THE UNIVERSITY OF ALBERTA

FINITE ELEMENT MODELLING OF FLUID MOTION AND DAMPED ACOUSTIC WAVES IN PIPES

by

© JAMES GORDON HILDEBRANDT

A THESIS

SUBMITTED TO THE FACULTY OF GRADUATE STUDIES AND RESEARCH

IN PARTIAL FULFILMENT OF THE REQUIREMENTS FOR THE DEGREE

OF MASTERS OF SCIENCE

MECHANICAL ENGINEERING

EDMONTON, ALBERTA

FALL 1982

Abstract

This work is an analysis of the fluid behavior in a pipe subject to a harmonically varying pressure gradient. From this basis the acoustic properties are obtained and these are compared to experimental data.

This analysis considers the affect of the inertia, the viscosity and the pipe configuration on the fluid motion. Galerkin's method of weighted residuals is used to derive a Finite Element model from a simplified Navier-Stokes momentum equation. A four node isoparametric element is used to determine the velocity distribution at two times of the harmonic cycle, at the beginning of the cycle (when pressure gradient is a maximum), and at 90° into the cycle (when pressure gradient is going through zero). Using the mean of these velocities the resistivity and the effective density are found as functions of frequency.

For a pipe of uniform cross-sectional area the impedance is directly found from the resistivity and the effective density via an exact equation. To find the impedance for a pipe with an area varying along the axis a second Finite Element is developed which requires these same parameters.

Results are presented for the cases of a circular pipe, triangular pipe, square pipe, two parallel walls and a rectangular pipe with an aspect ratio of five. Good agreement is found between the predicted and the experimental results.

Acknowledgments

I would like to express my sincere gratitude to Dr. A. Craggs for his guidance of this work. It has been very rewarding working with him.

Special thanks to Ron Pelot for his companionship and his interest in this work which brought to light many facets of this topic. Thanks also to Roger Toogood for providing much assistance in the technical aspects and the preparation of the presentation of this work. In the latter area thanks are also expressed to Waqar-Ul-Haque and Richard Carlson. Fellow graduate students and the academic staff are thanked for providing a stimulating and challenging atmosphere in which to learn and work.

Funding was partly provided by a scholarship from Natural Sciences and Engineering Research Council Canada.

Thanks to General Motors Corp. for providing data and a specimen for testing.

Table of Contents

List of Figures

Definition of Symbols

ρ_o	Static value of density.
C	Speed of sound in tube.
ρ_e	Effective density.
R	Resistivity.
ω	Circular frequency (rad/sec).
k	Wave number (ω/C).
μ	Dynamic viscosity.
r_h	Hydraulic radius (2area/perimeter).
K	Dimensionless frequency $r_h(\rho_o\omega/\mu)^{1/2}$.
U	Particle velocity, in X direction.
$\overline{U}$	Mean velocity across pipe.
$\dot{U}$	Particle acceleration, in X direction.
$\{\ \}$	Column matrix.
$[\ ]$	Rectangular matrix.
j	Imaginary unity.
$\hat{P}$	Maximum acoustic pressure.
$\hat{U}$	Argument of fluid velocity.
Rf	Reflection factor.
$\|Rf\|$	Magnitude of reflection factor.
Z	Specific impedence.
β	Phase angle.
τ	Shear stress.
F	Biot's [1] correction function.
γ	Ratio of specific heats for a gas.
Ni	Interpolation function.

Ci	Parameters of the field variable, in this work is either the velocity at a point or its derivative.
Domain	Entire pipe area.
S	Boundary enclosing the pipe area.
Re(u)	Real part of the complex variable u.
Im(u)	Imaginary part of the complex variable u.

1. Introduction

The problem to be considered is the analysis of the acoustic properties of pipes of arbitrary cross-section in which viscous and inertial forces of the fluid are included. Previous work in this area has been restricted by the analytical methods to the cases of channels and cylindrical pipes.

A review given by Zwikker and Kosten [19] covers and builds on the contributions of Helmholtz, Kirchhoff [11] and Rayleigh [15] in the analysis of fluid motion in pipes. The first analysis of unsteady fluid motion near a wall was developed by Stokes and this analysis was applied to the cases of channels and pipes by Helmholtz who considered only the viscous and inertial forces. Kirchhoff [11] made a major contribution by including viscosity and effects arising from the generation of heat and its conduction to and from the walls of the tube. Rayleigh [15] built on these works to develop a theory of the fluid motion for cases when the viscosity dominates and when viscosity is very small. Rayleigh [15] was the first to suggest that the acoustic properties of a wall made of numerous fine channels could simulate the properties of a porous sound absorbing wall.

The general characteristics of fluid motion in round pipes can best be described through examining the extreme cases at low and high frequencies. The most important

difference is whether the viscous or the inertial forces dominate.

At low frequencies or when the tube is very small the viscous property of the fluid determines its motion. The characteristics of the motion are as follows. The mean velocity of the fluid is proportional to and in phase with the pressure gradient. A boundary condition of viscous flow is that the velocity at the pipe wall is zero. At these low frequencies in a round pipe the velocity profile is approximately a paraboliod of revolution. The temperature of the fluid is held constant by the conduction of heat to the walls of the pipe, which in most cases has a much larger heat capacity than the fluid. (The heat here mentioned refers to that which is generated by the compression and expansion of the fluid). This results in the speed of sound propagation in the pipes being at its lower limit which is 290 m/s for air.

At high frequencies the fluid motion is complicated by two factors. The first and most important factor is the inertia of the fluid. When the inertial forces dominate over the viscous forces the fluid motion lags behind the pressure gradient. Under harmonically varying pressure gradients, as frequency increases, the motion lag approaches 90°. In addition the velocity profile flattens and, for a given pressure gradient, the peak velocities achieved decrease with increasing frequency. This situation is similar to a damper-mass system; if the forcing function is kept

constant, the amplitude of vibration decreases when the frequency increases.

A more involved factor influencing the fluid motion at high frequencies is the conduction of heat. At high frequencies the fluid does not communicate heat fast enough to the pipe walls to make reasonable the assumption of constant temperature throughout the fluid. This in itself has three effects. The first effect is that the speed of sound approaches the adiabatic speed of sound which is 343 m/s for air. Since the walls of the pipe have a decreased influence on the temperature there exists a significant temperature difference between the walls and the fluid at the axis of the pipe. Thus the viscosity is no longer constant. The third effect is the introduction of another mechanism for dissipation in the form of thermal processes. Even at high frequencies, however, the dissipation of the wave energy is dominated by viscous forces.

Biot [1] develops a function in an attempt to describe the interaction of the viscous and the inertial forces in narrow channels and round pipes. This function is applicable to absorptive material but here it is used mainly as a comparison to the numerical analysis.

Biot's function is related to the momentum balance as follows

$$-\partial P/\partial X = \rho_e\big|_{K=0}\,\dot{\overline{U}} - F_{(K)}\,R\big|_{K=0}\,\overline{U} \qquad 1.1$$

A more convenient form with which to analyze the acoustic properties is in the equation

$$-\partial P/\partial X = \rho_e \dot{\bar{U}} - R\bar{U} \qquad 1.2$$

where $\bar{U}$ is the complex mean velocity (averaged across the pipe at t=0 and t=90° in the cycle), $\dot{\bar{U}}$ is its time derivative, ρ_e is called the effective density and R is the resistivity. This relation assumes that the fluid velocity is constant across the pipe and equal to U. Kuttruff [12] assumes that the effective density and resistivity are constant but admits that from Cremer [4] this analysis is limited to conditions where $\rho_o \omega / R \leq 4$. The proceeding analysis is not under this constraint.

It can be reasoned that the parameters of effective density and resistivity must change with frequency by simply contrasting the fluid motion characteristics at low and high frequencies. For example at high frequencies the analogy to the damper-mass system shows that the magnitude of the velocity decreases with frequency. This implies that the resistivity increases with frequency. These properties, which are functions of frequency, are also strongly dependent on the type of pipe considered.

The dependence on the type of pipe considered is due to the different fluid motion found in different pipes. The simplest example is to consider steady state flow in pipes. The shear stresses on the walls of non-circular pipes can be extremely variable along the perimeter of the pipe. Thus it is reasonable to say that the fluid behavior, and thus the acoustic properties, in non-circular pipes at various

frequencies are significantly different from those of the cases already studied, i.e. the channel and cylinder.

The aim of this thesis is to develop an analysis of fluid motion which is applicable to pipes of any arbitrary cross-section.

Biot's [1] function for the channels and the cylindrical pipe is used to confirm the results obtained. Biot [1] states that these two cases represent extreme cases. So the function for any other case should lie between these two functions. It is found that the cases of non-circular pipes do not behave quite as predictably as this reasoning suggests.

More importantly, the intent of this analysis is to find how the resistivity and effective density vary with frequency for a number of shapes of pipe. With these relations it is possible to use the work of Zwikker and Kosten [19] and that of Craggs [2] to deduce first the input impedance, then directly the absorption, of a matrix of finite pipes. This done it is possible to confirm the analysis by experiment. This was done along with the above analysis.

The presentation of the analysis proceeds as follows. In Chapter 2 the method of analysing the problem is covered. This begins with the assumptions which lead to the governing equations. The method of solution to the governing equations, the finite element method, is then developed.

Chapter 3 presents the solution of the governing equations as applied to triangular pipes and square pipes. Comparison is made of the results of the analysis to Biot's [1] functions.

Chapter 4 shows the types of meshes used and the convergence of the bulk properties due to changing the type of mesh.

The resulting shear stresses on the walls of the triangular pipe and square pipe at various frequencies are noted in Chapter 5.

The relationship between the fluid motion and the acoustic properties of resistivity and effective density are derived in Chapter 6. These properties are presented, as predicted by the numerical model, for the cylindrical, triangular, square, and rectangular pipes as well as for the slit. Also included are two ways of finding the impedance for a finite pipe with one end closed. The first way is from the exact equation for a pipe which is uniform along its length. The second is a finite element method which can model a pipe varying in area along its axis.

The impedance tube experiment, the predicted absorption of the numerical model, and the most critical assumptions of the analysis are discussed in Chapter 7.

A summary of the work and the conclusions drawn from it are contained in Chapter 8.

2. Calculating Velocity Distributions due to Oscillating Pressure Gradients

2.1 Deriving Velocity Profiles in Small pipes

The first area to be examined is the fluid velocity distribution across a pipe with the fluid being subjected to an oscillatory pressure gradient. The importance of this is to provide the mean velocity as a function of time. This information directly leads to two important bulk properties: the resistivity R, and effective fluid density, ρ_e. These two properties depend on the cross-sectional geometry of the pipe and frequency of the oscillatory pressure gradient.

The acoustic impedance can be determined knowing only the resistivity, effective density, and the length between the open end where the wave enters and the rigid terminus. In practice the acoustic impedance and attenuation are required for an assembly or panel of parallel pipes of similar cross-sectional geometry which may be used for absorbing sound. Each pipe in the assembly affects the portion of the sound wave which strikes it independently and identically to the surrounding pipes, therefore the reflected wave from the single pipe will have the same strength and phase as the reflected wave from the assembly of pipes.

Pipes of circular cross-section are modelled to compare with the previously known analytical results. Pipes of

triangular and square cross-section are modelled to compare with the experimental results. Small pipes of triangular and square cross-section are quite practical due to their perfect packing density and ease of manufacture.

2.2 Assumptions

To find the velocity distribution certain assumptions can be made.

1) The fluid is Newtonian.

2) The walls of the pipe are rigid and stationary.

3) The pressure gradient is strictly axial.

4) The inlet effects are negligible.

5) The fluid temperature is constant.

6) The fluid density is constant.

The inlet effects are neglected because for significant sound absorption the pipes must be fairly thin and long to provide, in essence, a large area to act on the fluid. For steady flow, the section of pipe taken for the flow to go from the initially flat velocity profile to its steady state parabolic velocity profile (for laminar flow) is proportional to the Reynolds number [16]. In oscillating flow the inlet effects decrease for the following reasons. First of all the Reynolds number (based on instantaneous velocity) decreases with increasing frequency, and second the velocity distribution changes from a parabolic to a flattened profile thus localizing the shear to the walls and

thus the pseudo-steady-state condition is more easily established. The effect of the inlet on pulsatile fluid motion is covered briefly by McDonald [14] .

A more significant assumption is that there is no temperature gradient in the fluid. This allows the use of a constant viscosity across the pipe at all times but it means the absorption of the model will be low because the thermal process being neglected is a mechanism of dissipation. This assumption means that the isothermal speed of sound C=290 m/s should be used.

It is also assumed that the density variation is negligible. Although this analysis is to be applied to determine the characteristics of sound waves in pipes the fluid motion can be found first by assuming the fluid is incompressible. This is reasonable since even a sound pressure level of 100 dB creates a density variation which is five orders of magnitude smaller than the average density.

2.3 Governing Equations

With the above assumptions the Navier-Stokes momentum equation [16] is

$$-\frac{\partial P}{\partial X} = \rho_a \frac{\partial U}{\partial t} - \mu \nabla^2 U \qquad 2.1$$

For fluid motion in a stationary pipe the boundary condition is U=0 at the pipe wall. The Cartesian coordinate system is used with the X direction being along the axis of the pipe.

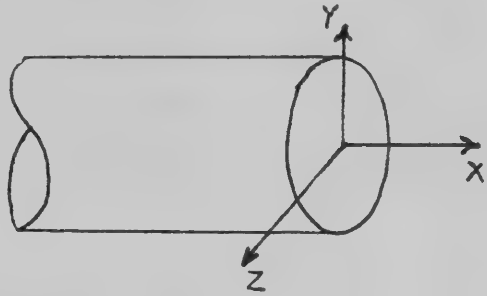

The second governing equation is the wave equation, as derived in Appendix A. This equation provides the form of the pressure variation needed. In one dimension the equation is

$$C^2 \frac{\partial^2 P}{\partial X^2} = \frac{\partial^2 P}{\partial t^2} \qquad 2.2$$

The resulting pressure is

$$P_{(x,t)} = \hat{P} \exp\{j(\omega t - kX)\} \qquad 2.3$$

where P is the peak pressure, ω is the circular frequency, k is the wave number $k= \omega /C$, and C is the sonic speed.

The velocity must assume the same form.

$$U_{(x,y,z,t)} = \hat{U}_{(y,z)} \exp\{j(\omega t - kX)\} \qquad 2.4$$

The phase difference between the velocity and the pressure is expressed by the complex quantity $\hat{U}$. The velocity output

of the computer program will be in terms of Ur and Ui, which are the real and imaginary parts of $\hat{U}$ respectively

$$\hat{U} = U_r + jU_i \qquad 2.5$$

Looking at one position of the pipe, say X=0, and replacing the exponential notation with its equivalent gives us

$$U(o,y,z,t)=(Ur+jUi)(\cos(\omega t)+j\sin(\omega t)) \qquad 2.6$$

Our input quantity is pressure so P is set to be real only

$$P = \hat{P} \cos(\omega t) \qquad 2.7$$

Since only the real part of these quantities has physical significance

$$U(o,y,z,t) = Ur \cos(\omega t) - Ui \sin(\omega t) \qquad 2.8$$

Ur is the velocity distribution at t=0 and the negative of Ui is the velocity distribution at ω t=90°.

Substituting this harmonic velocity into the momentum equation yields

$$-\frac{\partial P}{\partial X} = j \rho_o \omega U - \mu \nabla^2 U \qquad 2.9$$

2.4 Galerkin' s Method and the Finite Element Method

Analytical solutions to the above equation have been found in the case of a round pipe as well as for two infinite parallel plates, referred to hereafter as a slit. To solve for the velocity profile, however, in a pipe with an arbitrary cross-section, numerical techniques must be employed.

The numerical technique chosen is Galerkin's method [1] which is a specific form of the weighted residuals method. Huebner [10], who provides some excellent examples of the use of Galerkin's method in finite elements, offers the following which can be taken as a synopsis of the method.

> "Applying the method of weighted residuals involves basically two steps. The first is to assume the general functional behavior of the dependent field variable in some way so as to approximately satisfy the given differential equation and boundary conditions. Substitution of this approximation into the original differential equation and boundary conditions then results in some error called a residual. This residual is required to vanish in some average sense over the entire solution domain".
> "The second step is to solve the equation (or equations) resulting from the first step and thereby specialize the general functional form to a

---

[1]For further discussion see Refs. 6 and 8. The original work by Galerkin is not readily accessible but brief accounts are contained in various Russian publications eg. Refs. 5 and 9.

particular function, which then becomes the approximate solution sought".

Let us expand this with the simplified momentum equation (2.9) in mind. The field variable is the velocity U. The domain of interest is the YZ plane bounded by the pipe walls, S.

First U is approximated by $\tilde{u}$, where either the functional behavior of $\tilde{u}$ is specified in terms of unknown parameters, or the functional dependence on all but one of the independent variables is specified while the functional dependence on the remaining independent variable is left unspecified. Then the dependent variable is approximated by

$$U \simeq \tilde{u} = \sum_{i=1}^{m} N_i C_i \qquad 2.10$$

where Ni are the assumed functions and Ci are either the unknown parameters or unknown functions of one of the independent variables. The m is the number of unknown parameters with which U is approximated. The m functions Ni are generally chosen to satisfy the boundary conditions.

When the approximation $\tilde{u}$ is substituted into the momentum equation (2.9) there will likely be some error called the residual, ϵ .

$$\epsilon = \frac{\partial P}{\partial X} + j\, \rho_o\, \omega\, \tilde{u} - \mu\, \nabla^2\, \tilde{u} \qquad 2.11$$

The focus of the method of weighted residuals is to determine the m unknowns Ci in such a way that the residual over the entire domain is small.

Therefore we choose m linearly independent weighting functions Wi and specify that the weighted average of the error vanish over the domain. That is if

$$\int_{\text{Domain}} \varepsilon W_i \, dA = 0 \qquad 2.12$$

then the residual is small in some sense. Note that minimizing the error of the differential equation does not necessarily mean that the error of the solution has been minimized by the same weighting functions.

At this point a broad choice of weighting functions are available. For this problem, however, Galerkin's criterion determines the weighting functions. Galerkin's criterion is that the weighting functions are the same as the approximating functions used to represent U, that is Wi=Ni for i=1,2,...m.

2.5 Discretization

So far the entire solution domain has been considered. This requires that the approximating functions identically satisfy the boundary conditions. This can mean that the functions can be quite involved if the shape of the boundary is irregular. Since the differential equation holds at any

point in the domain, it also holds for any collection of points defining an arbitrary subdomain or element of the whole domain. Focusing on this element generally allows a simplification of the approximating function. The shape of the domain is then approximated by an assembly of such elements.

Now, looking at a typical element, the functions Ni are the interpolation functions defined over the element, and the undetermined parameters Ci are the values of the field variables or their derivatives at the nodes. For each element, then,

$$\int_{D^{(e)}} \left\{\frac{\partial \rho^{(e)}}{\partial X} + j\rho_o \omega U^{(e)} - \mu \nabla^2 U\right\} Ni^{(e)}\, dA^{(e)} = 0 \qquad 2.13$$

where

$$U^{(e)} = \sum_{i=1}^{r} NiCi = \lfloor N^{(e)} \rfloor \{Ci^{(e)}\} \qquad 2.14$$

where r is the number of unkown parameters of each element i.e. the product of the number of nodes per element and the number of unknowns per node. The unknowns are velocity if the lowest order interpolation function is used or the unknowns may also include the derivatives of the velocity if a higher order function is used. Henceforth U will represent the approximate velocity.

The only problem remaining before assembling the elements and solving the equations is that the interpolation function must ensure continuity of the function between elements. The interpolation functions must be chosen such

that, at the element boundaries, continuity of the field variable, as well as continuity of its partial derivatives is satisfied (up to one order less than the highest-order derivative appearing in the expression to be integrated). The higher the order of continuity required, the fewer suitable interpolation functions available.

Applying integration by parts to the integral expression, equation (2.9), reduces the order of the derivatives and the required order of the approximating function. Integration by parts also conveniently introduces the natural boundary conditions.

Appendix B shows the detailed derivation of the matrix equations. For this work the simplest quadrilateral element was used. It has only one degree of freedom at each node and thus can only assume a linear variation between nodes. Figure 2.1 shows a typical element and the interpolation function in the transformed ZY plane.

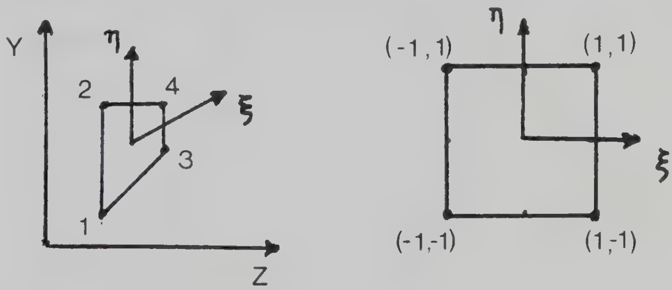

$$U = \frac{1}{4} \times \{U_1(1-\eta)(1-\xi)+U_2(1+\eta)(1-\xi)+U_3(1-\eta)(1+\xi)+U_4(1+\eta)(1+\xi)\} \quad 2.15$$

Figure 2.1 Coordinate Systems

The YZ plane is the physical plane. The $\eta\xi$ plane is the natural coordinate system. This transformation allows us

to perform the necessary integrations using Gauss quadrature in an orthogonal plane and yet allowing the element to assume the shape of practically any quadrilateral in the ZY plane. The transformation from one plane to the other is performed by the same function as the interpolation function.

$$Z = \frac{1}{4} x \{Z_1(1-\xi)(1-\eta)+Z_2(1-\xi)(1+\eta) +$$
$$Z_3(1+\xi)(1-\eta) + Z_4(1+\xi)(1+\eta)\} \qquad 2.16$$

$$Y = \frac{1}{4} x \{Y_1(1-\xi)(1-\eta) + Z_2(1-\xi)(1+\eta) +$$
$$Y_3(1+\xi)(1-\eta) + Y_4(1+\xi)(1+\eta) \qquad 2.17$$

Elements calculated by this procedure are termed isoparametric.

2.6 Matrix Equations

After applying Galerkin's method to the differential equation, equation (2.13) must be solved for each element domain. In matrix notation

$$\int_D Ni \frac{\partial P}{\partial X} \quad dA = \{P\} \qquad 2.18$$

$$j\rho_o\omega \int_D Ni \quad U \quad dA = j\rho_o\omega \quad [Me] \{U\} \qquad 2.19$$

$$\mu \int_D Ni \, \nabla^2 U \, dA = \mu \, [De] \{U\} \qquad 2.20$$

Where {P} is an array containing the force of pressure assigned to each node, that is, the larger the element the larger the values of force at each node. {U} is the array of

the velocities at each node in the element, [Me] is called the mass matrix, it represents the mass of the element, and [De] is the stiffness matrix. So the equation can be written for each element as

$$\{P\} = (\mu[De] + j\,\rho_o\omega\,[Me])\,\{U\} \qquad 2.21$$

These elemental equations are assembled into global matrices producing simultaneous equations to be solved.

If a certain procedure is applied to the global numbering of the mesh an important process can be applied to the global matrices. The process is partitioning. The required system is numbering the nodes on the interior of the pipe first leaving the boundary nodes to be numbered last. The resulting global matrix will have all of the information relevent to the interior nodes in the top left corner and all of the information relevent to the boundary nodes in the bottom left corner. This will provide a direct means to finding the shear forces on the pipe walls after solving for the velocities at the interior nodes.

Define:

DOF = number of degrees of freedom at each node allowed by interpolation functions.

NK = DOF times the number of nodes on pipe wall.

NI = DOF times the number of nodes inside pipe i.e. where u is not constrained by the boundary conditions.

NT = NK + NI

Array size	Array	Comments
NIx1	$\{U\}$	= matrix of velocities at interior nodes.
NKx1	$\{Uo\}$	= matrix of velocities at nodes on pipe wall, (filled with zeros).
NIx1	$\{P\}$	= force due to the pressure at each internal node
NKx1	$\{F\}$	= force due to shear at each node on pipe wall.
NTxNT	$[Ma]$	= assembly of all mass matrices [Me].
NIxNI	$[M_{ff}]$	= subset of [Ma] , represents mass of fluid around each interior node
NKxNI	$[M_{cf}]$	= subset of [Ma] , represents mass of fluid around each node on pipe wall.
NTxNT	$[Da]$	= assembly of all stiffness matrices [De].
NIxNI	$[D_{ff}]$	= subset of [Da] , represents stiffness of fluid at each interior pipe node.
NKxNI	$[D_{cf}]$	= subset of [Da] , stiffness of fluid at nodes on pipe walls

The partitioning appears as follows

$$[Ma] = \begin{bmatrix} M_{ff} & M_{fc} \\ & \\ M_{cf} & M_{cc} \end{bmatrix} \qquad [Da] = \begin{bmatrix} D_{ff} & D_{fc} \\ & \\ D_{cf} & D_{cc} \end{bmatrix} \qquad 2.22$$

(a) (b)

The result of assembling all the elemental equations is

$$\begin{Bmatrix} \{P\} \\ --- \\ \{F\} \end{Bmatrix} = \left(\mu \begin{bmatrix} D_{ff} & D_{fc} \\ & \\ D_{cf} & D_{cc} \end{bmatrix} + j \rho_o \omega \begin{bmatrix} M_{ff} & M_{fc} \\ & \\ M_{cf} & M_{cc} \end{bmatrix} \right) \begin{Bmatrix} \{U\} \\ \\ \{U_o\} \end{Bmatrix} \qquad 2.23$$

Only {U} and {F} are unknown. {U} is solved from

$$\{U\} = (\mu[D_{ff}] + j \rho_o \omega [M_{ff}])^{-1} \qquad \{P\} \qquad 2.24$$

It is interesting to see that the shear forces on the nodes of the walls can now be obtained by a single matrix multiplication

$$\{F\} = (\mu[D_{cf}] + j \rho_o \omega [M_{cf}]) \qquad \{U\} \qquad 2.25$$

This last step is made easy because of the aforementioned numbering scheme. This could be made without this scheme but only if intricate matrix manipulations are made to put the resulting matrices into the form already shown above.

Some computing facilities can not solve systems which consist of complex variables, as these do. Therefore it may be desirable to express the above in terms of real matrices only. The complex equation to find {U} can be written in terms of real numbers only as

$$\begin{Bmatrix} Ur \\ \\ Ui \end{Bmatrix} = \left[\begin{array}{c|c} \mu[D_{ff}] & -\rho_o \omega [M_{ff}] \\ \hline \rho_o \omega [M_{ff}] & \mu [D_{ff}] \end{array} \right]^{-1} \begin{Bmatrix} Pr \\ \\ Pi \end{Bmatrix} \qquad 2.24\,a$$

where subscript r denotes the real part and subscript i the imaginary part of the quantity at each node.

Similarly treating the shear force equation results in

$$\begin{Bmatrix} Fr \\ Fi \end{Bmatrix} = \begin{bmatrix} \mu[Dcf] & -\rho_0 \omega [Mcf] \\ \rho_0 \omega [Mcf] & \mu[Dcf] \end{bmatrix} \begin{Bmatrix} Ur \\ Ui \end{Bmatrix} \qquad 2.25\,a$$

Thus the stage has been reached where the problem has been reduced to determining an appropriate mesh of elements and solving sets of linear equations.

Determining the best element mesh, it will be shown in the next chapter, is done interactively with the velocity distribution.

The assumptions made and numerical technique employed provide a basis on which to obtain the fluid motion and ultimately the acoustic characteristics of a pipe. Up to this point it is difficult to see what limitations might occur under these assumptions and the numerical analysis. On examination of the results it can be seen that the analysis is limited to certain frequencies. By choosing an appropriate finite element mesh, however, the range is considerably extended. This will be further discussed in chapter 4.

This leads to the initial results, the velocity profiles.

3. Resulting Velocity Distributions

3.1 Interaction of Inertia and Viscosity

Now consider the properties of the velocity associated with an oscillatory pressure gradient. A physical description will be given followed by the Finite Element results. First of all note a parameter commonly related to pulsatile flow problems, K, defined as [1]

$$K = r \left(\frac{\rho_o \omega}{\mu} \right)^{1/2} \qquad 3.1$$

K is similar to Reynold's number in that it compares the inertial to the viscous forces. Commonly K is called either the acoustic Reynold's number or the dimensionless frequency.

The first feature of the fluid motion to be noted is that there is a phase lag between the pressure gradient and the fluid movement. The fluid near the wall is almost in phase with the pressure gradient. This is because the viscous losses at the wall prevent this layer from gaining much momentum. The less momentum the greater the ease of the fluid to follow the pressure gradient reversals. The fluid near the axis of the pipe, which is least affected by the walls, achieves the highest momentum, and lags the most

----

[1] r is some typical dimension. For a slit r is half the width for all other cases it is taken as the wetted perimeter radius or hydraulic radius defined as twice the area divided by the perimeter.

behind the pressure reversals. At high values of K there is less time in the cycle for the wall shear to translate to the centrally located fluid and the velocity profile of the interior fluid becomes flattened. The fluid in the central part of the tube is virtually unsheared and the very high velocity gradients are found near the wall. Thus the fluid behaves like a solid core surrounded by a thin viscous fluid (See Figure 3.1). According to McDonald [14] at a relatively high frequency of K=20 the region of high velocity gradient, where the viscosity is of any importance, is virtually confined to the outer 5 per cent of the tube radius (See Figure 3.2).

3.2 Velocities in Triangular and Square Pipes

The velocity distributions for the triangular and square pipes are shown for various frequencies in Figures 3.3 to Figures 3.11.

It is easy to see the similarity of these flows to those of the round pipe, as just described. As the frequency increases the velocity distribution in the middle of the pipe flattens and becomes more out of phase with the pressure gradient. Correspondingly the peaks in the corners of the pipe at t=0 become accentuated. The three dimensional figures do not have the same velocity scale. To show the relative changes of the velocities as the frequency increases see Figure 3.12 and Figure 3.13 . Shown here are

the velocity profiles for a round pipe with the frequency changing but with the pressure gradient held constant. Figure 3.13 is the velocity profile at time t=0 in the cycle. Figure 3.14 is the velocity profile at time $\omega t=90°$, note that the scale of both figures is the same.

It might be noticed that the velocity profiles for the triangular and square pipes contain some irregulaties. The major cause of these irregularities is the process used for plotting. The input data for the plotting program must be from a mesh of uniform spacing throughout. This means that the output of the F.E programs must be used to interpolate values at each grid point for the uniform mesh. These interpolations were handled by a system library program which unfortunately did not use the same interpolation functions as those of the elements. At high values of K the irregularities are especially prominant near the edges of the pipe. The points that suddenly stick out are points where the nodes of the original Finite Element grid points are. The velocities in the corners of the pipes are better represented because the original grid contains a higher concentration of nodes in the corners. Some other irregularities originate in the plotting program itself. This is seen from the erratic lines drawn along the edge of the square pipe even though the input function is zero along the edge.

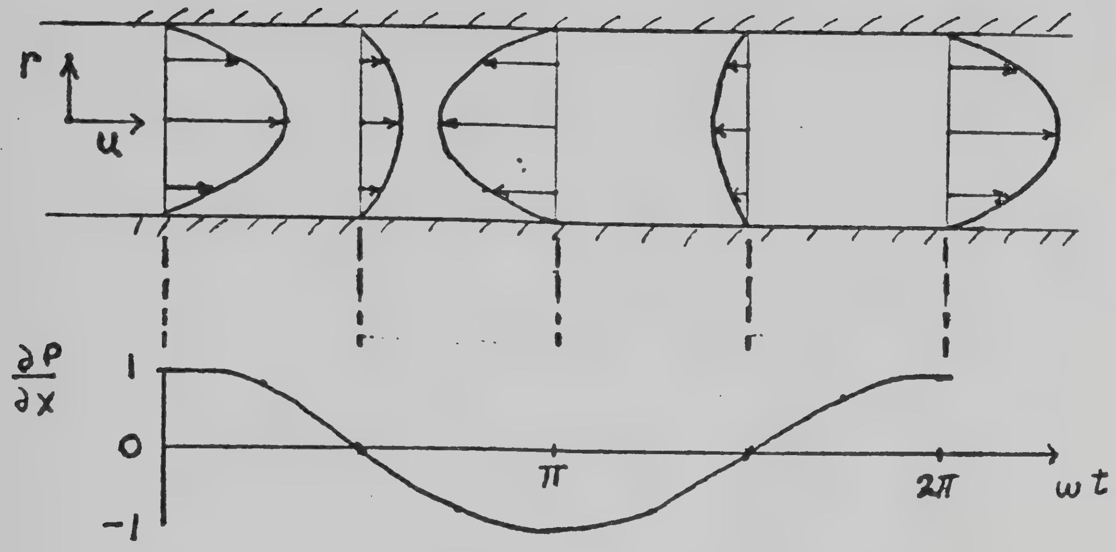

a) Low Frequency, K ≃ 1.

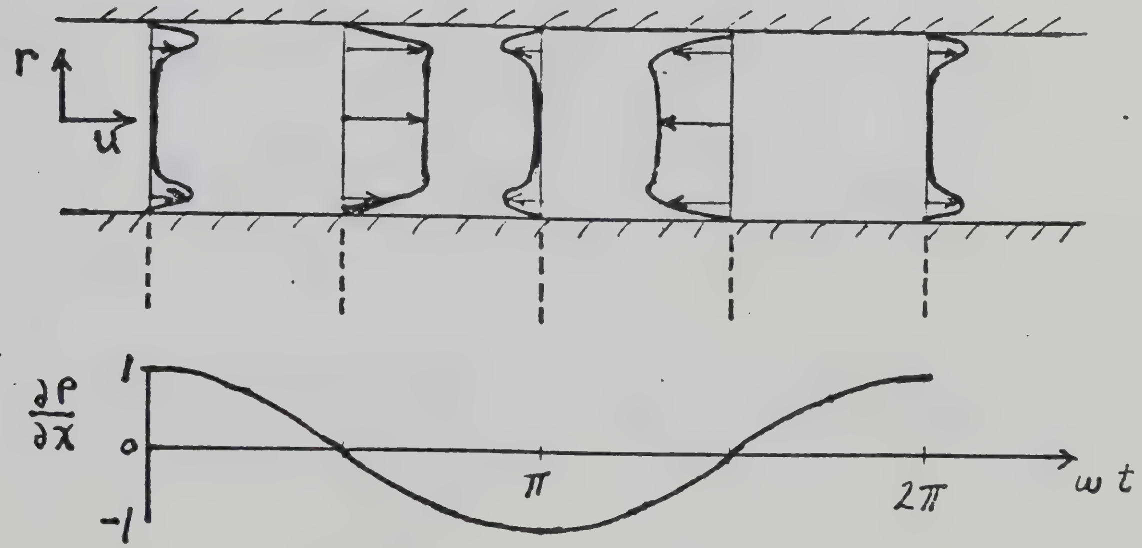

b) High Frequency, K ≃ 10.

Figure 3.1 Velocity Profiles in circular pipe at various times in the cycle.

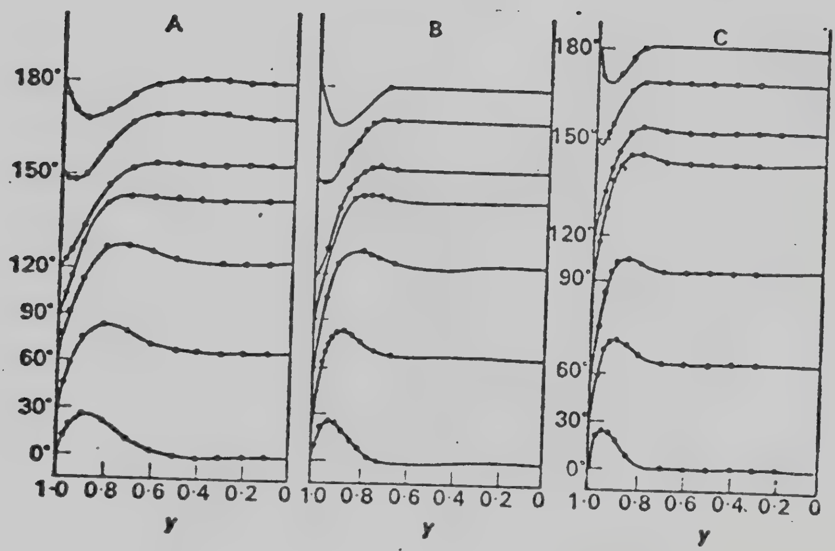

Figure 3.2 Velocity profiles of a cylindrical pipe created by a pressure gradient of a sinusoidal wave form. Profiles are given for half the tube at intervals of 30° from 0° to 180°.

A. $K = r(\frac{\rho\omega}{\mu})^{\frac{1}{2}} = 10$

B. $K = 15$

C. $K = 20$

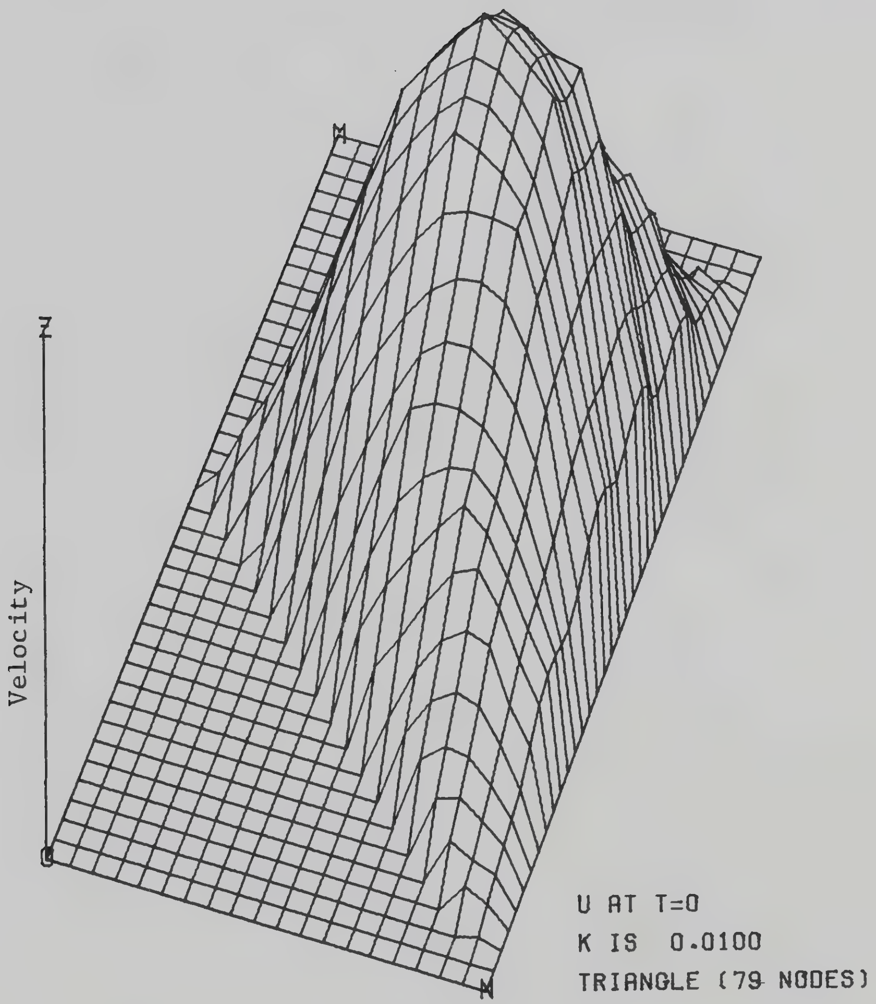

Figure 3.3 Velocity profile in triangular pipe

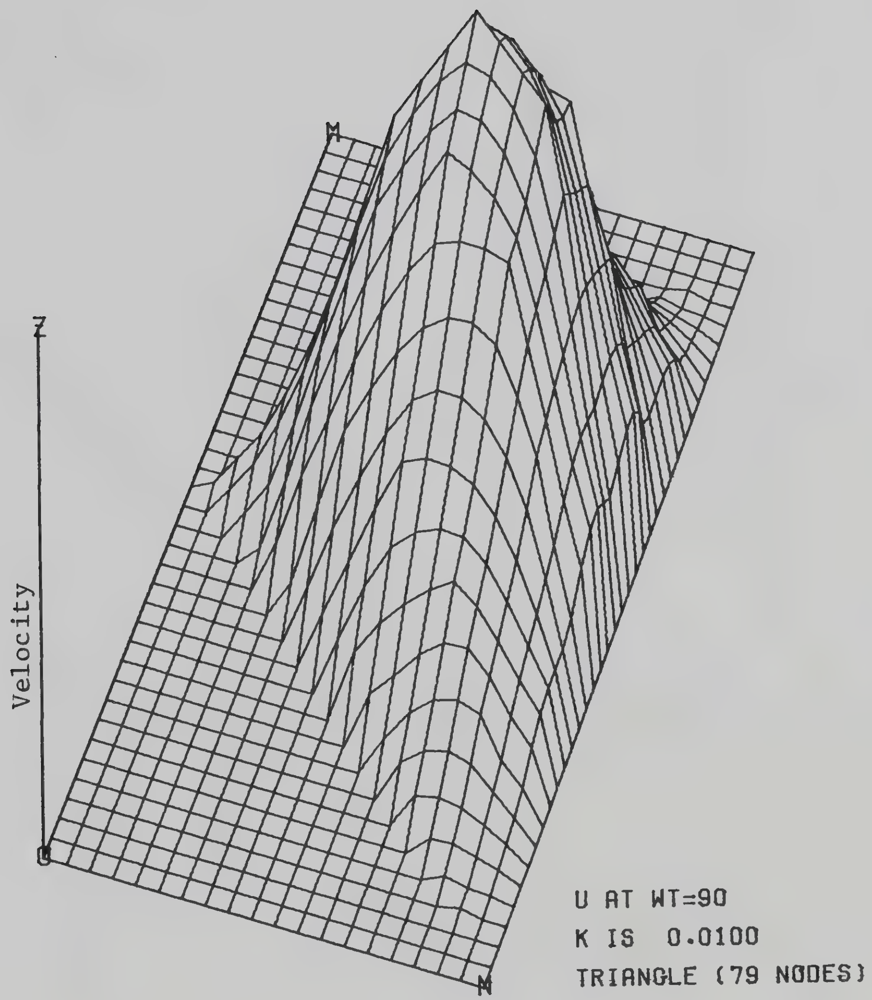

Figure 3.4 Velocity profile in triangular pipe.

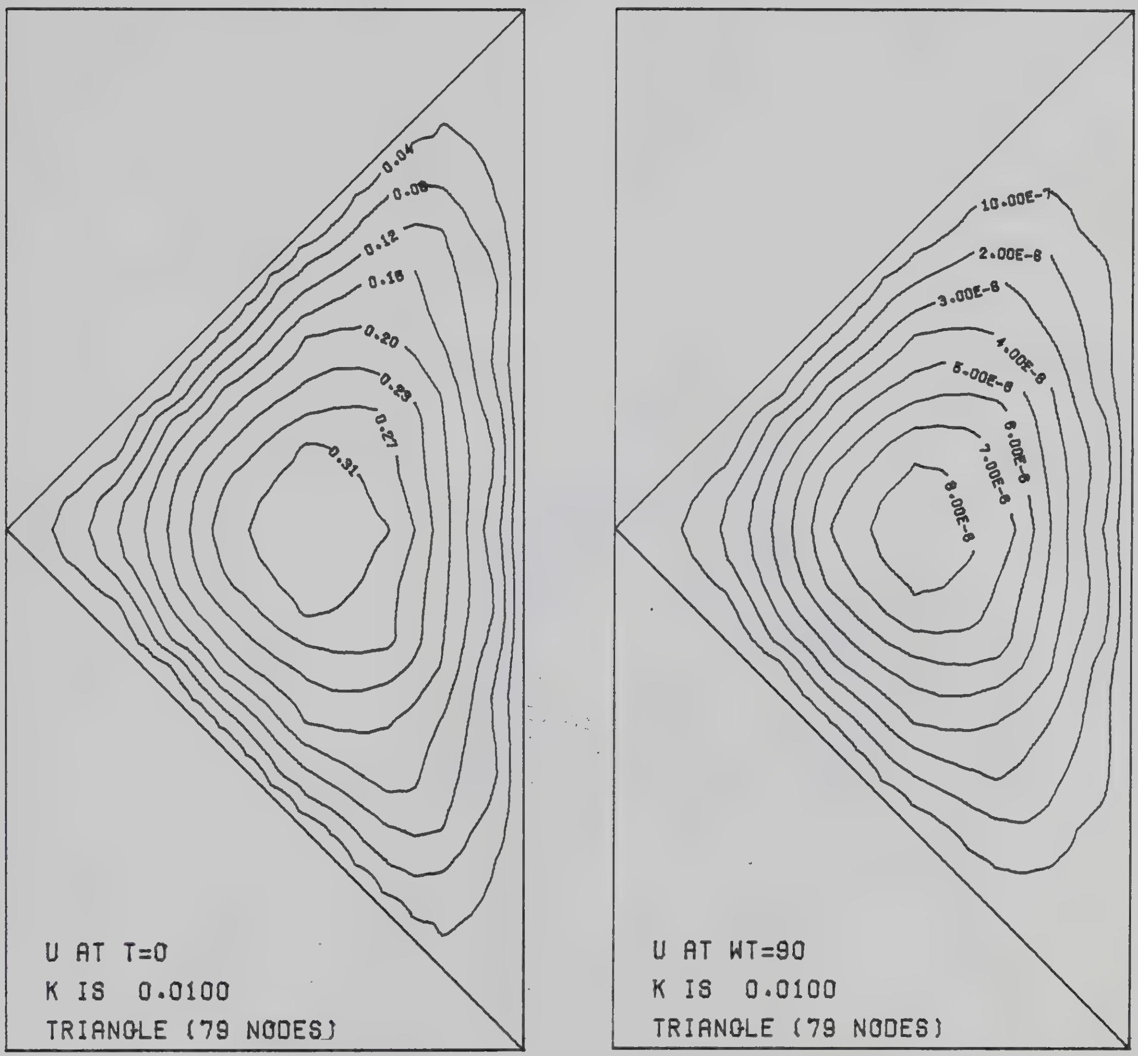

Figure 3.5 Contours of velocity in triangular pipe.

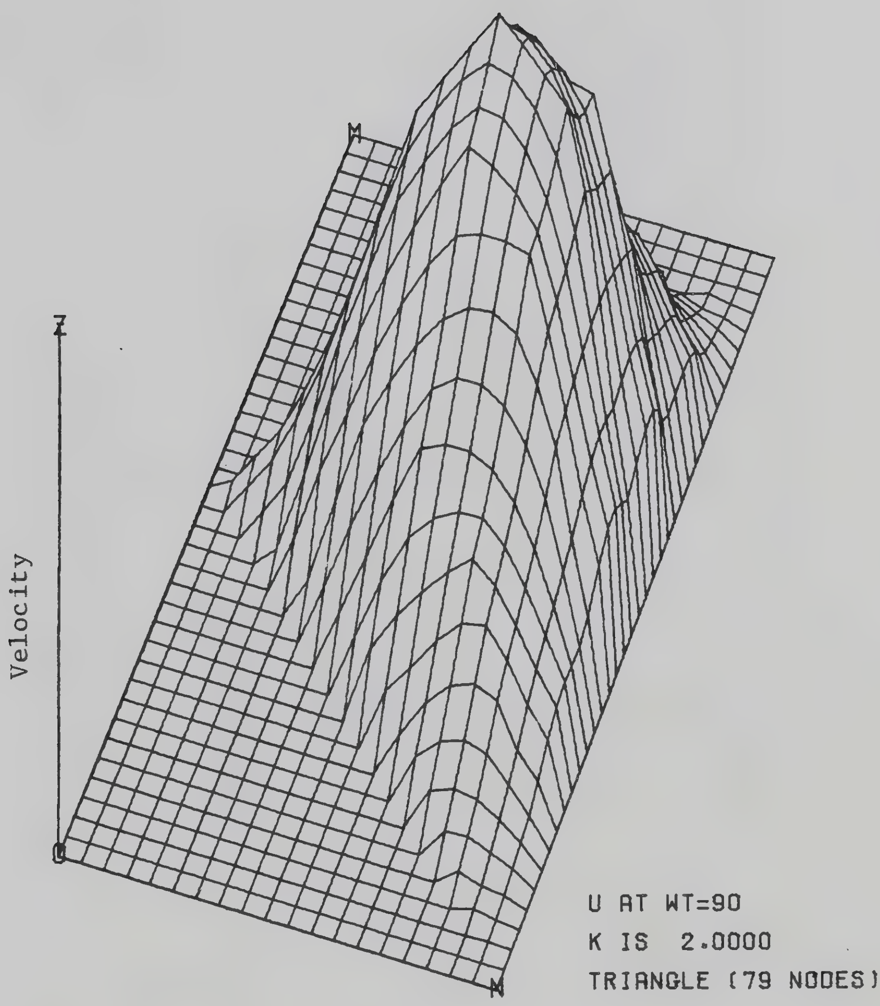

Figure 3.6 Velocity profile in triangular pipe.

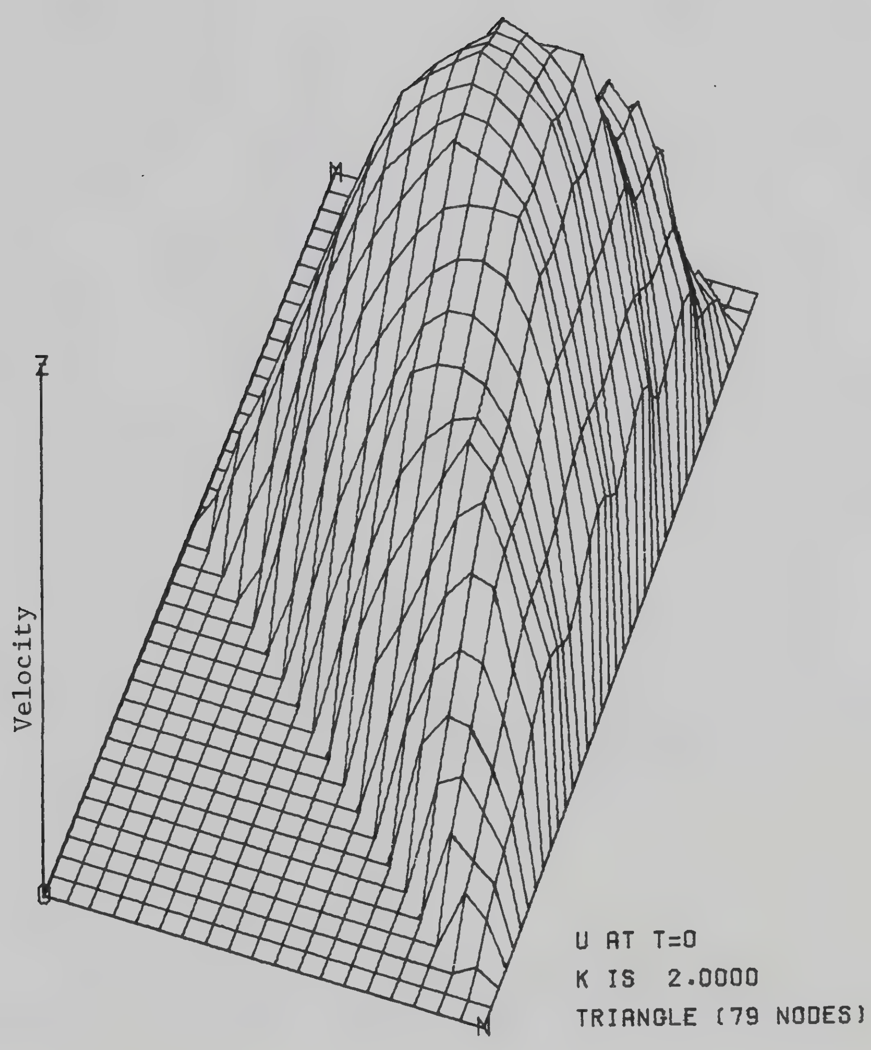

Figure 3.7 Velocity profile in triangular pipe.

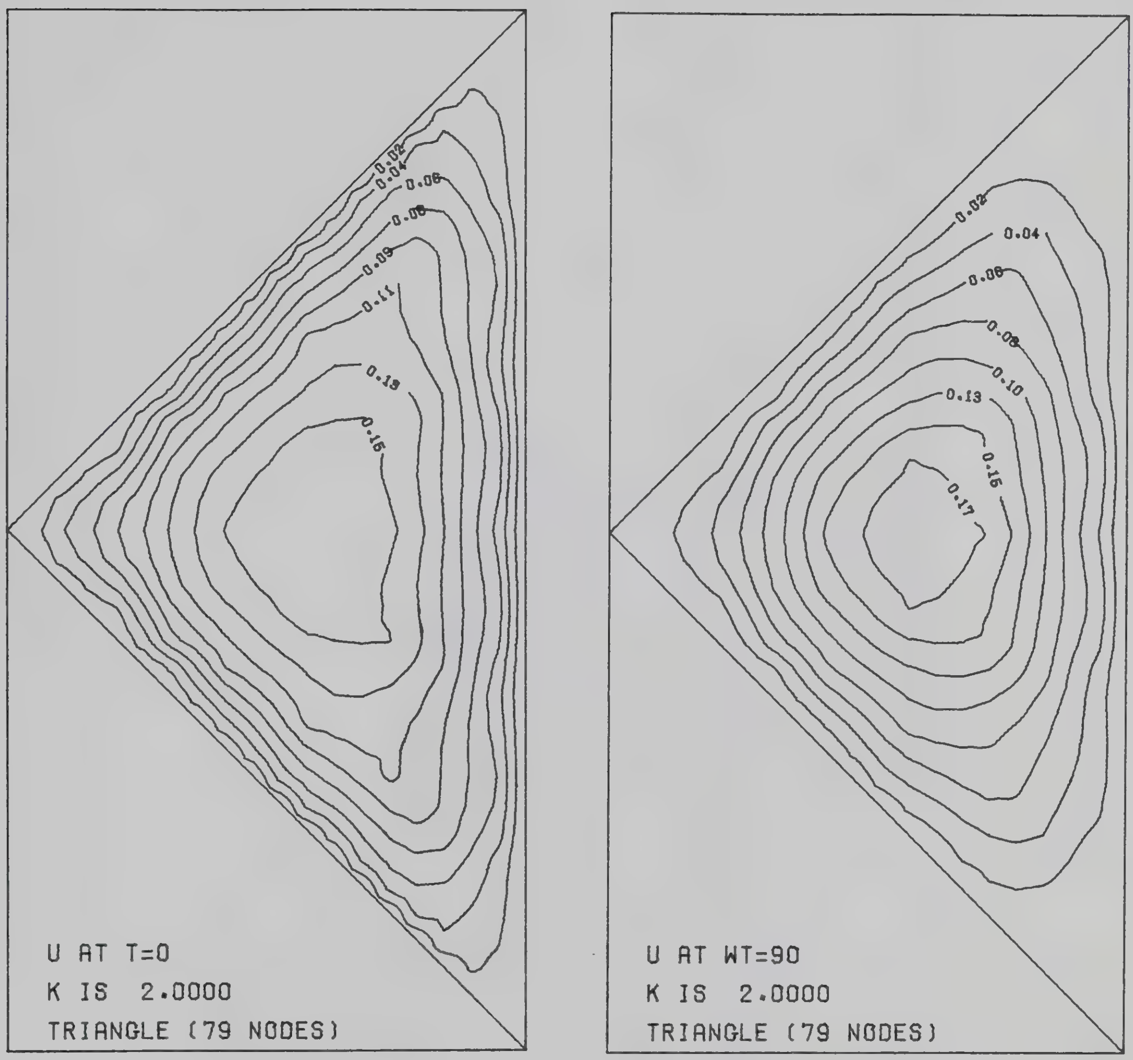

Figure 3.8 Contours of velocity in triangular pipe.

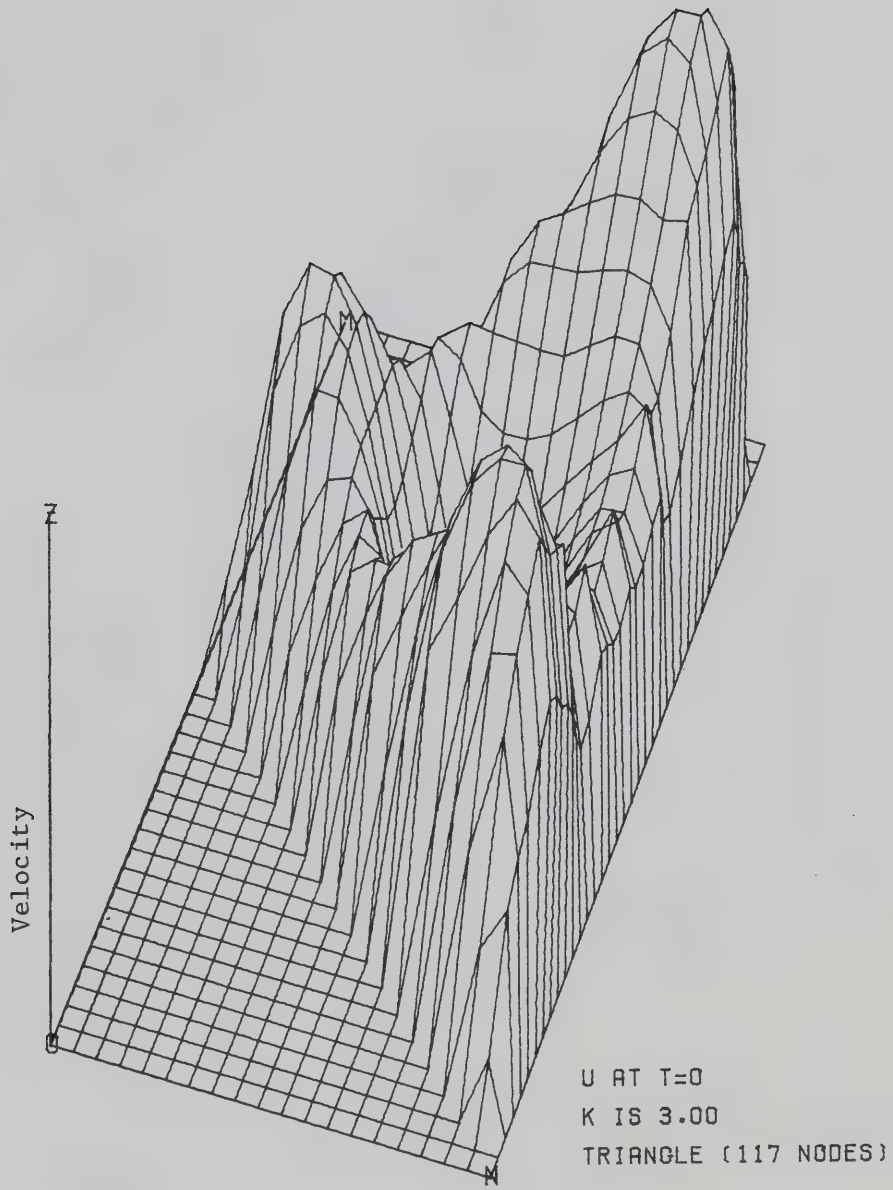

Figure 3.9 Velocity profile in triangular pipe.

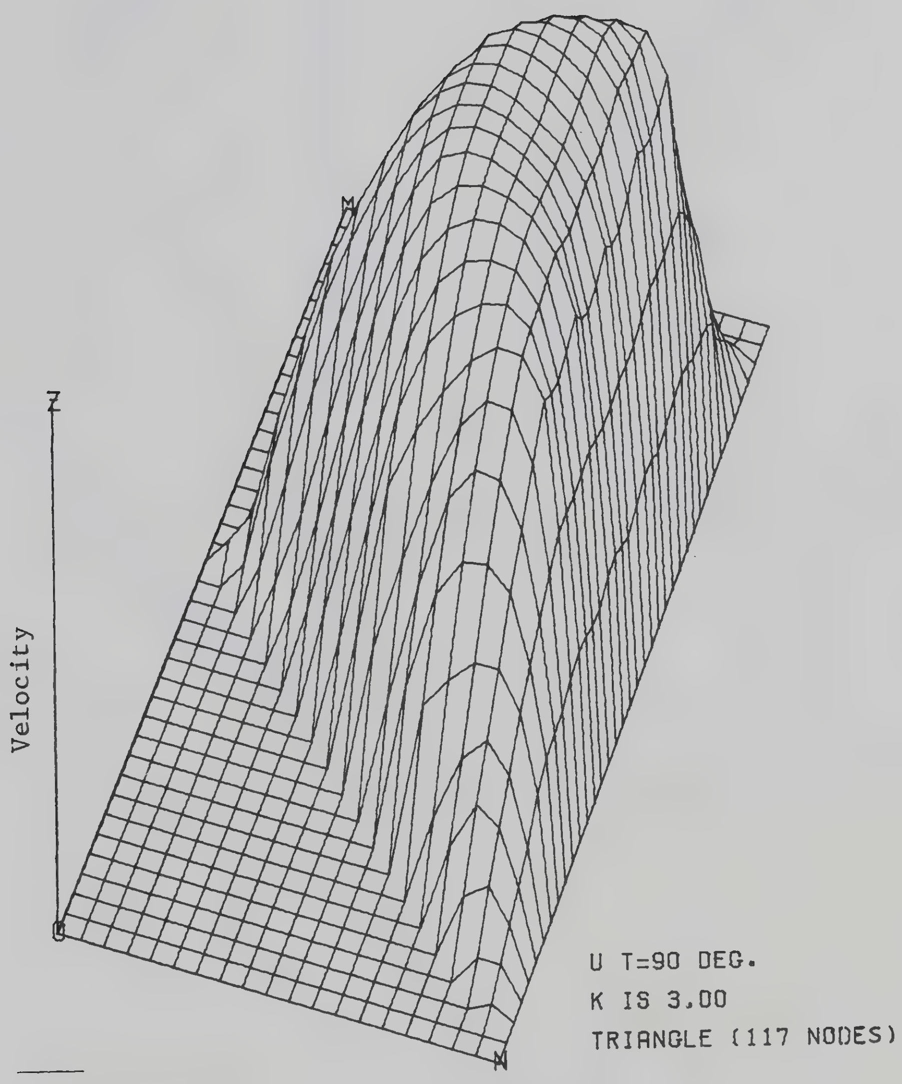

Figure 3.10 Velocity profile in triangular pipe.

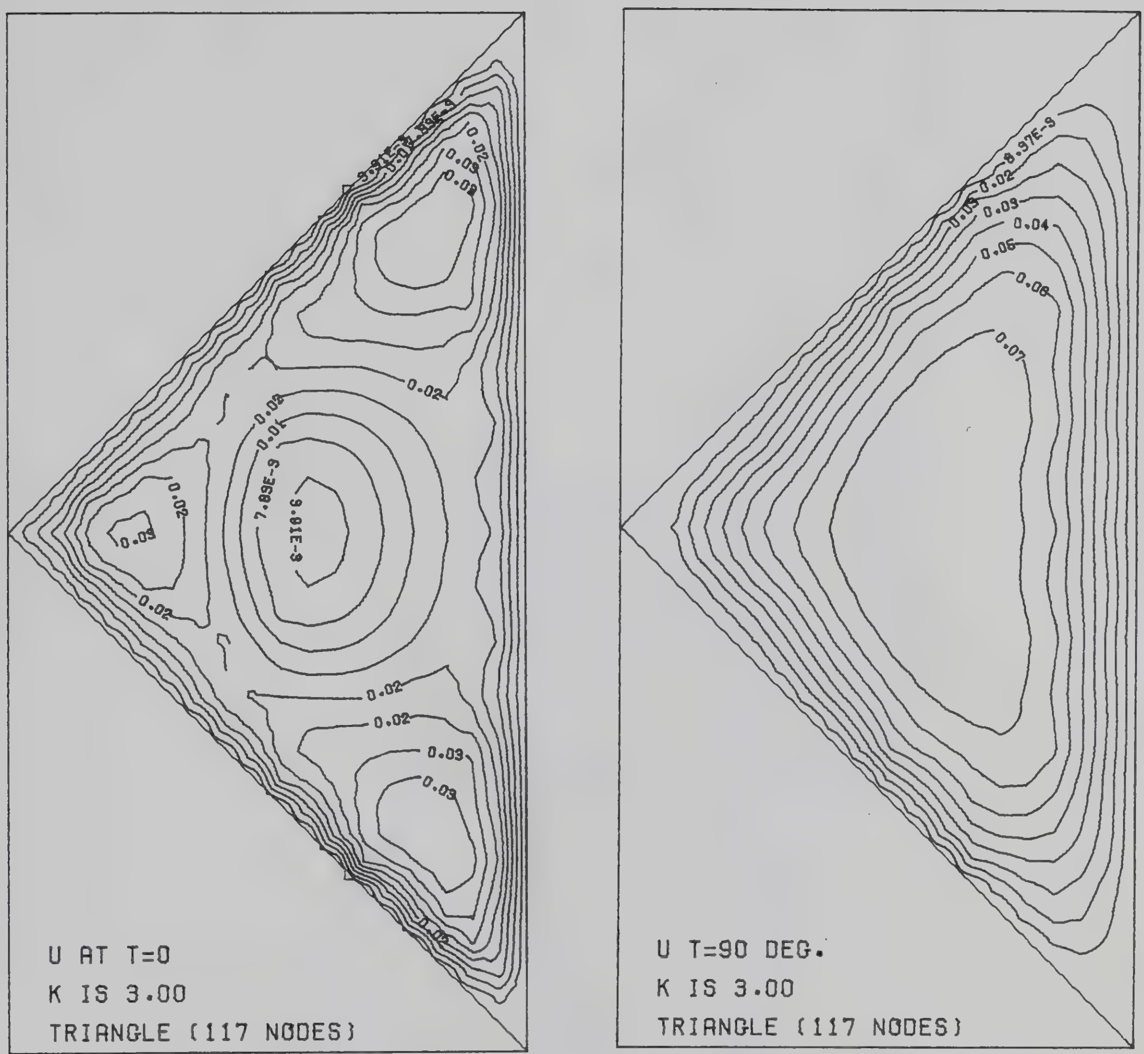

Figure 3.11 Contours of velocity in triangular pipe.

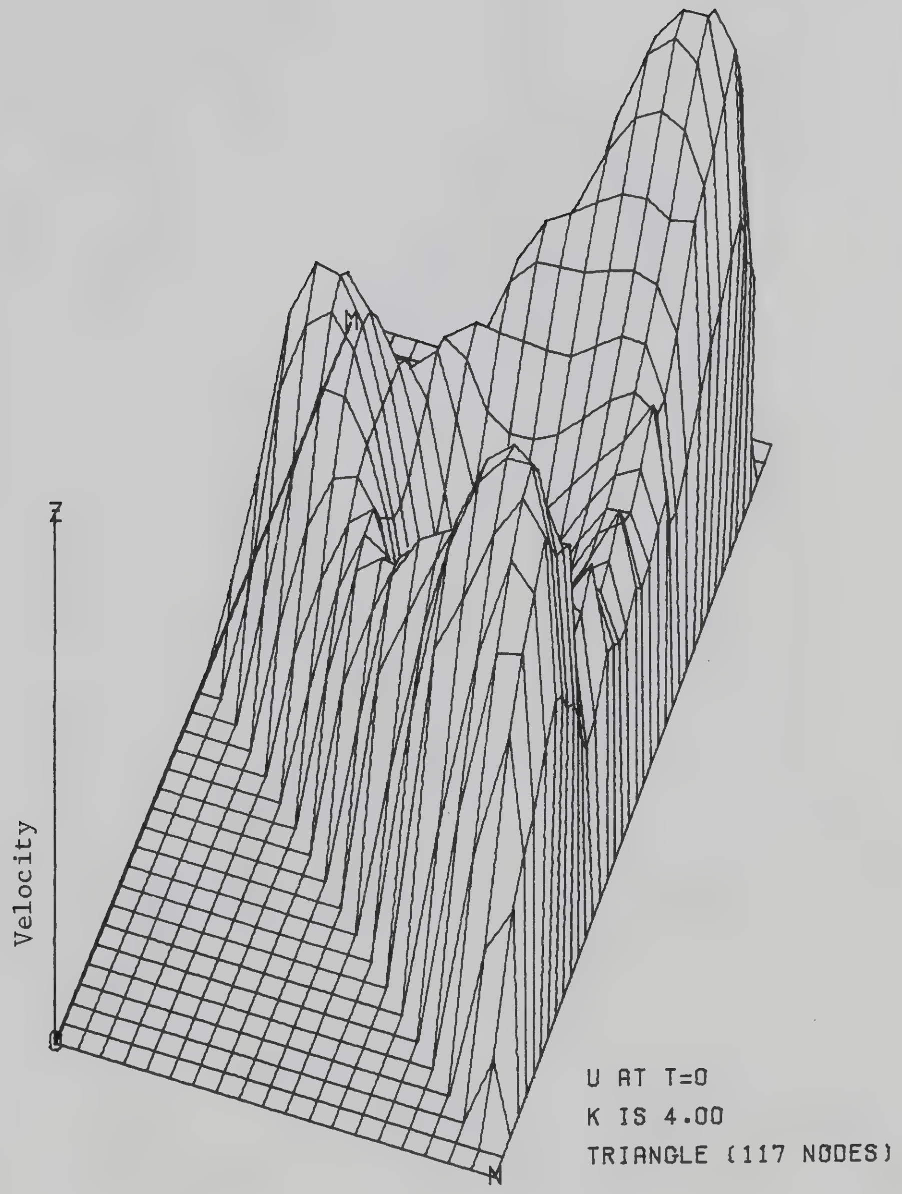

Figure 3.12 Velocity profile in triangular pipe.

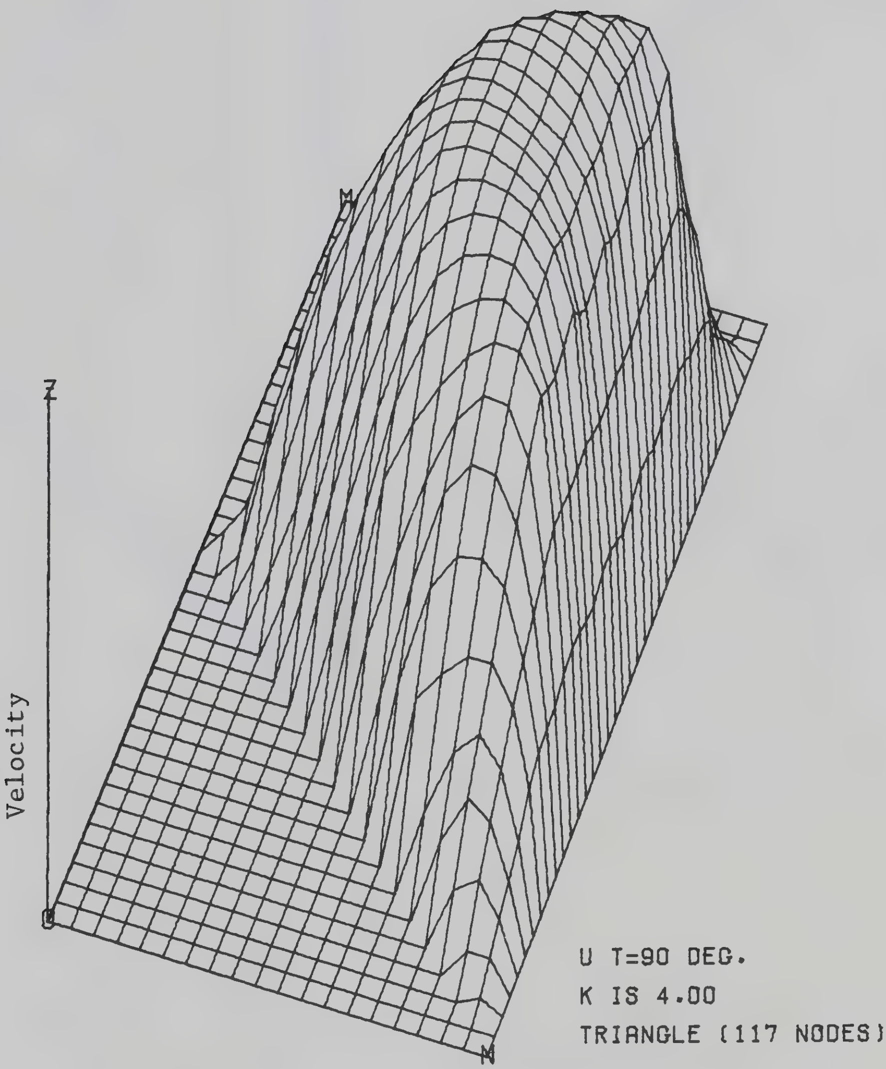

Figure 3.13 Velocity profile in triangular pipe.

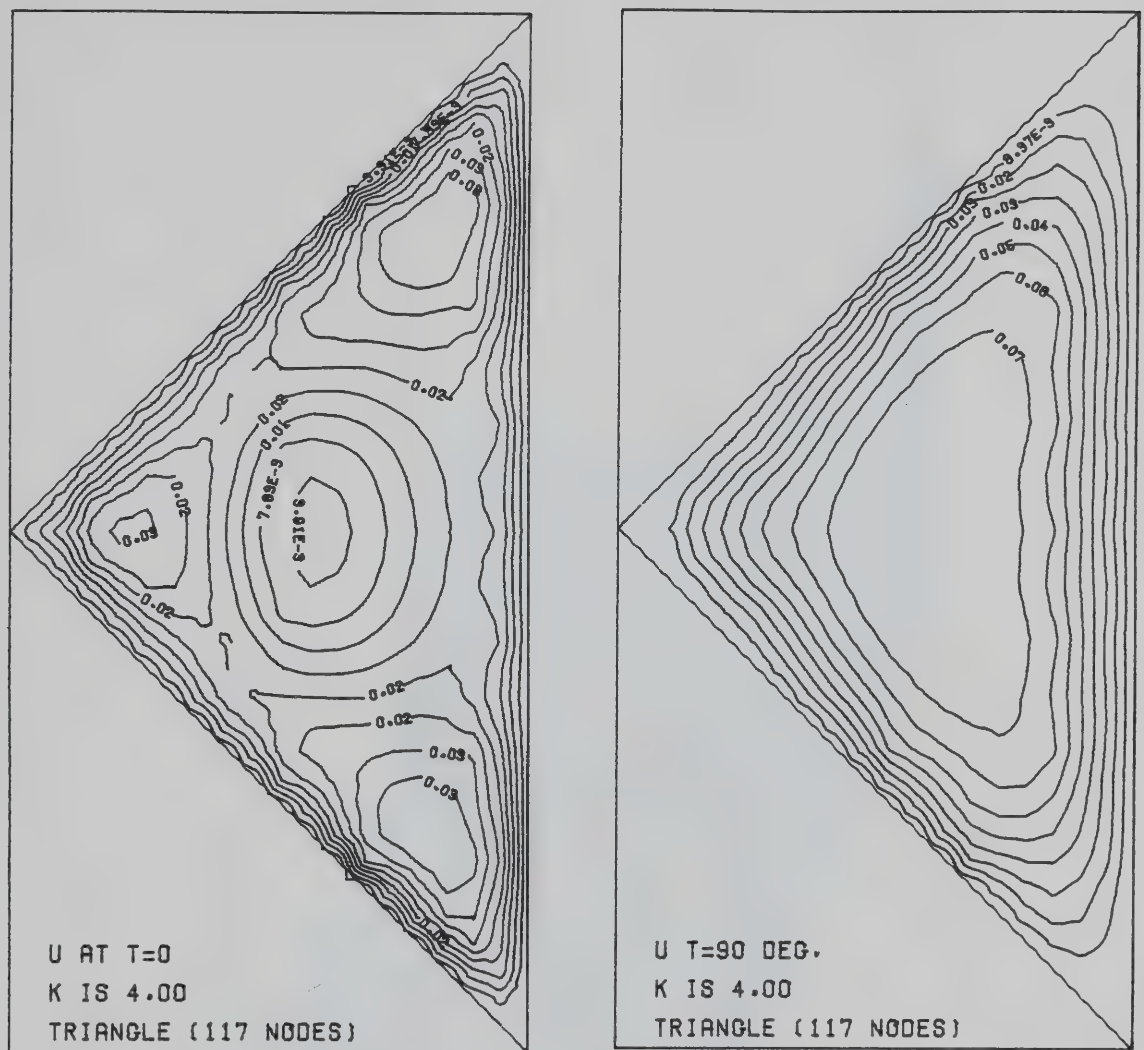

Figure 3.14 Contours of velocity in triangular pipe.

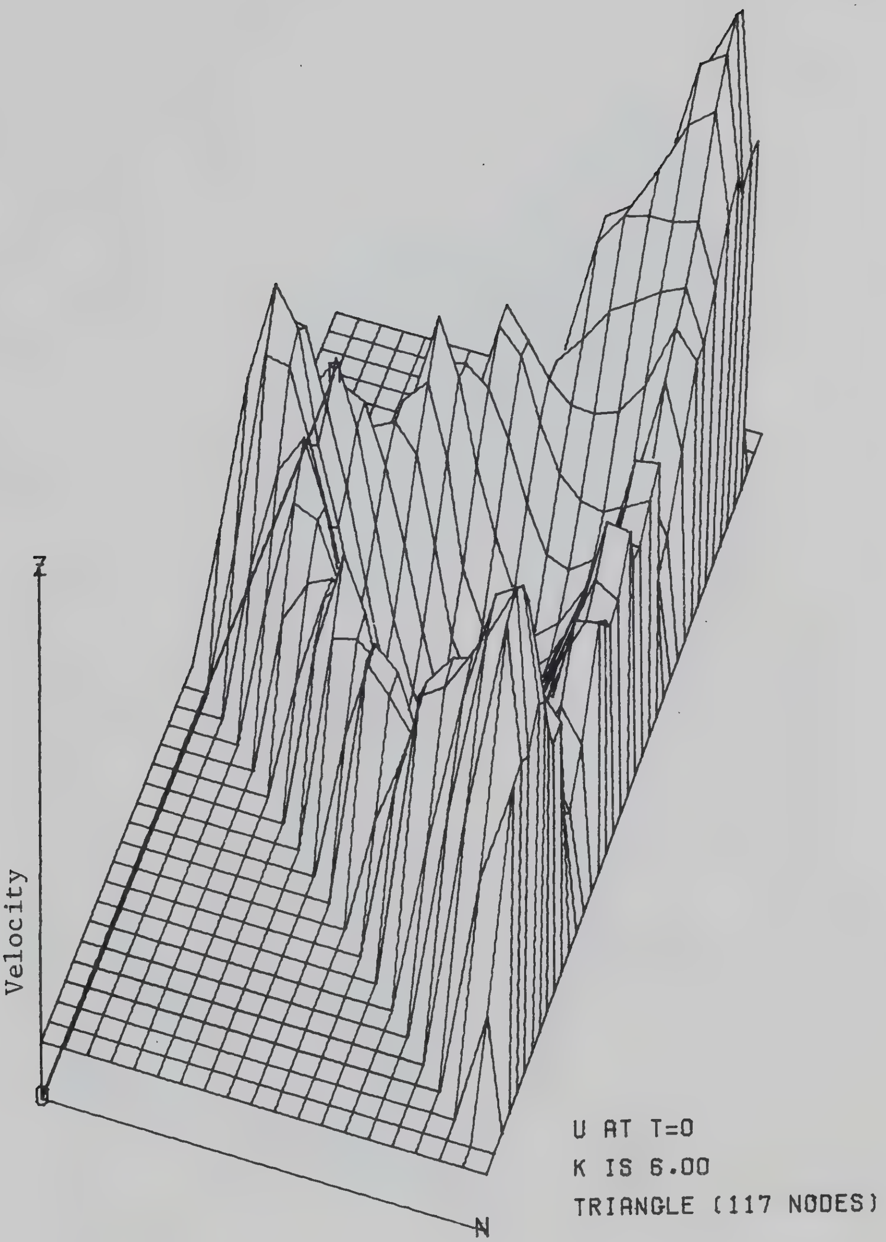

Figure 3.15 Velocity profile in triangular pipe.

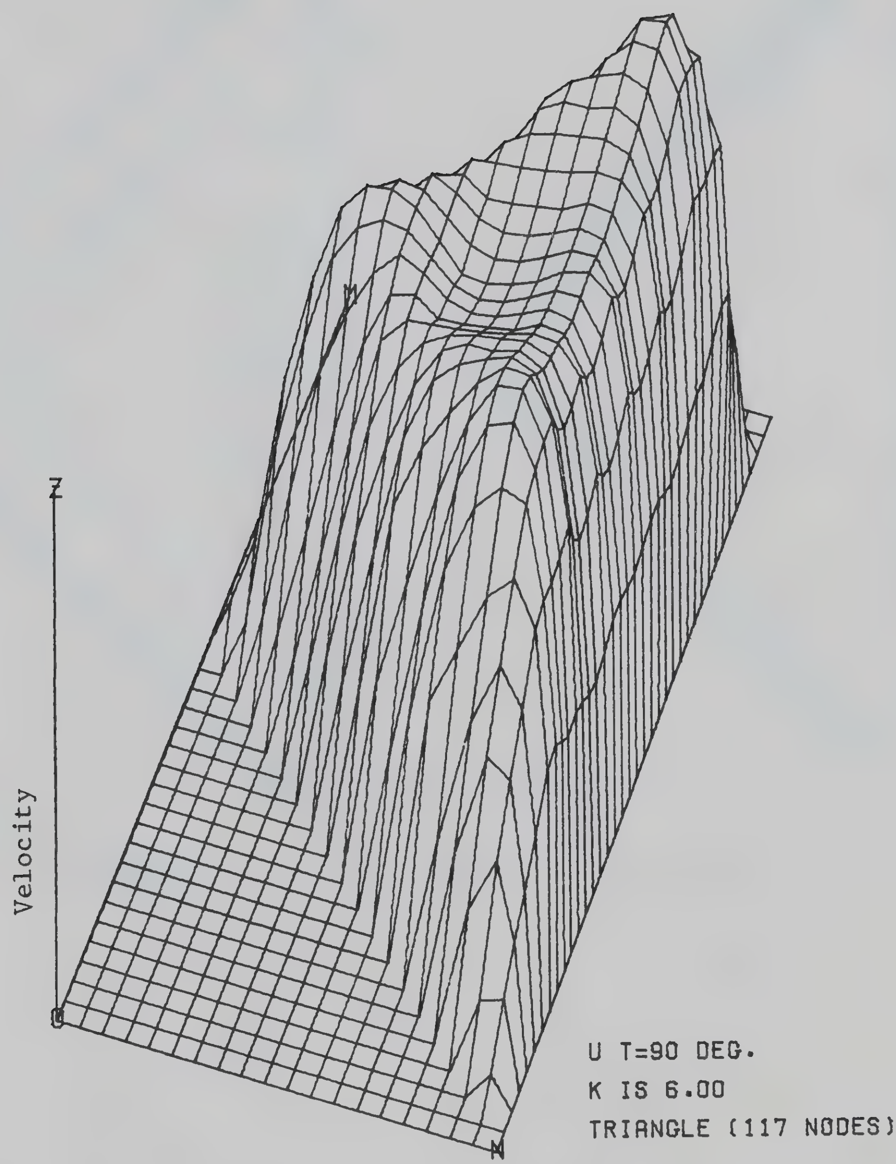

Figure 3.16 Velocity profile in triangular pipe.

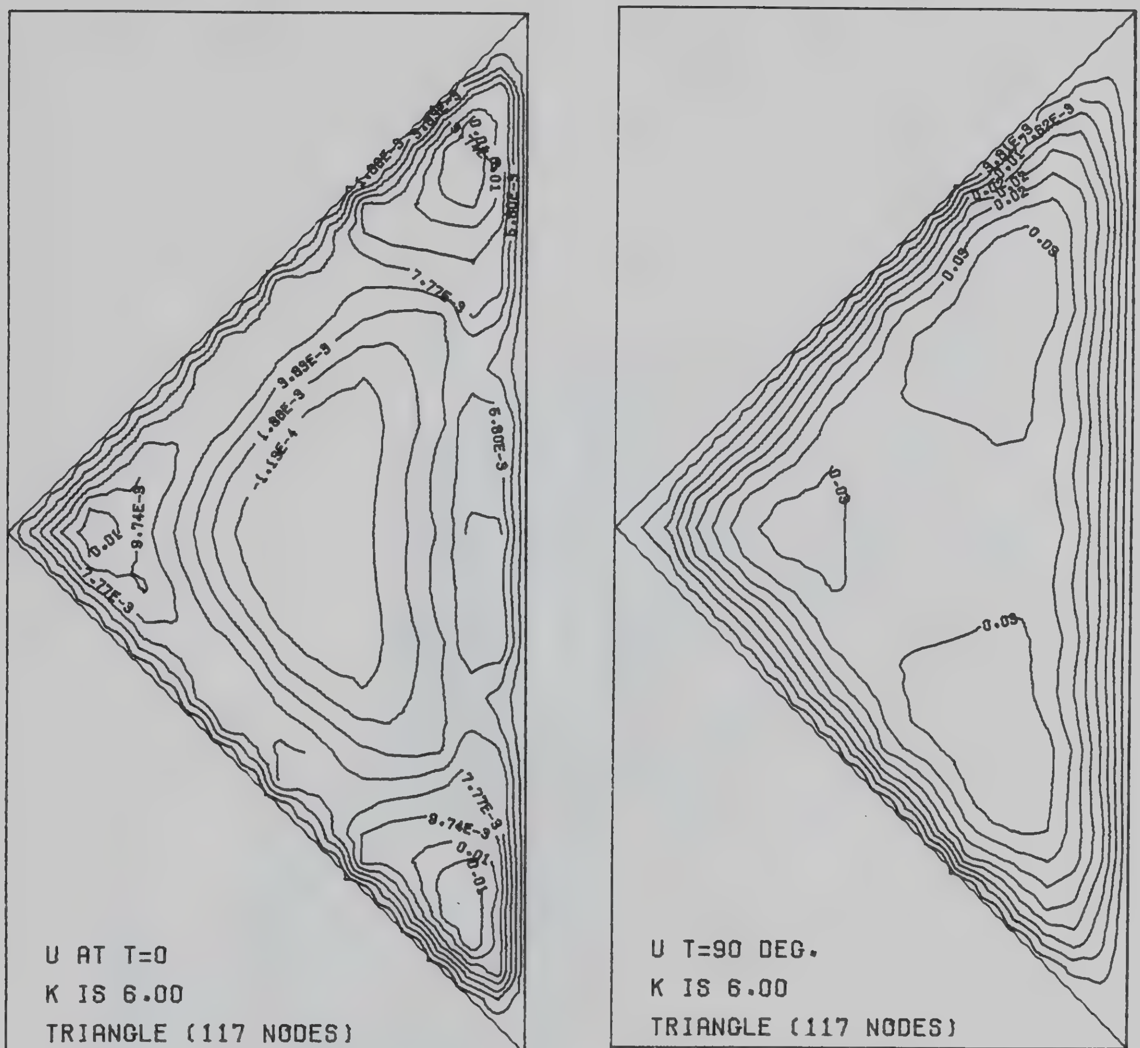

Figure 3.17 Contours of velocity in triangular pipe.

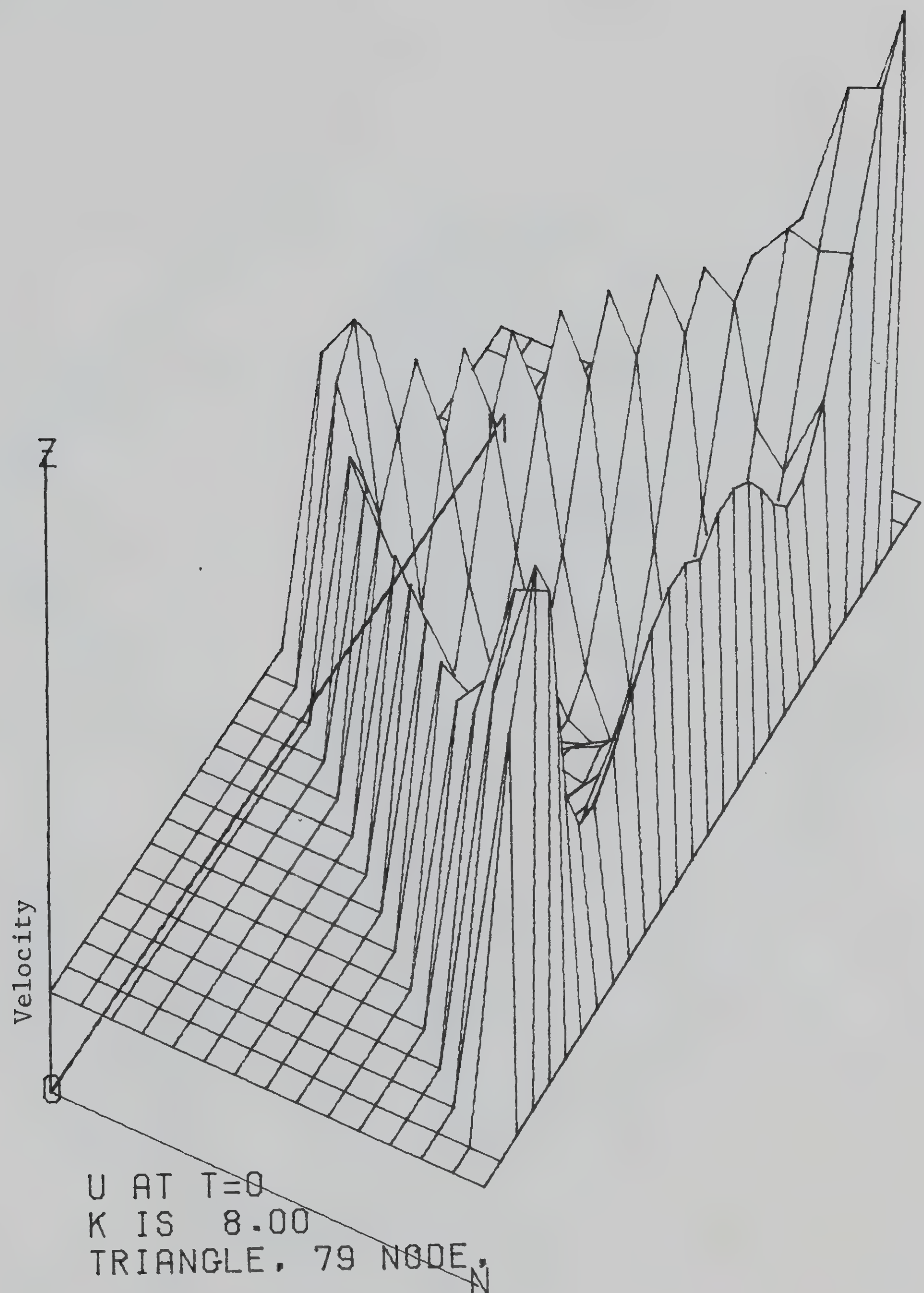

Figure 3.18 Velocity profile in triangular pipe.

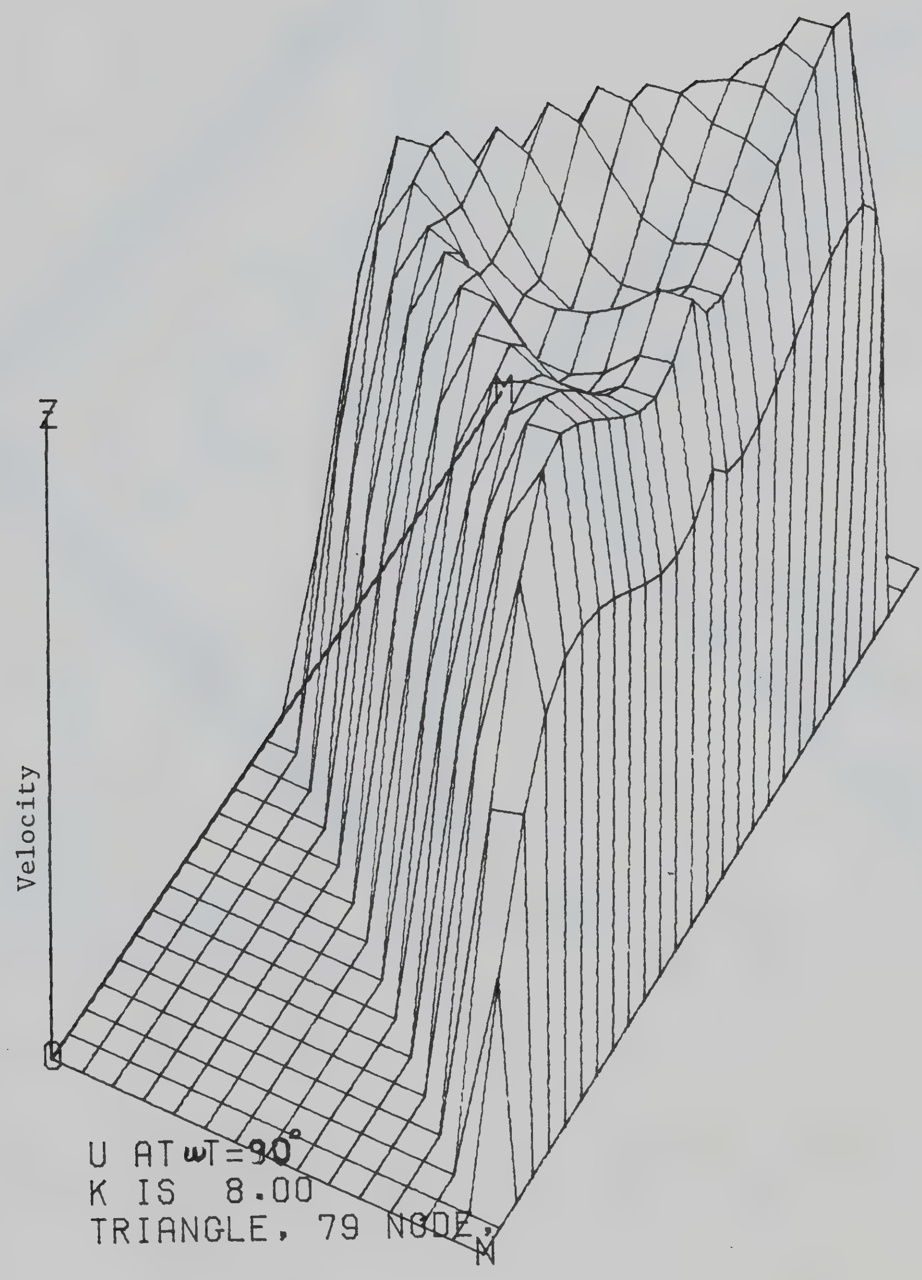

Figure 3.19 Velocity profile in triangular pipe.

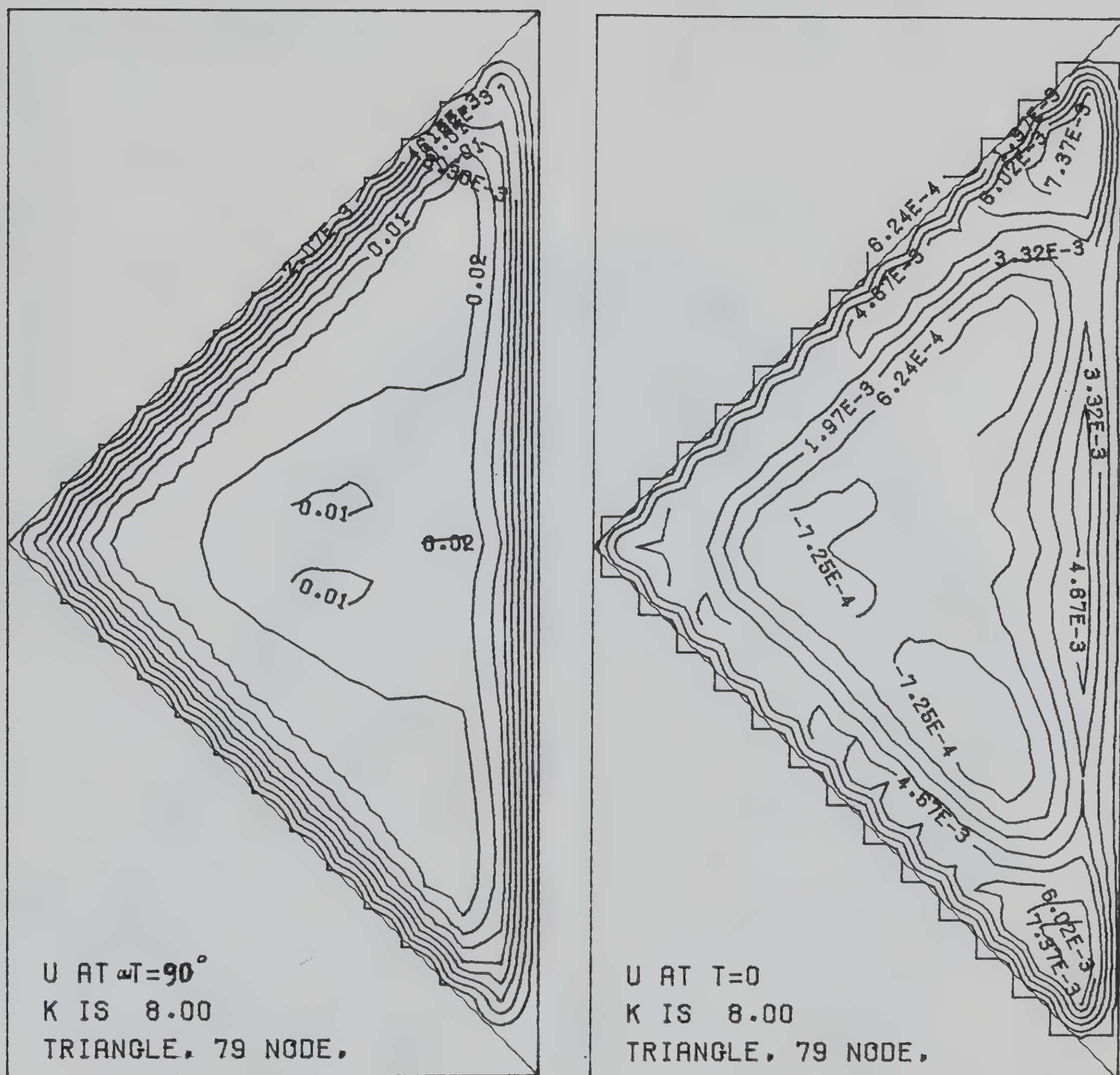

Figure 3.20 Contours of velocity in triangular pipe.

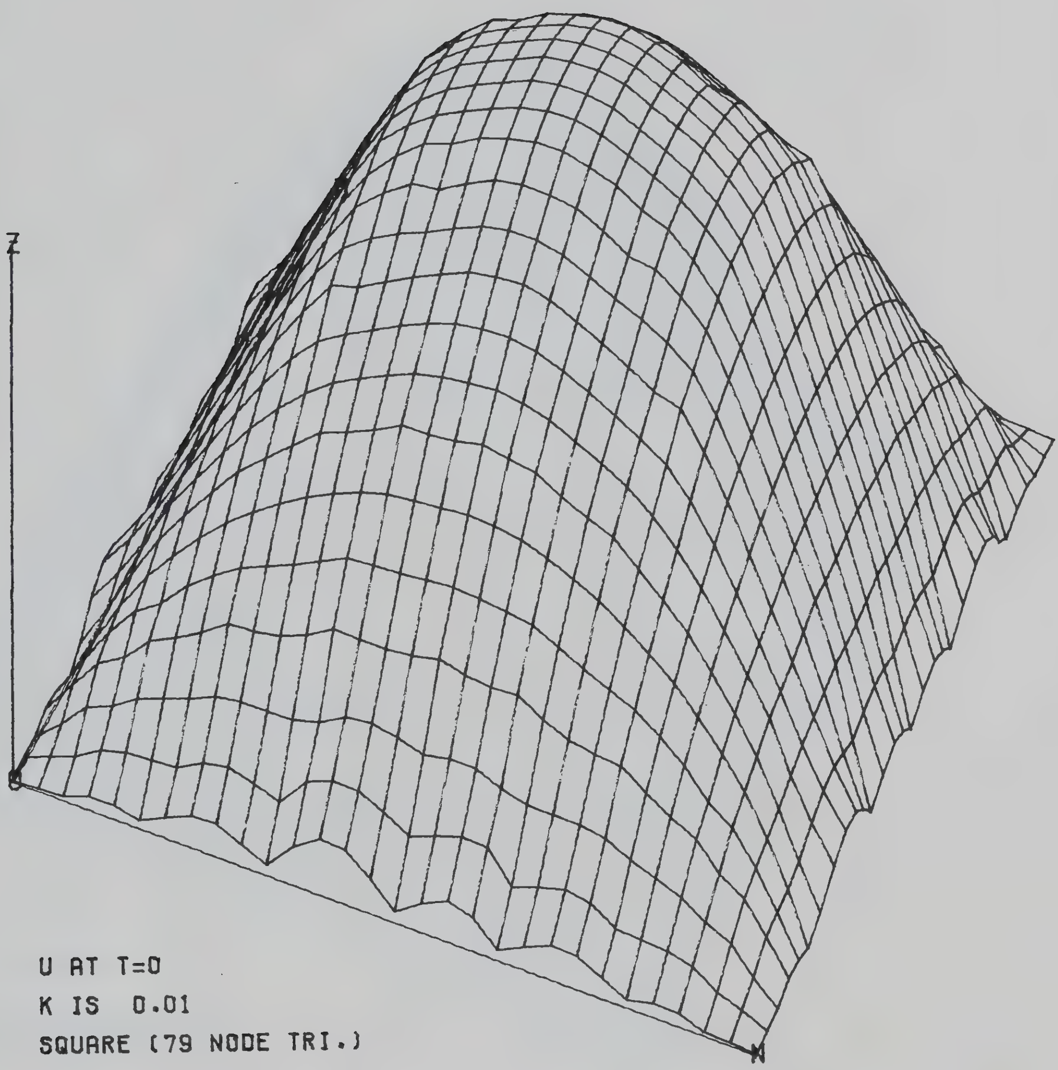

Figure 3.21 Velocity profile in square pipe.

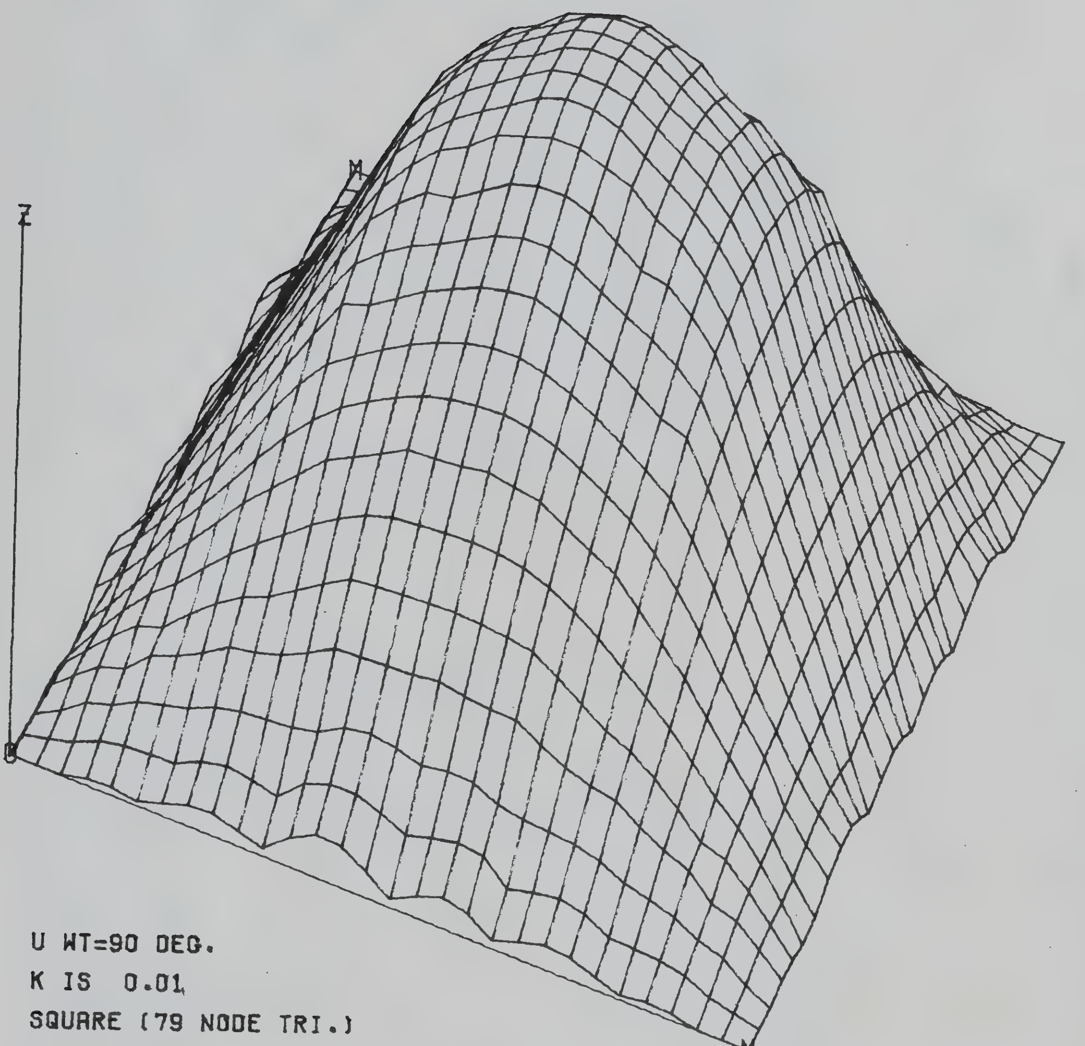

Figure 3.22 Velocity profile in square pipe.

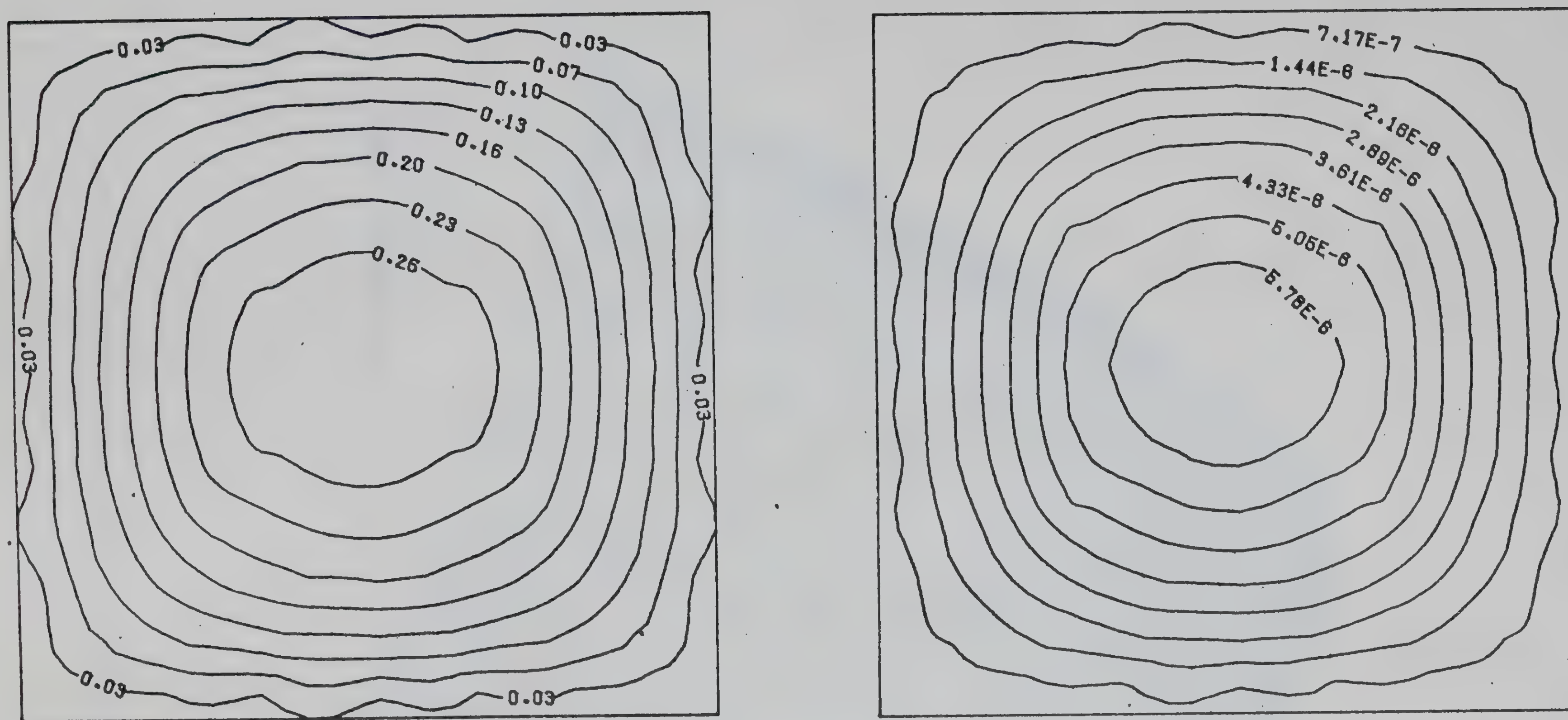

(a) U at t=0
K = 0.01

(b) U at ωt = 90°
K = 0.01

Figure 3.23 Contours of velocity in square pipe.

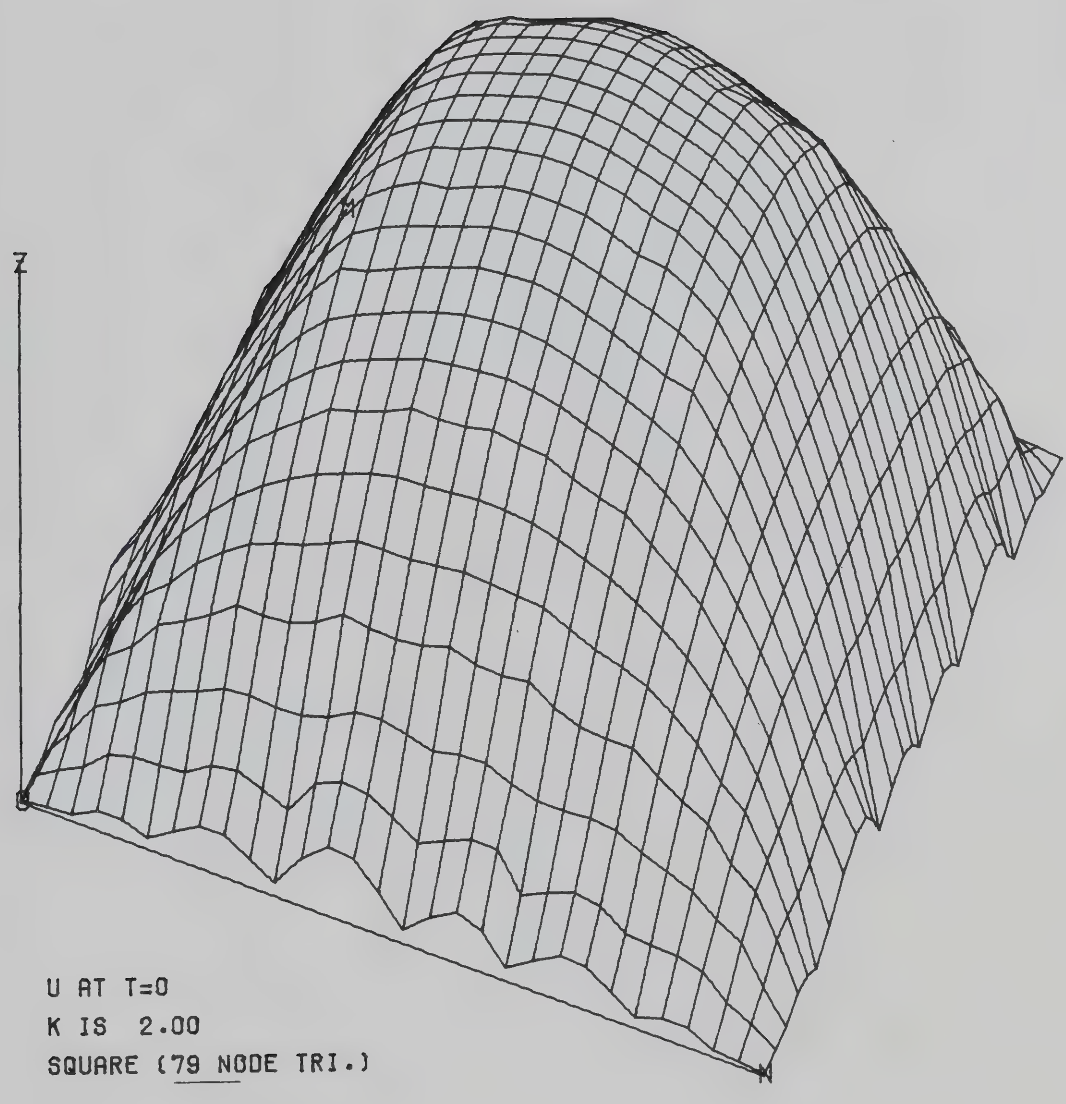

Figure 3.24 Velocity profile in square pipe.

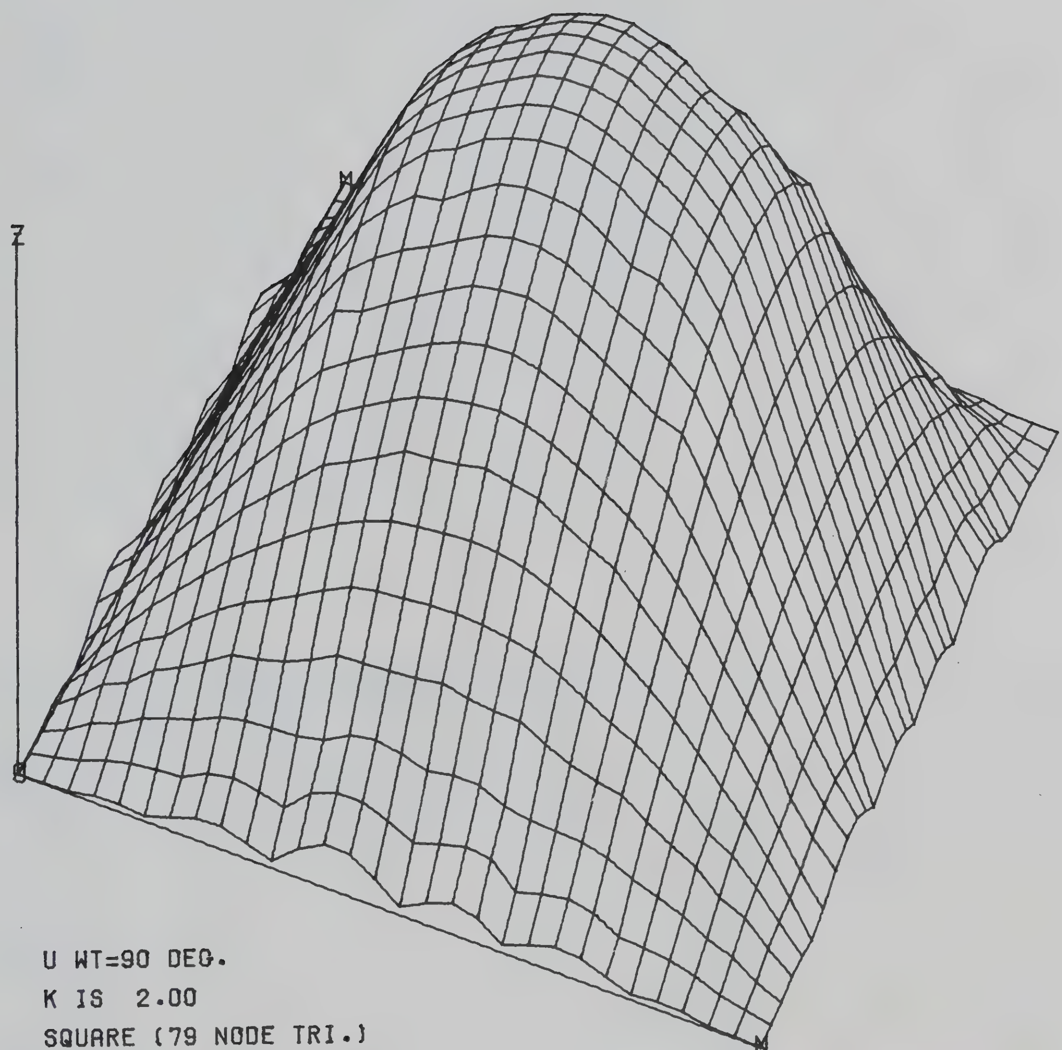

Figure 3.25 Velocity profile in square pipe.

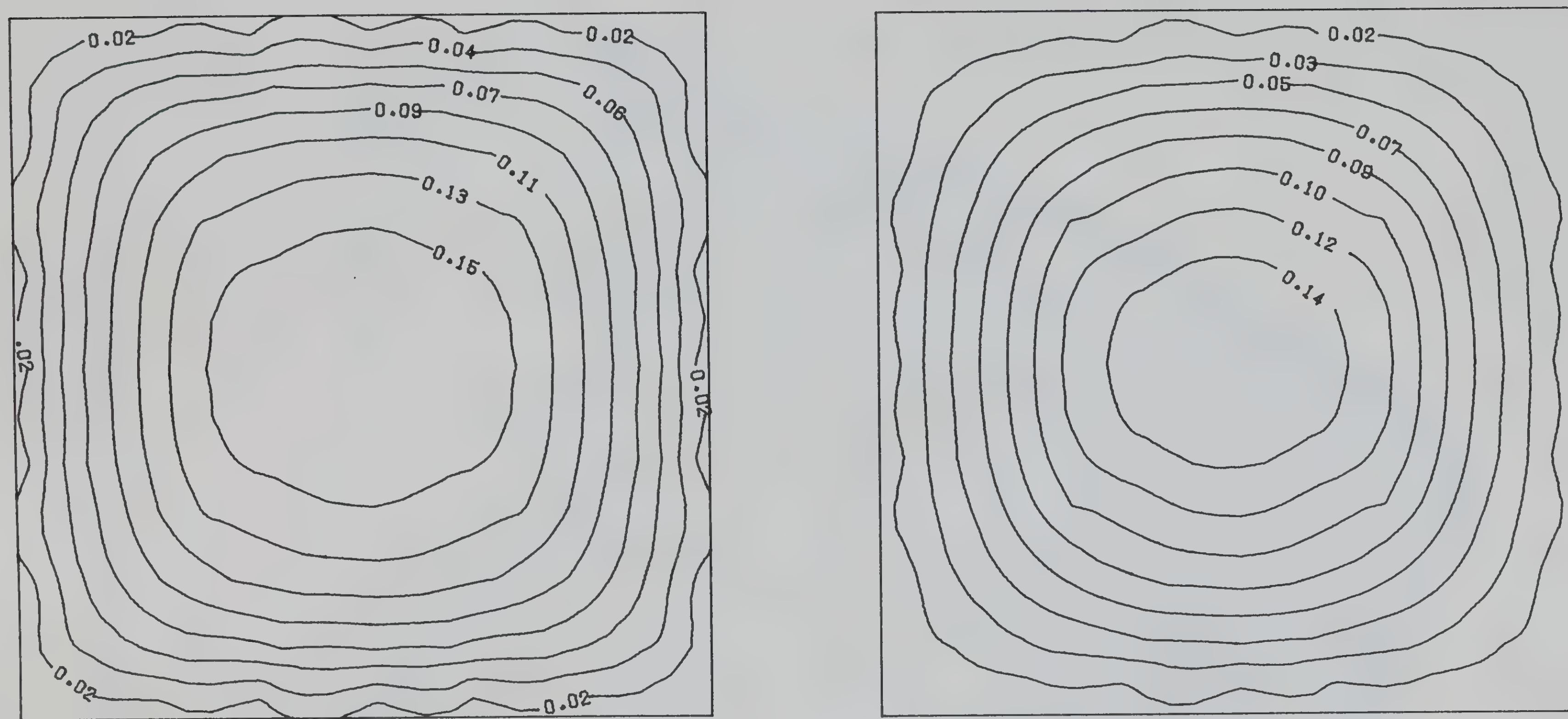

(a) U at t = 0
K = 2

(b) U at ωt = 90°
K = 2

Figure 3.26 Contours of velocity in square pipe.

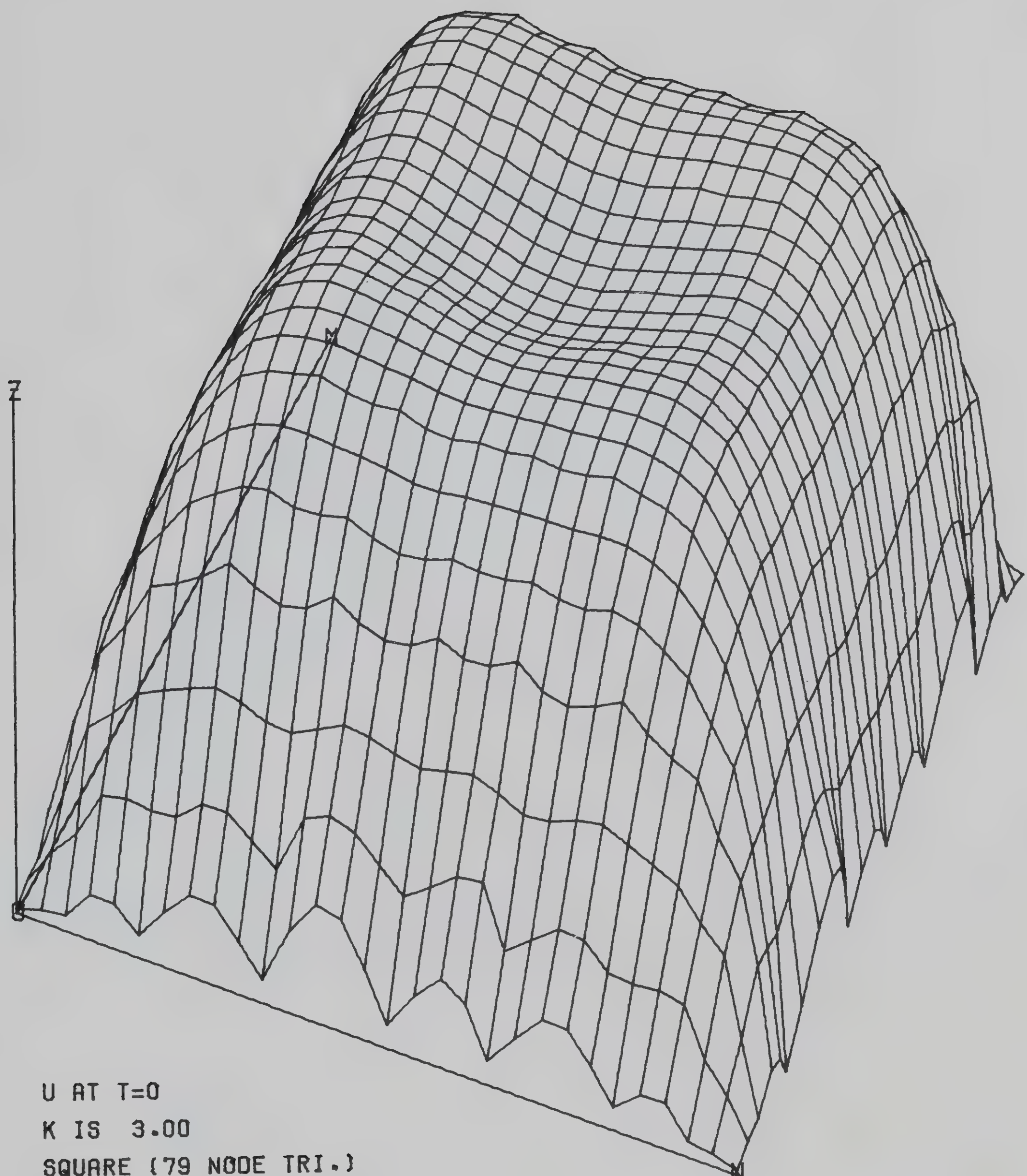

Figure 3.27 Velocity profile in square pipe.

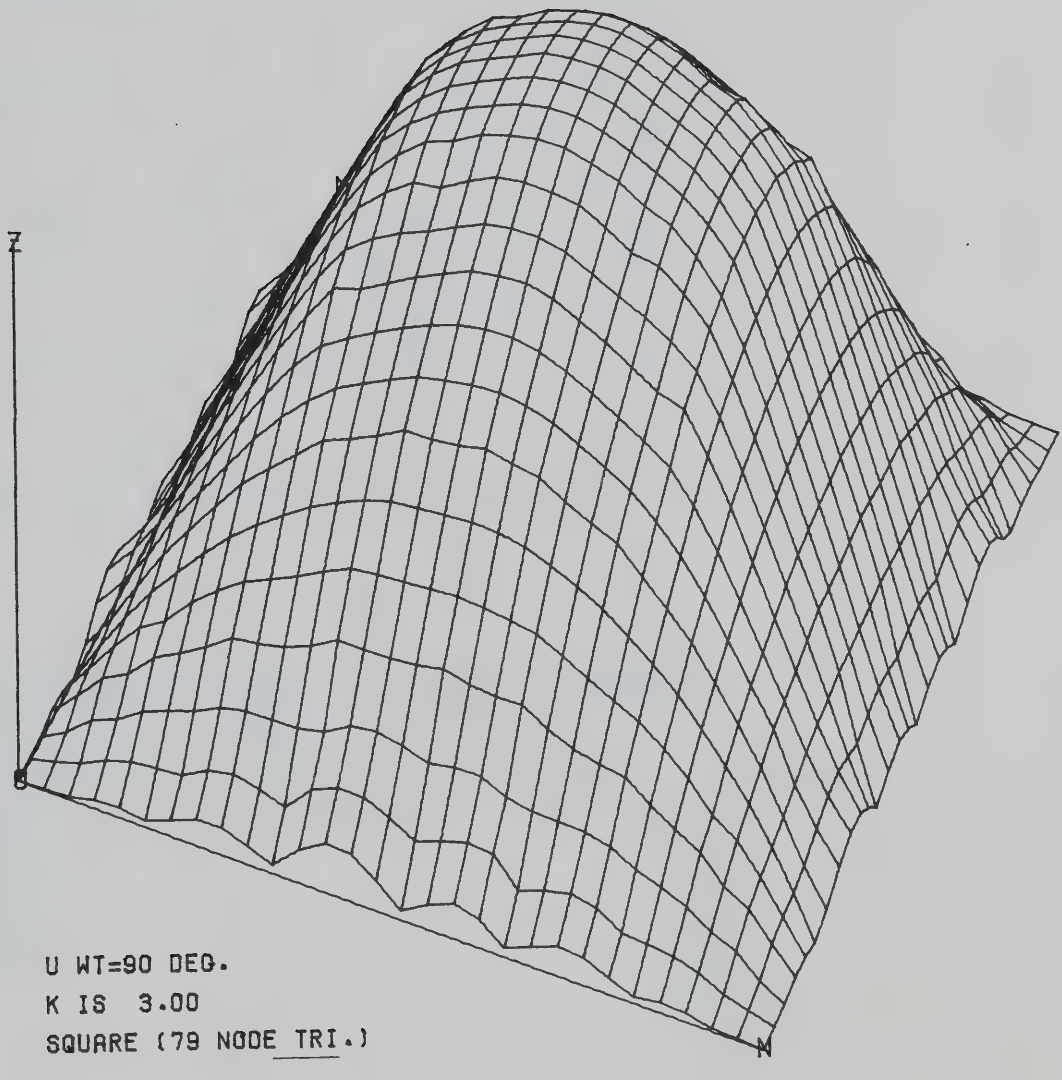

Figure 3.28 Velocity profile in square pipe.

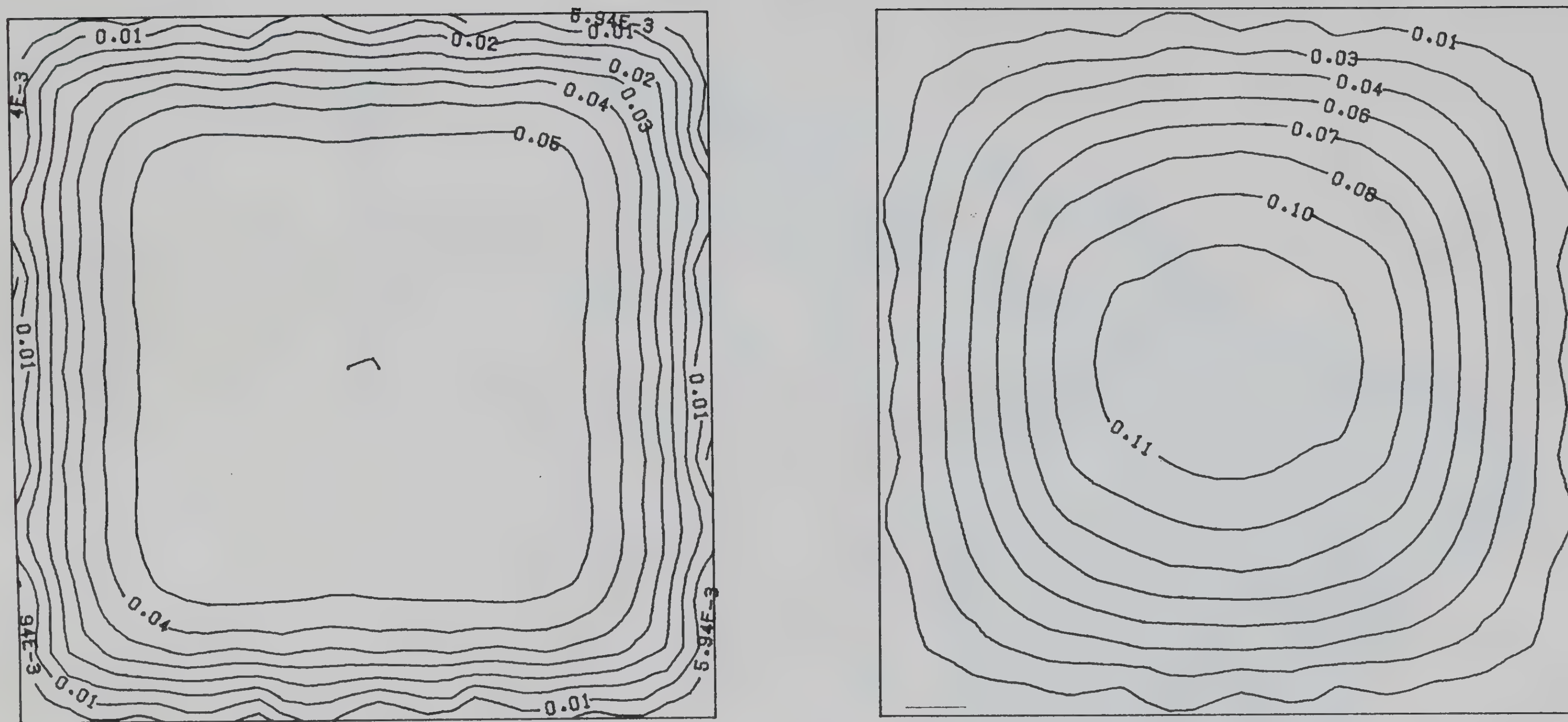

(a) U at t= 0
K = 3

(b) U at ωt = 90°
K = 3

Figure 3.29 Contours of velocity in square pipe.

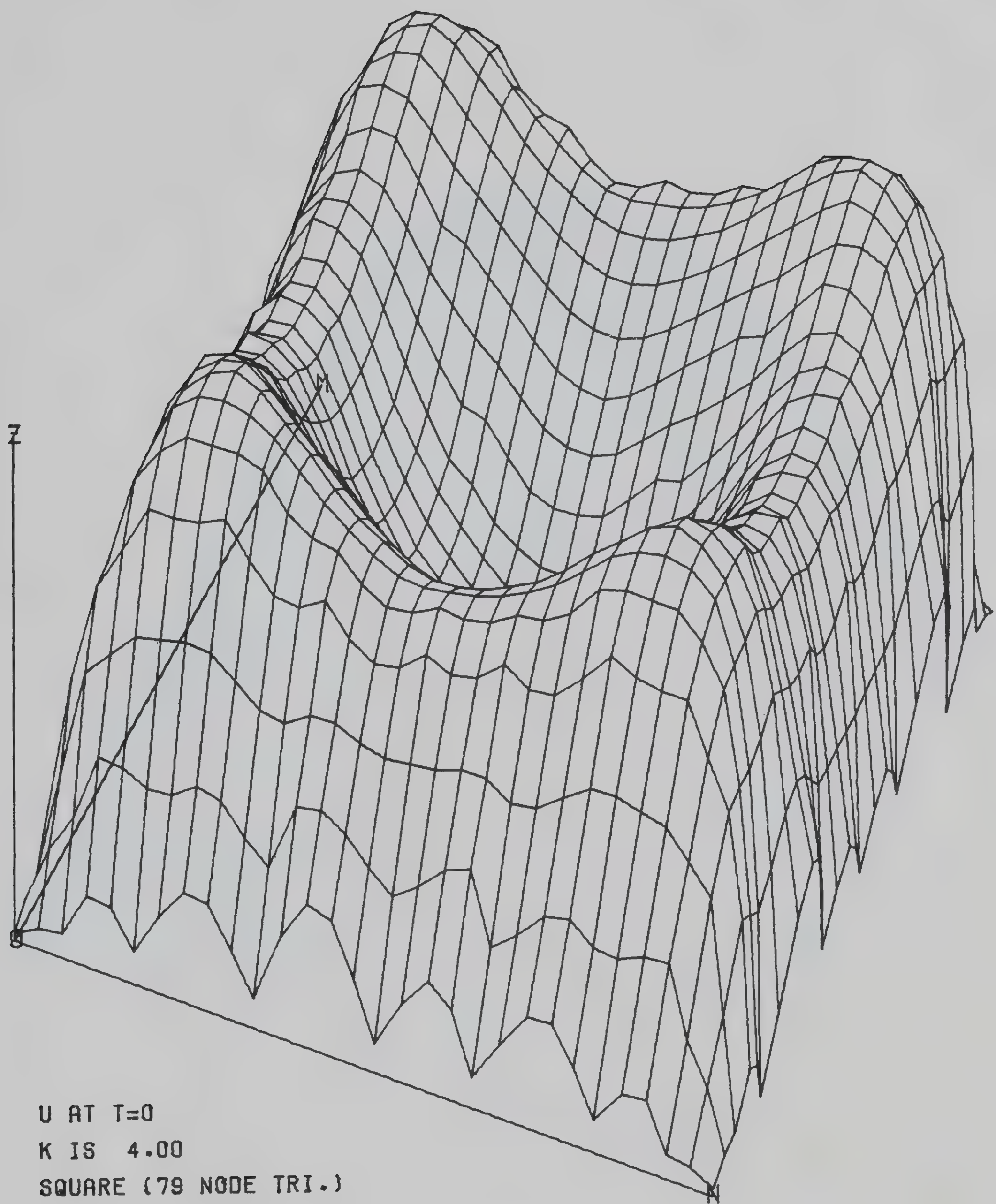

Figure 3.30 Velocity profile in square pipe.

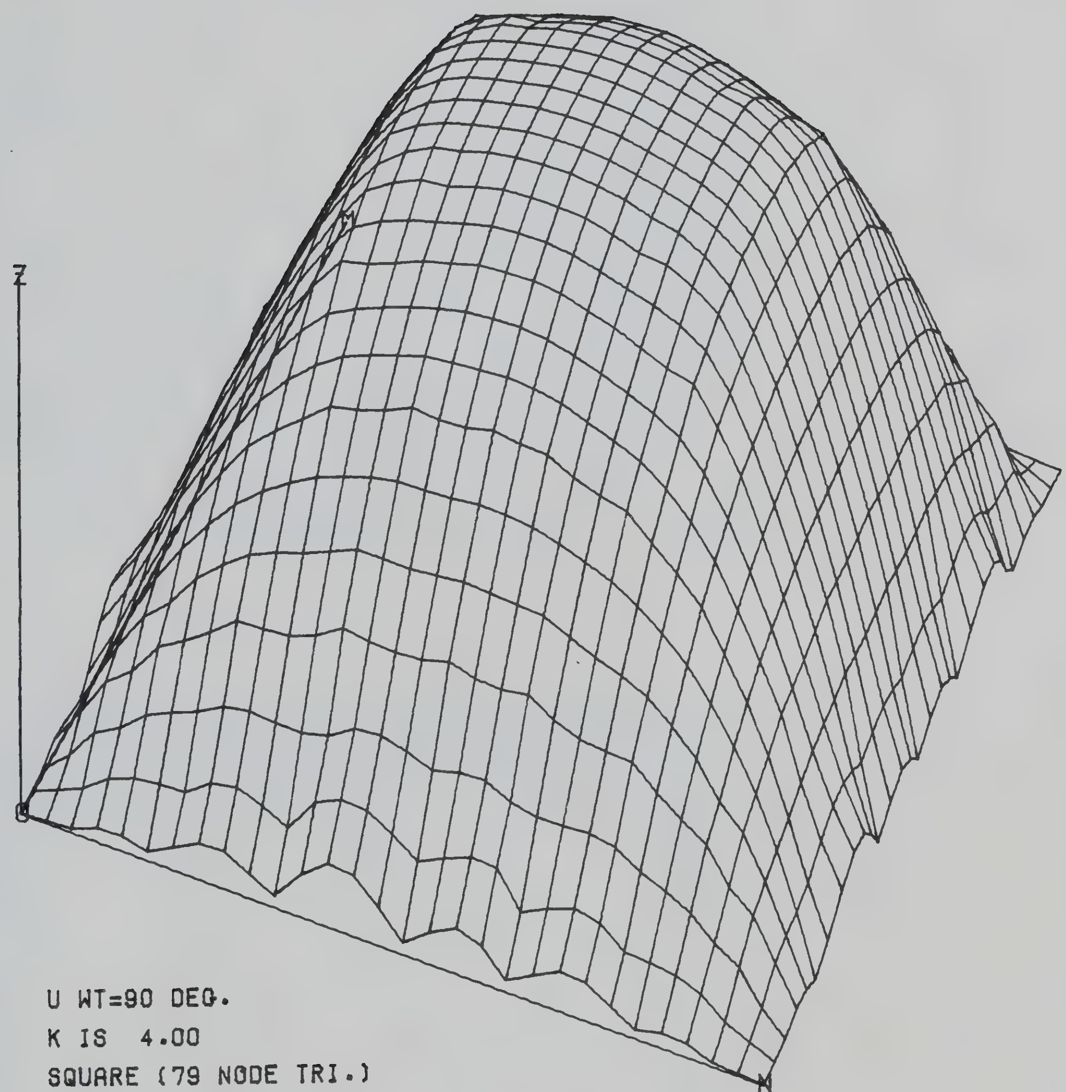

Figure 3.31 Velocity profile in square pipe.

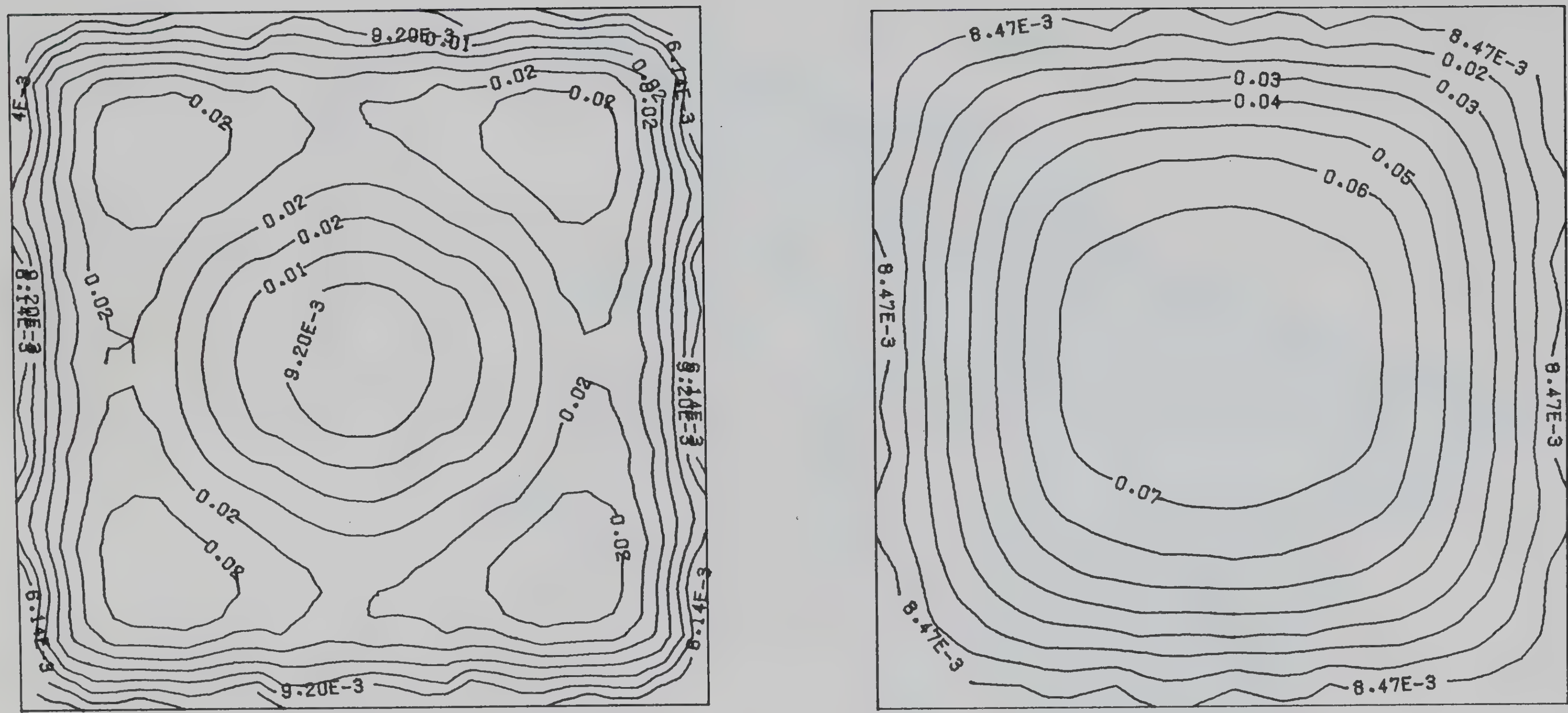

(a) U at t = 0
K = 4

(b) U at ωt = 90°
K = 4

Figure 3.32 Contours of velocity in square pipe.

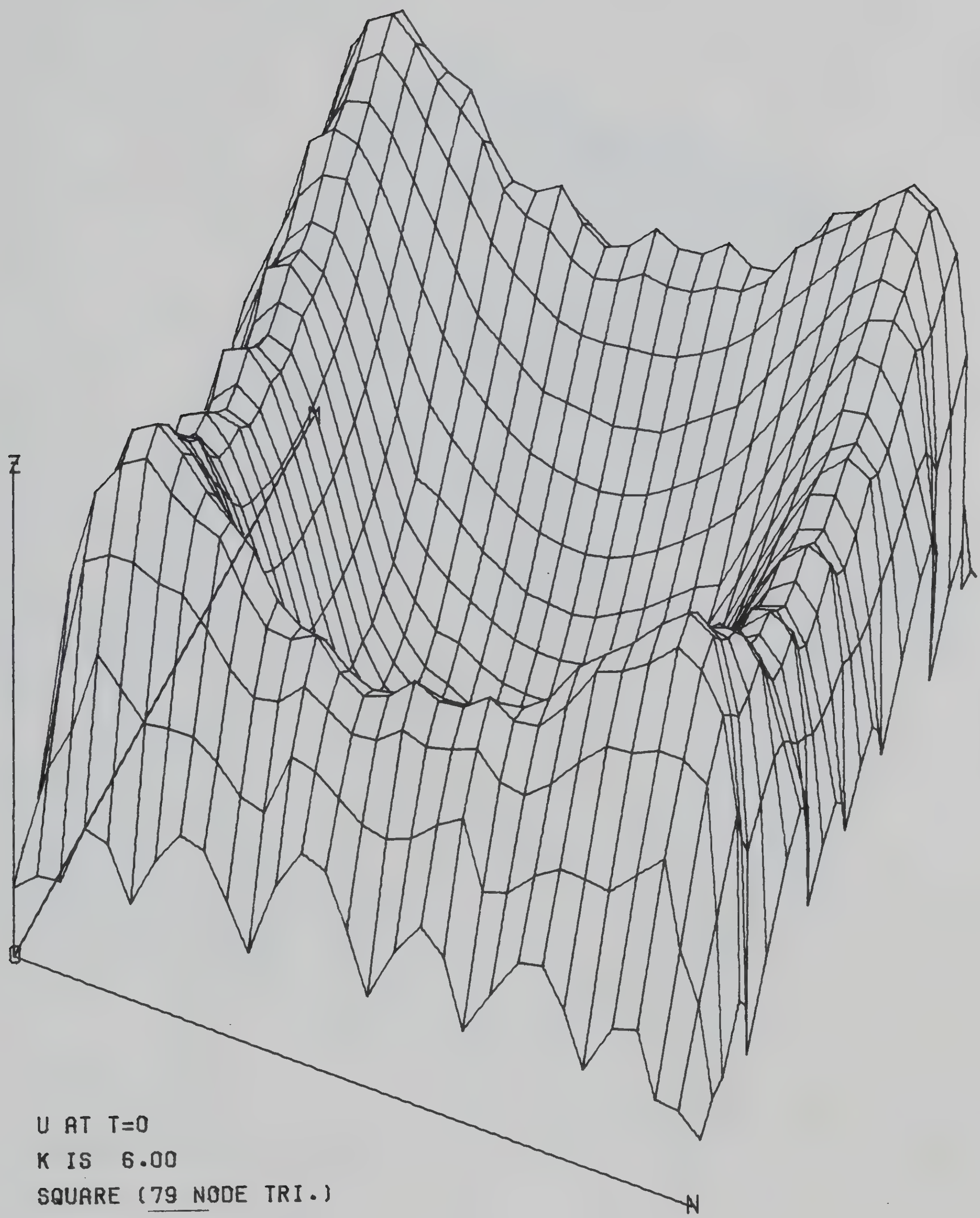

Figure 3.33 Velocity profile in square pipe.

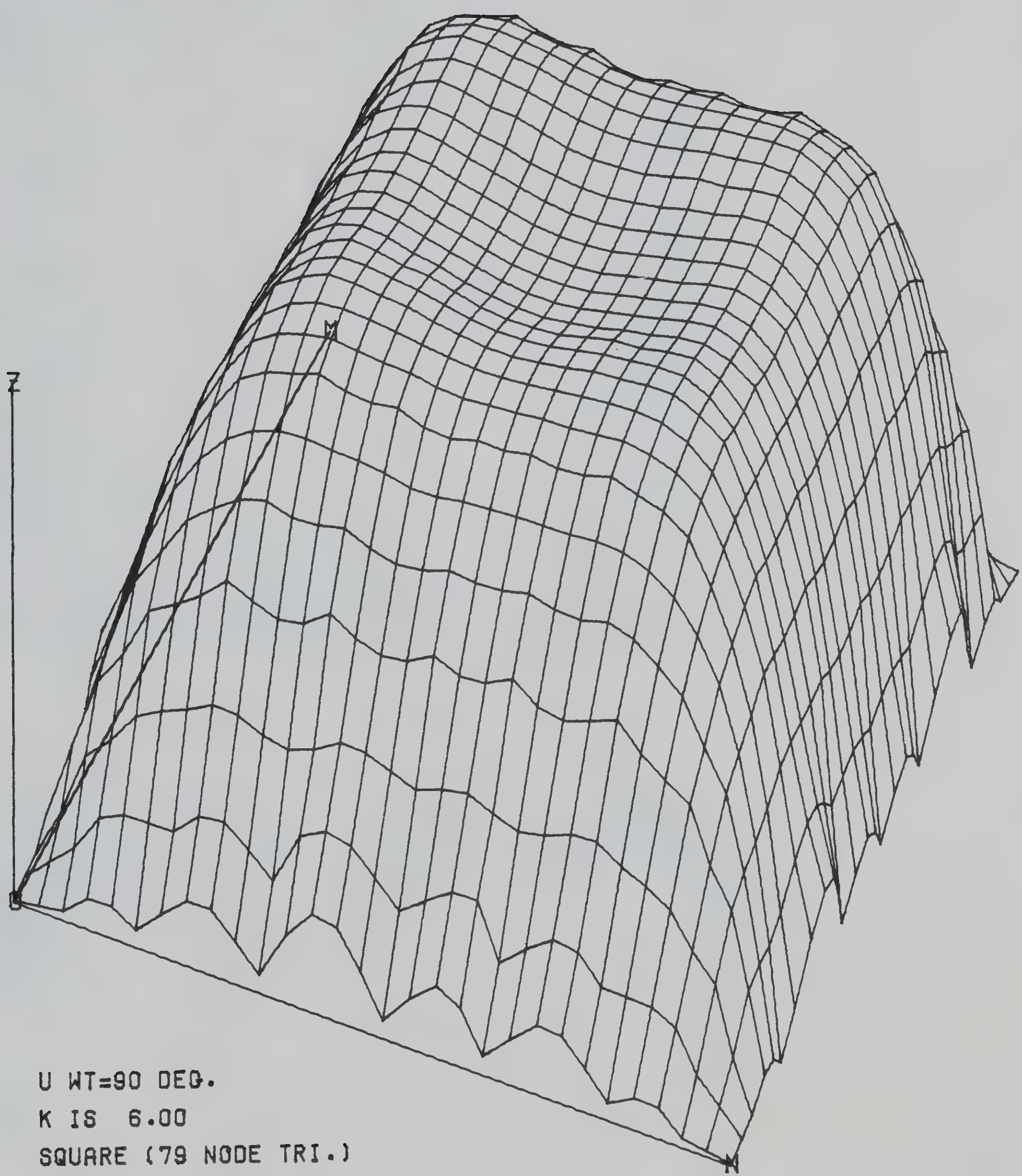

Figure 3.34 Velocity profile in square pipe.

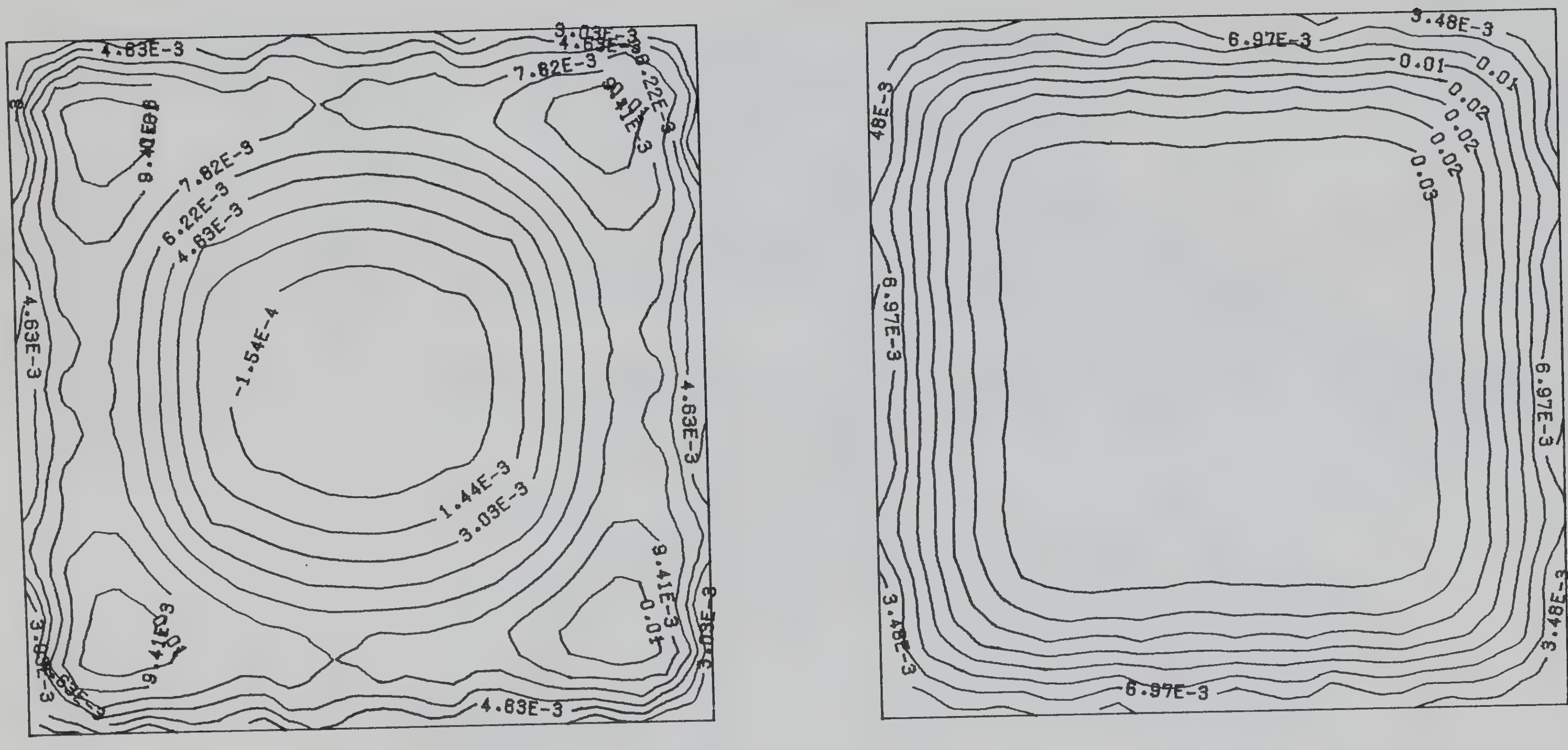

(a) U at t = 0
K = 6

(b) U at $\omega t = 90°$
K = 6

Figure 3.35 Contours of velocity in square pipe.

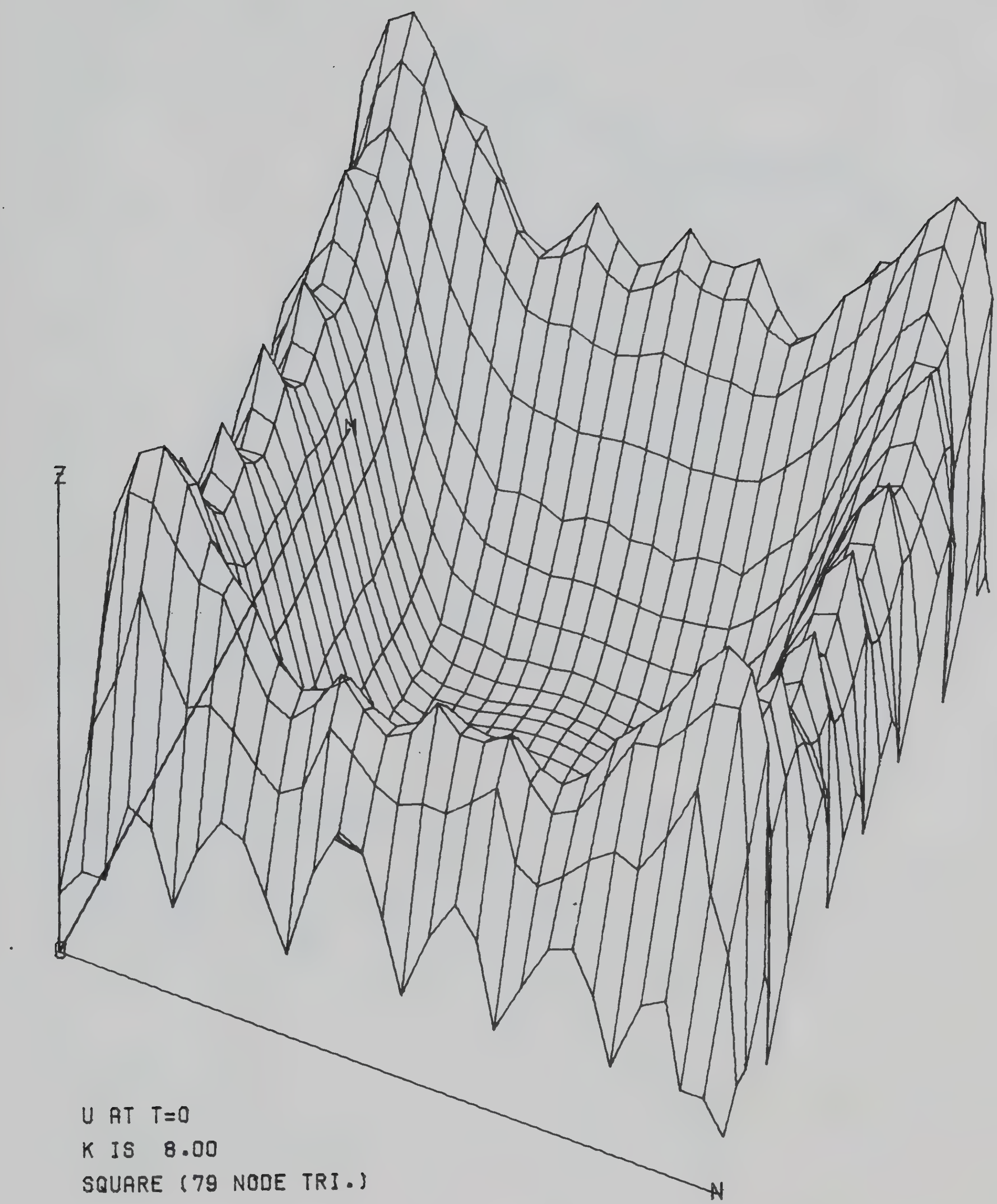

Figure 3.36 Velocity profile in square pipe.

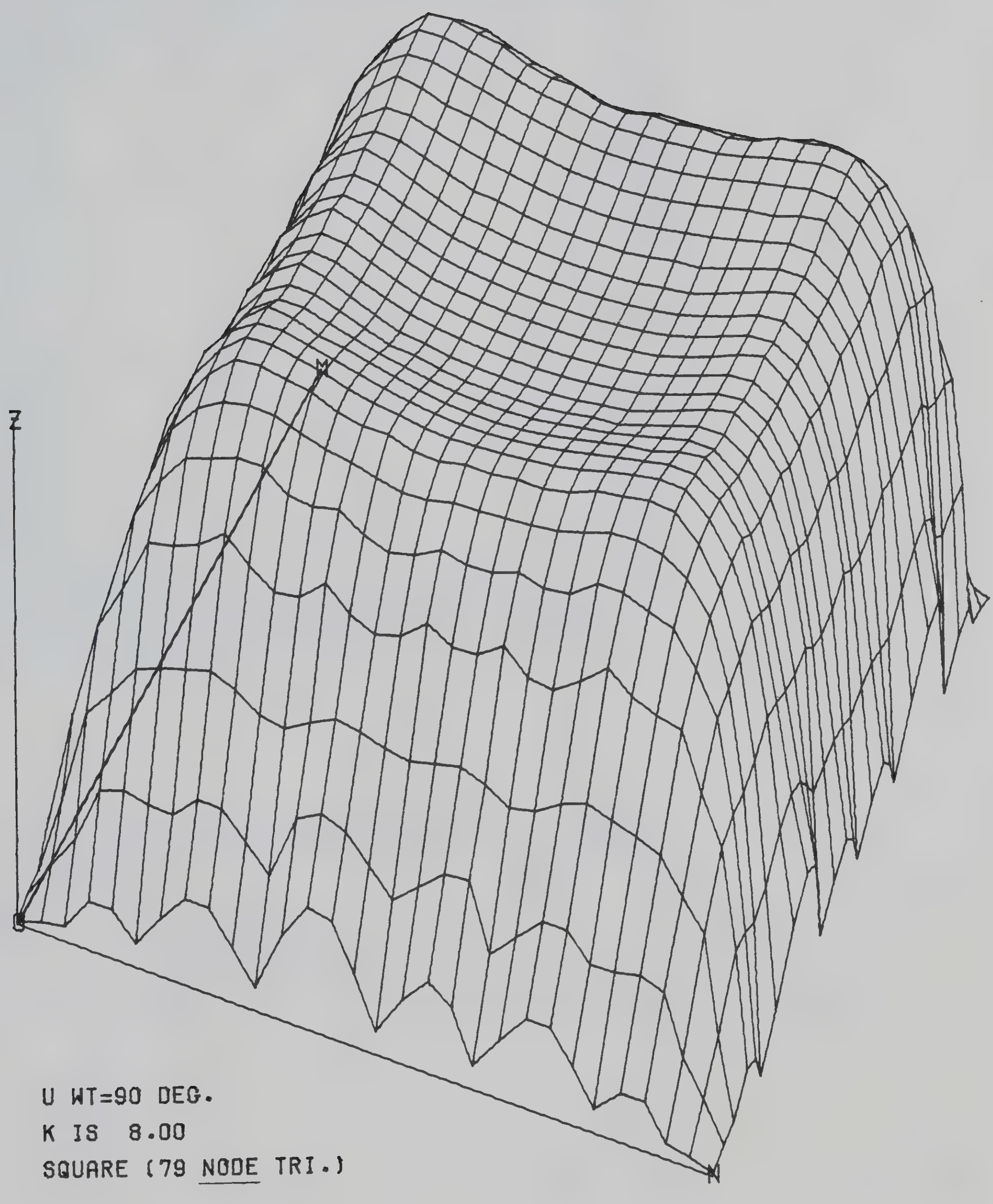

Figure 3.37 Velocity profile in square pipe.

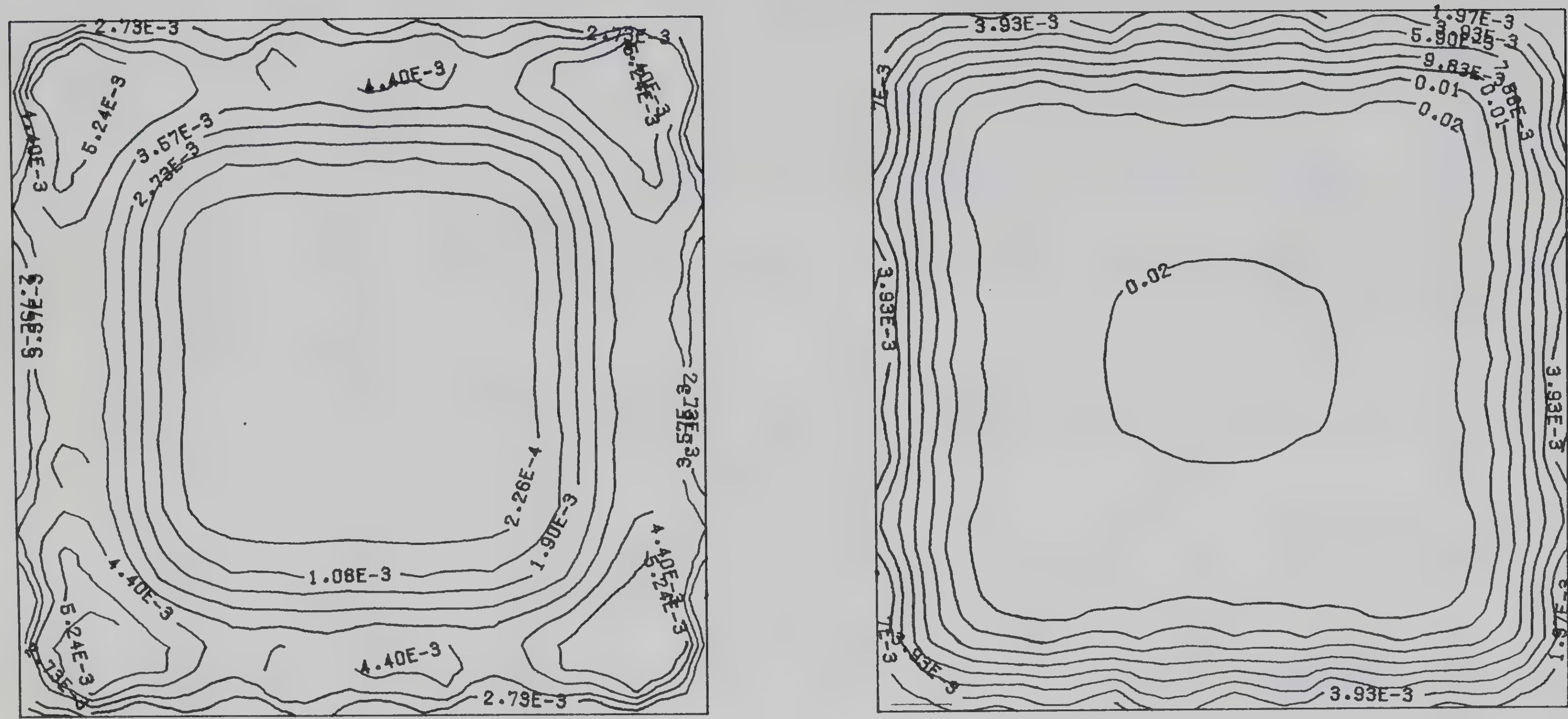

(a) U at t = 0
K = 8

(b) U at ωt = 90°
K = 8

Figure 3.38 Contours of velocity in square pipe.

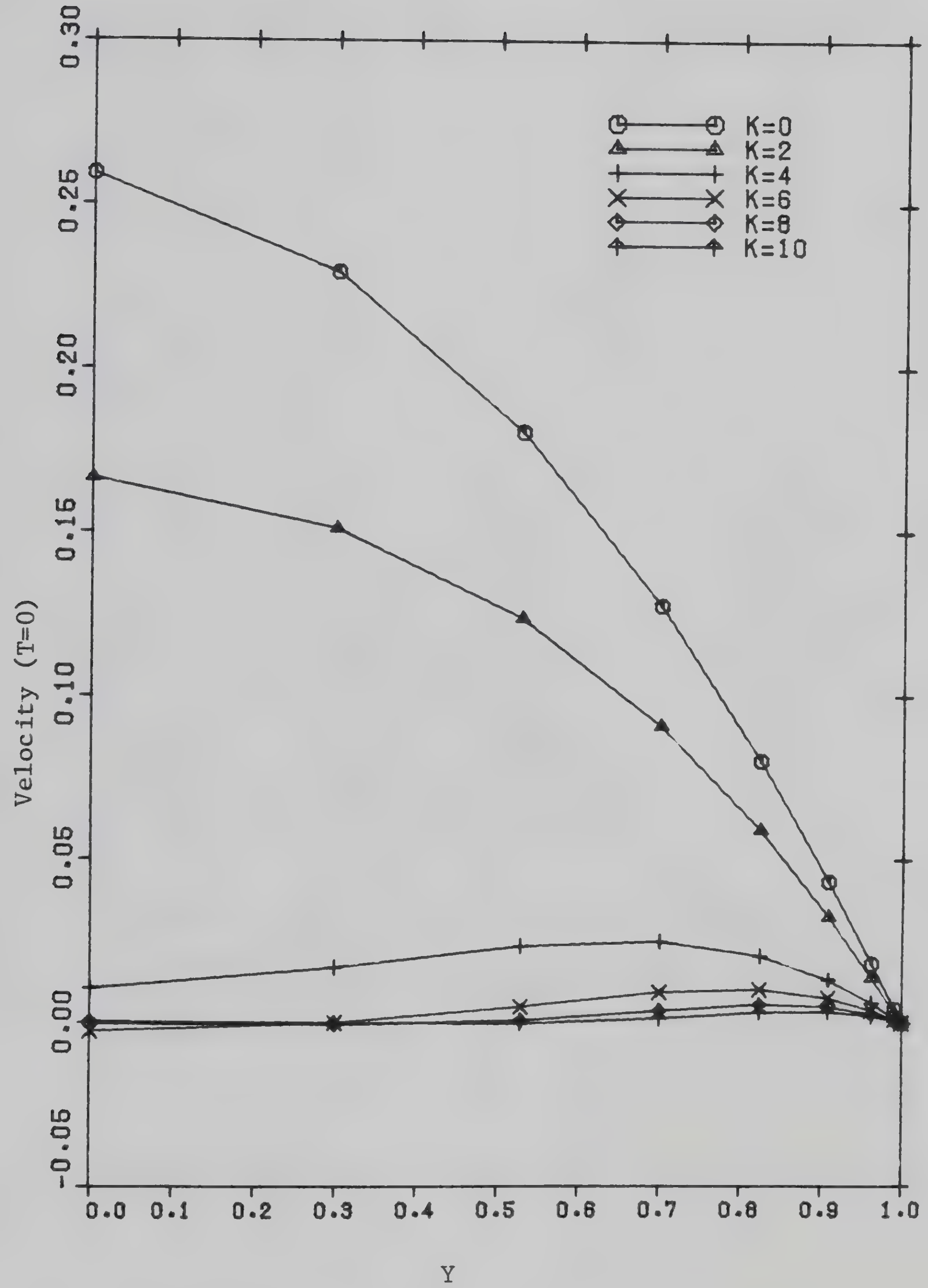

Figure 3.39 Circular pipe velocity profile at t=0 for various K. Pressure gradient held constant.

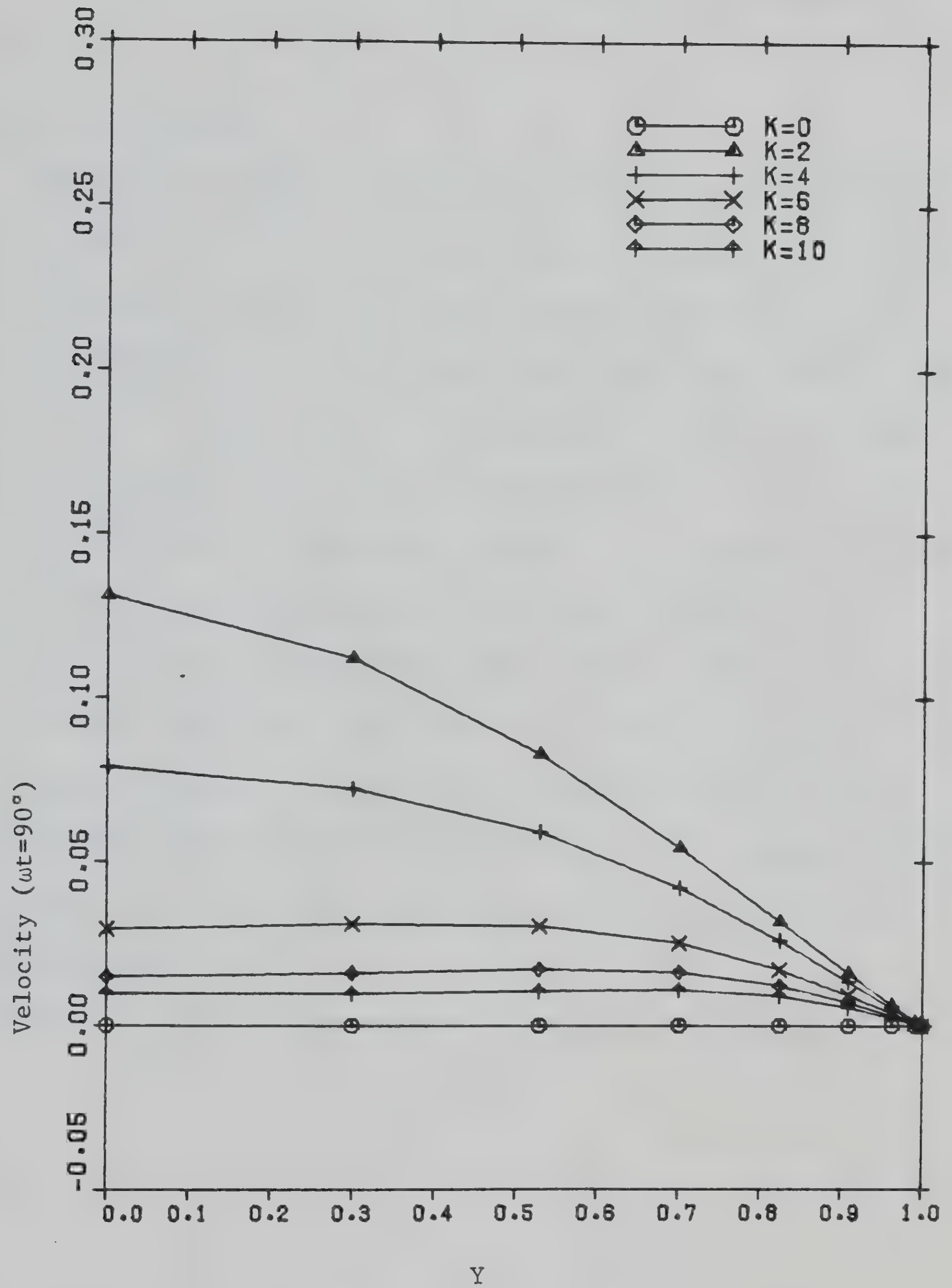

Figure 3.40 Circular pipe velocity profile at $\omega t=90°$ for various K. Pressure gradient held constant.

4. Convergence and Influence of Mesh type

4.1 Biot's Function

The mean values of the real and imaginary velocities will be used to arrive at the acoustic properties of the pipe. In order to test the mean values predicted by the numerical model some analytical work relating similar mean properties to frequency is introduced. It has only been possible to apply this work to propagation in a circular pipe and between two parallel plates - heretofore assumed to produce functions which would represent bounds on the possible functions. The principle results of this section are the Biot functions and these are derived primarily to verify the results of the finite element program. This verification has also provided insight into optimizing the convergence of the bulk properties through changing the finite element mesh.

Biot [1] defines a term F(K) (compare to equation 1.1),

$$F_{(K)} = \frac{2b_1}{C'\mu} \frac{\tau}{\bar{U}} \qquad 4.1$$

μ is the dynamic viscosity, τ is the shear stress, $\bar{U}$ is the average velocity over a cross-section, (F, τ, and $\bar{U}$ are all complex and functions of K). For a slit b_1 is half the distance between the parallel walls. For a circular pipe, b_1

is the radius, for the other pipes it is the hydraulic radius.

Biot [1] describes this function F as a measure of the deviation from steady flow. Therefore, the constant c is introduced. Its purpose is to make the function F equal unity at K=0 . The analytical solutions show that for a circular pipe C=8 and for the parallel walls C=6. The numerical model solutions find that for a triangular pipe C=6.68 for a square pipe C=7.14 and for a rectangular pipe with an aspect ratio of five C=9.59 .

The real part of the function F versus K and the imaginary part versus K are shown respectively in Figures 4.1 and 4.2. These graphs compare the curves for the case of the parallel walls, the circular, triangular and square pipes as well as for a rectangular pipe with an aspect ratio of 5.

According to Biot [1] for the circular pipe the functions at high K asymptotically become parallel to straight lines

$$F = K / \sqrt{(32)} = 0.177 \text{ K}. \qquad 4.2$$

For the slit the curves asymptotically become parallel to

$$F = K / \sqrt{(18)} = 0.236 \text{ K}. \qquad 4.3$$

Biot [1] mentions that the slit and the circular pipe should represent the extreme aspect ratios thus the Biot curves for all of the other configurations should be between these two curves. The results presented here do not appear to confirm this. The curves for the rectangle lie just outside the curve of the circle. This discrepancy may be in the definition of a typical dimension to calculate the acoustic Reynolds number. At high aspect ratios there is a problem using the hydraulic radius as the typical dimension. As an example of this problem consider the slit. From the hydraulic radius equation, the radius is equal to the width of the slit whereas for Biot's work half the width is used in the calculation of K. This problem has been left unresolved. This does not detract from the validity of the computer program results since the equations are solved in terms of the actual frequency and actual pipe dimensions. The only area this influences is the principle of similar solutions for the high aspect ratio configurations.

If the aspect ratio is indeed a major factor determining the correction function it would be reasonable to expect a triangular pipe and especially a square pipe (as its aspect ratio is clearly unity) to have curves closer to that of the circular pipe as opposed to that of the slit. This conclusion is contradicted by the results in Figure 4.1 and Figure 4.15. This result is unexpected and can only suggest that there is another factor to be considered.

4.2 Mesh types

By comparing the Biot functions resulting from different element meshes information can be gleaned to help find the characteristics of a mesh which would minimize error.

First the easiest case to model is used to demonstrate some of the principles used in choosing appropriate meshes. This case is the circular pipe. Since the circle is axisymmetric a small sector of a circle can be used to model the entire pipe. See Figure 4.3

If an arc of 20° is chosen and 4 quadrilateral elements are used to define the sector the result is the same as a circle modelled by 72 elements.

As mentioned, the elements chosen assume linear variations and have only one unknown per node. If higher order elements are used the use of symmetry is more involved because the derivatives across unconstrained boundaries must be specified to be zero. A constrained boundary is wherever the velocity is set to zero to satisfy the boundary condition.

The grids shown are selected because, of the grids tried, they give the best results for the number of unconstrained nodes used. The CPU time required is approximately proportional to the square of the number of unconstrained nodes. As an example of the time required consider the triangular grid (see Figure 4.4) used to model the square pipe of Figure 4.6. The mesh uses 74

unconstrained nodes. To solve for the velocity distribution for a single frequency takes 3.31 CPU seconds on the Amdahl 470/V8. Most of the CPU is used to invert the matrix of equation 2.24. This grid gives the same result as if the square was modelled by 497 nodes. Using the grid of Figure 4.7 for a rectangular grid finding a single velocity profile takes 7.02 CPU sec.

The CPU time could be reduced by capitalizing on the fact that the matrix to be inverted is symmetric. In addition certain global numbering schemes allow one to minimize the space required by banding the matrix but the scheme desired to satisfy the partitioning is not compatible with banding.

Figures 4.8 and 4.9 show that the bulk fluid properties are easy to model at low frequencies but a finer finite element mesh is required to model the properties at high frequencies. It was found that accuracy of a particular number of elements could be improved simply by concentrating the nodes near the edge of the pipe. More nodes are required to model the large changes of the velocity gradients near the wall. Large changes are difficult to model in any numerical technique.

To concentrate elements in regions with high gradients, the uniform grid in the Z direction is transformed by the function

$$Znew = Z \cdot \exp(1-Z) \qquad 4.4$$

and the Y values are changed to maintain the straight sides

of the sector.

This new mesh is a tremendous improvement as can be seen by comparing Figure 4.8 and Figure 4.9 to Figure 4.10 and Figure 4.11. For the real part of the Biot function the analytical solution is almost indistinguishable from the finite element solution with only 4 elements. For the imaginary part this change gives each grid the accuracy of a uniform grid of roughly 4 times the number of elements of a uniform grid.

As mentioned the number of elements that effectively model a circular pipe depend on the angle of the sector and the number of elements in the arc. From this it might be incorrectly surmised that the accuracy can be doubled by halving the angle of the sector. If the arc is less than about 20° there is, in fact, very little gain in decreasing the angle of the arc. The spacing with respect to the pipe wall has a much greater significance. By simply looking at the velocity profiles some feeling can be acquired as to the best places for finer gridding i.e. at the largest changes of the velocity gradients. The grids modelling the triangular and square pipes contained a higher density of elements near the edges and corners of the pipe.

Figure 4.3 shows the type of grids used to model the circle. Velocities at the nodes on the circumference of the circle are set to zero.

Note that for the arc the element nearest the center is quite distorted from a square. Large distortions may cause

errors in the transformation from the orthogonal plane (in natural coordinates) to the global YZ plane. Care must be taken when generating meshes that unique mapping from one plane to the other takes place. The distortion is acceptable if the sign of the Jacobian used in transformations does not change over the domain. The distorted element mentioned above, by this criterion, is acceptable. Problems may occur if one of the interior angles of the quadrilateral is greater than 180°.

Figure 4.4 shows one of the best grids used to model a triangular pipe. Its hydraulic radius is one. The horizontal axis is Z, the vertical axis is Y. The triangle is modelled by a mesh covering only half of the entire domain. The part used by the program is shown by Figure 4.4(a). The other nodes are just a reflection over the Z axis. The velocities are constrained at the nodes on the line $Y = Z$ and $Z = 2.414$.

Figure 4.6 shows how the same mesh is used to model a square. The mesh is scaled down so that the hydraulic radius of the square is unity. In this case only the nodes on the line $Z = 1$ are constrained.

Figure 4.7 shows the effective grid to model the rectangle. Appropriate scaling factors in the Y and Z directions transformed this mesh into a rectangle with the desired aspect ratio and hydraulic radius. This mesh has 121 nodes and 100 elements. The basic grid is the portion of Figure 4.7 of where $0 \le Y \le 1$, $0 \le Z \le 1$, the constrained portion of

the boundary is at Y=1 and Z=1.

Chapter 6 contains another example and discussion of the affect the grid type has on two other bulk properties, resistivity and effective density.

By knowing the type of velocities say from a crude mesh a new mesh can be devised with nodes concentrated in the appropriate areas, thus minimizing the error in the bulk quantities. This is most important because the bulk quantities are needed to derive the acoustic properties of the pipe as will be discussed in chapter 6.

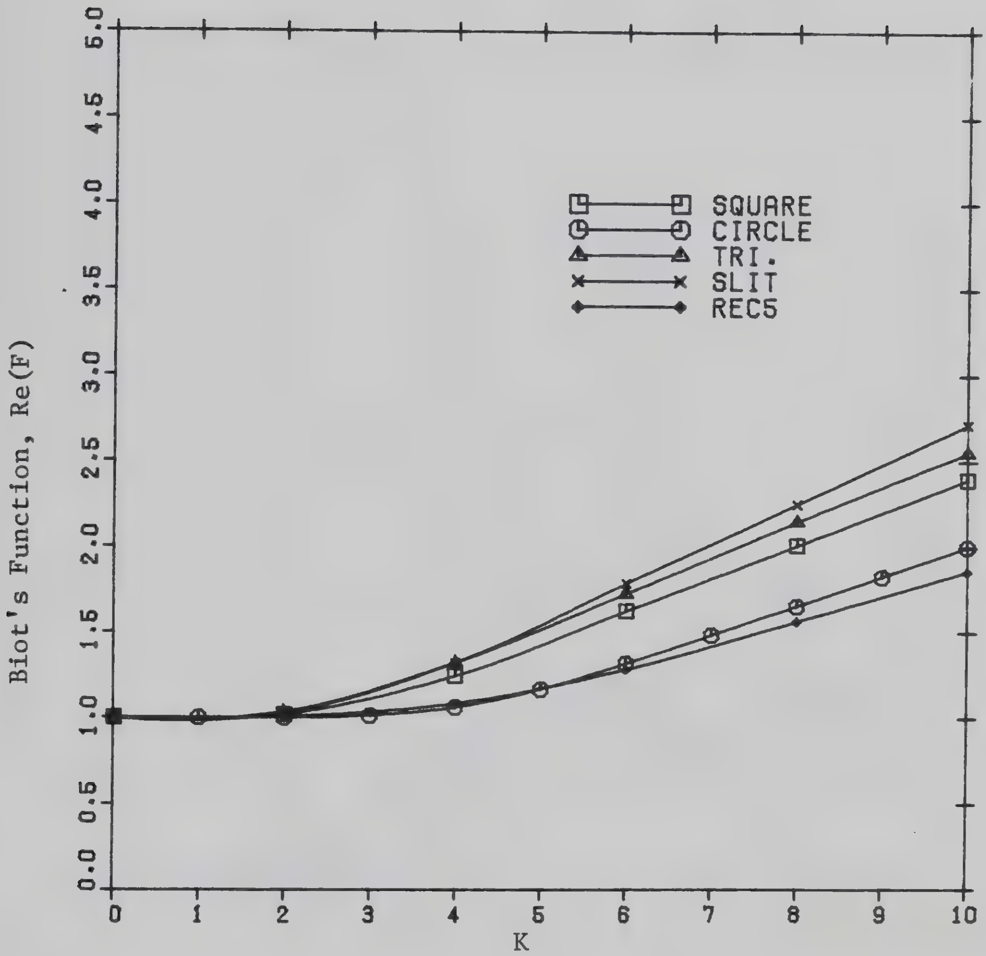

Figure 4.1 Real (F) vs. K
For slit, circle, triangle,square and
rectangle with aspect ratio of 5.

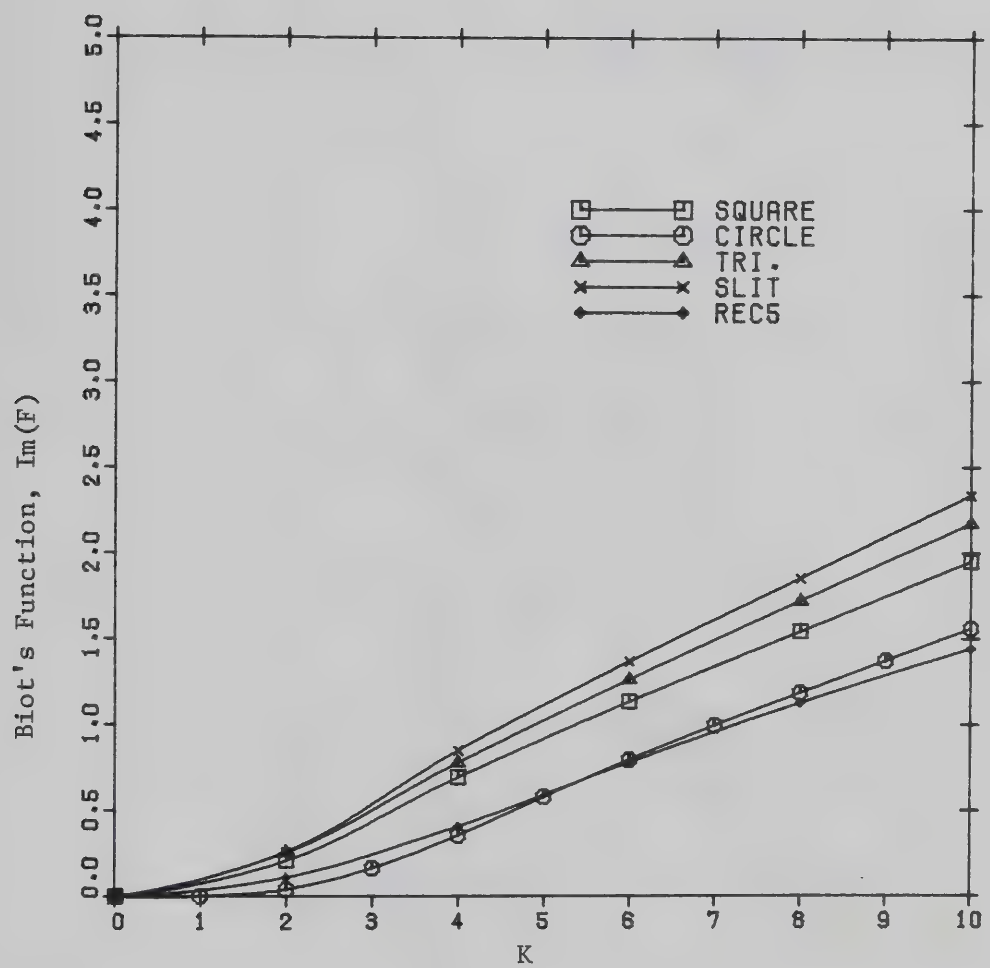

Figure 4.2 Imaginary (F) vs. K.
For slit, circle, triangle, square, and
rectangle with aspect ratio of 5.

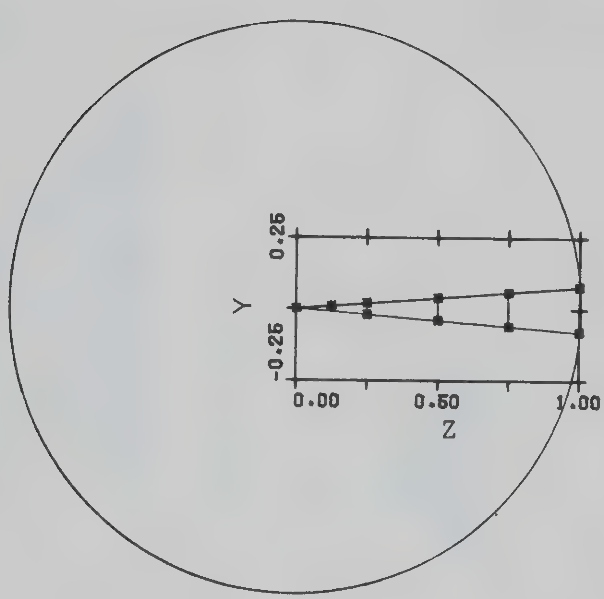

(a) For uniformly spaced elements.

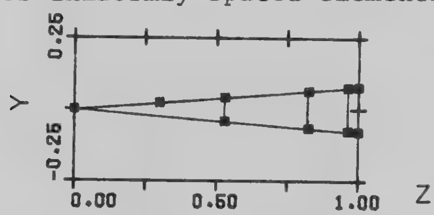

(b) Improved mesh with 4 elements.

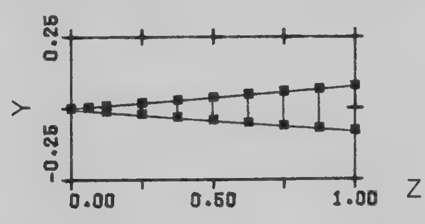

(c) Eight uniformly spaced elements.

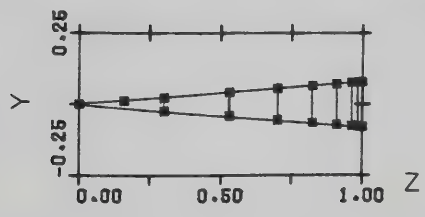

(d) Improved mesh with 8 elements.

Figure 4.3 Sample meshes to model circular pipe.

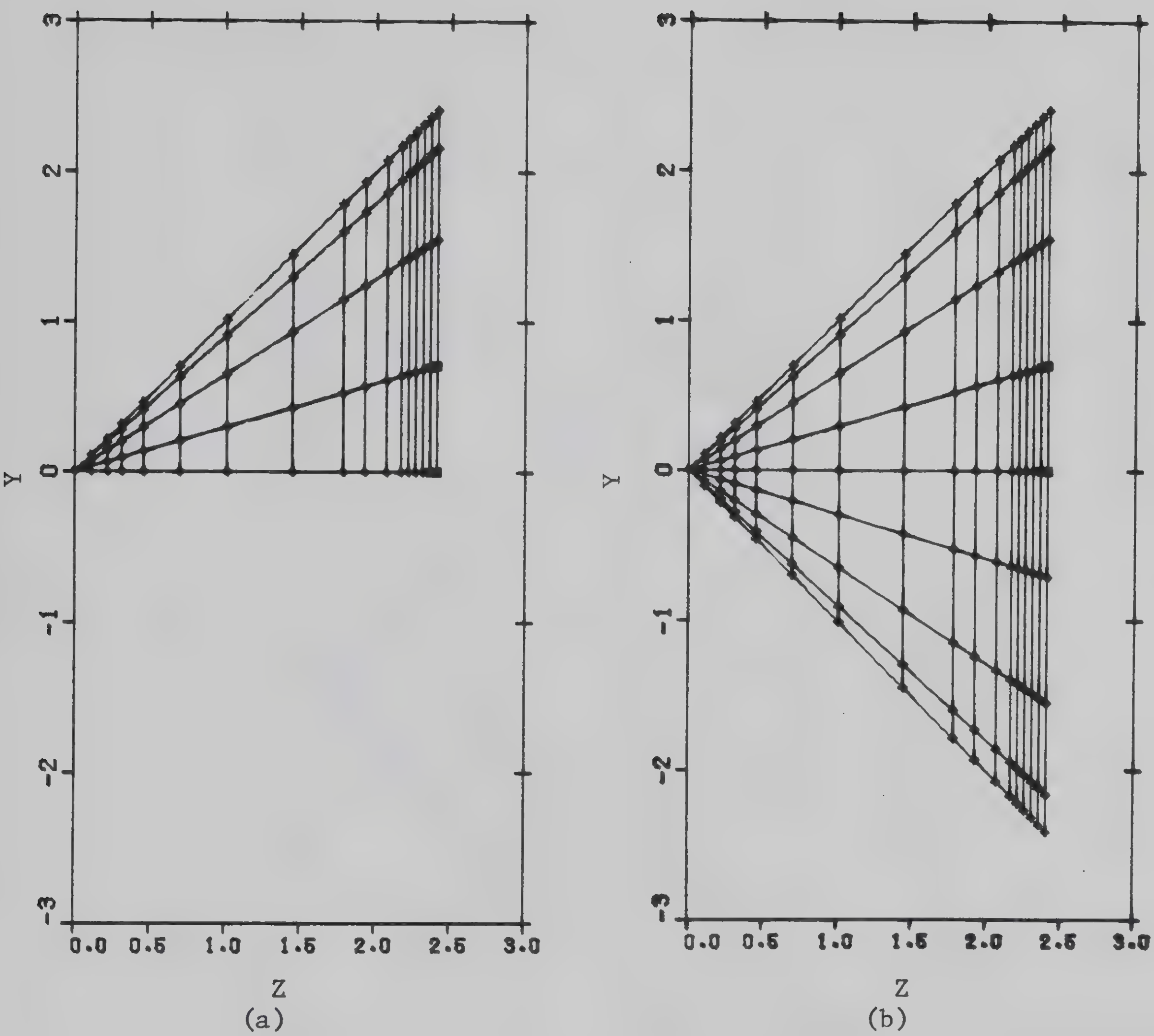

Figure 4.4. (a) Basic 79 node grid to model triangle and square.

(b) Effective grid of triangle using (a)

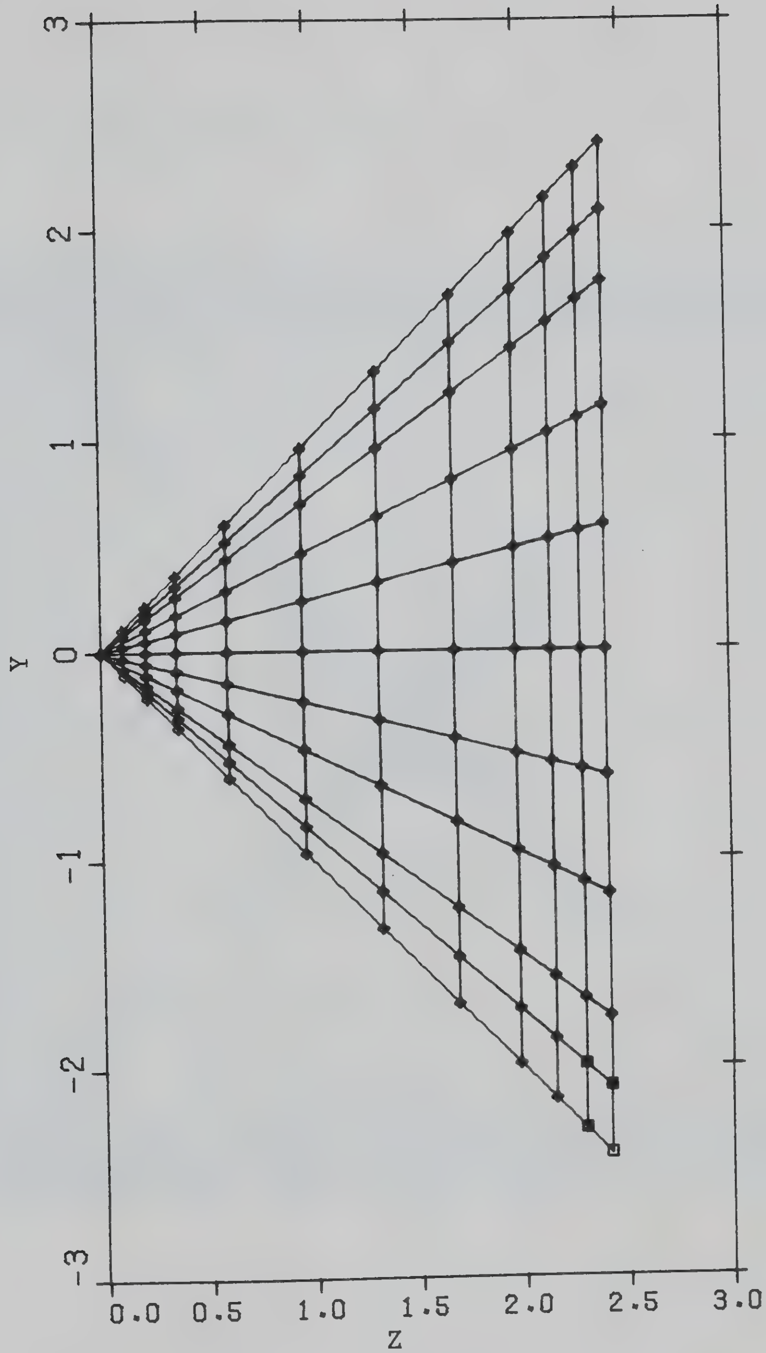

Figure 4.5 117 node grid for triangle.

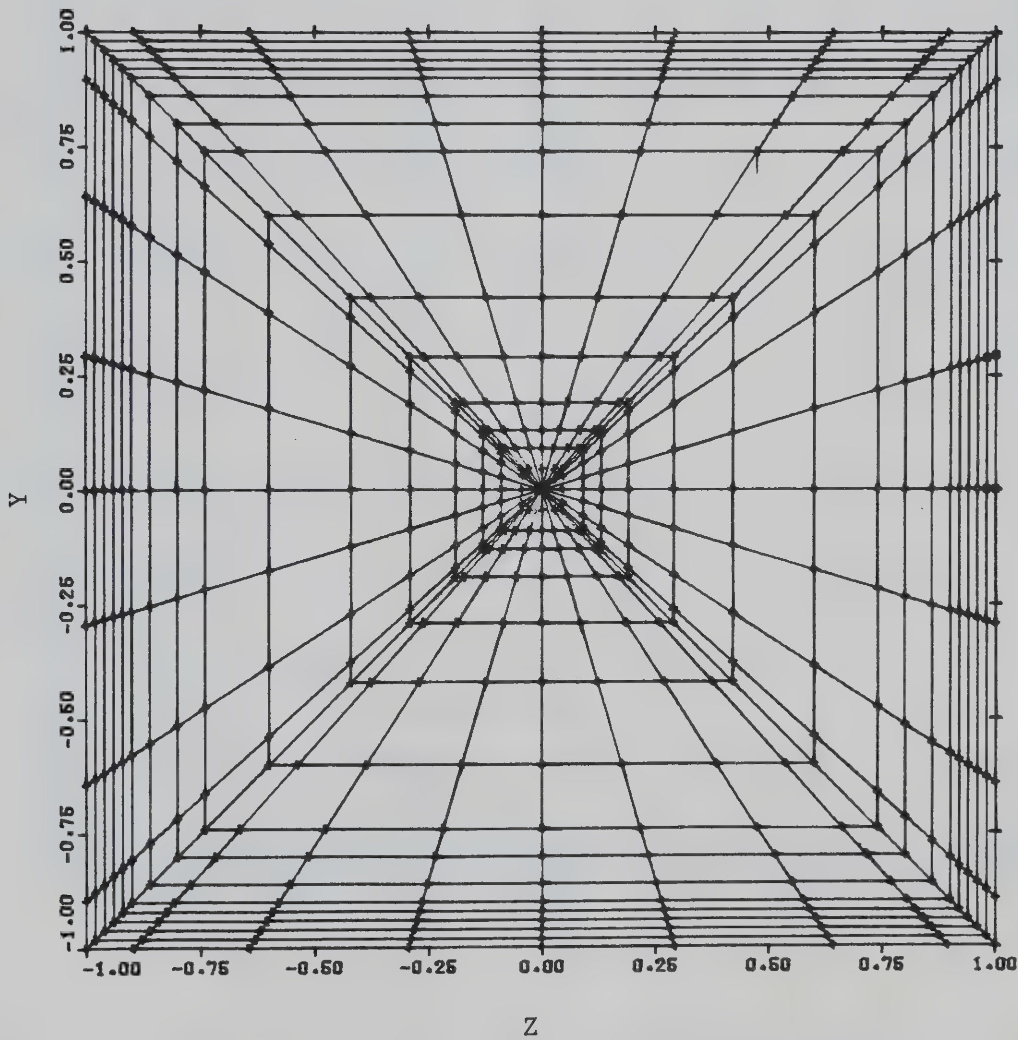

Figure 4.6 Effective grid using 79 node triangle.

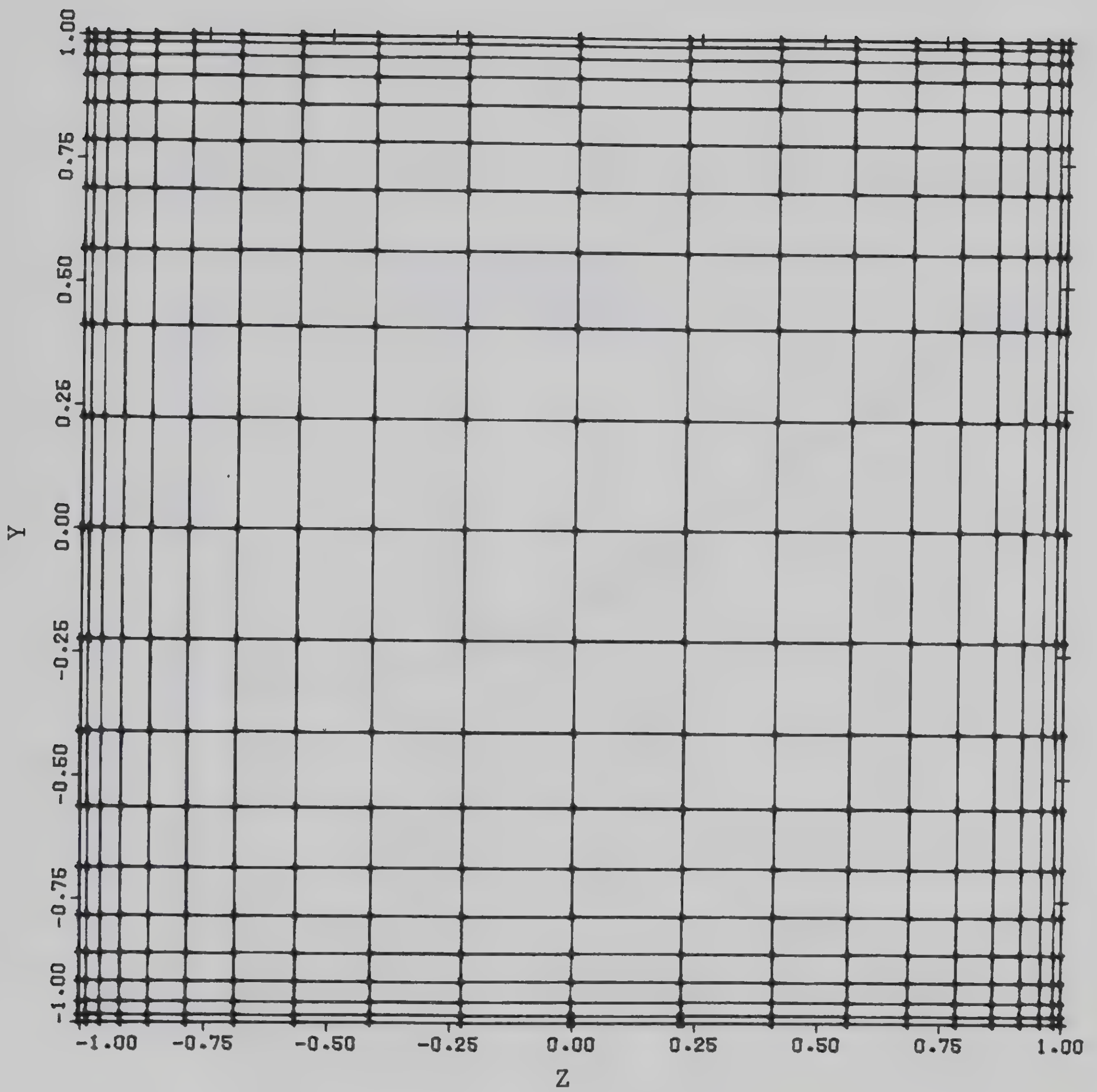

Figure 4.7 Effective grid for square or rectangle using 121 node portion in $0 \le Y \le 1$, $0 \le Z \le 1$.

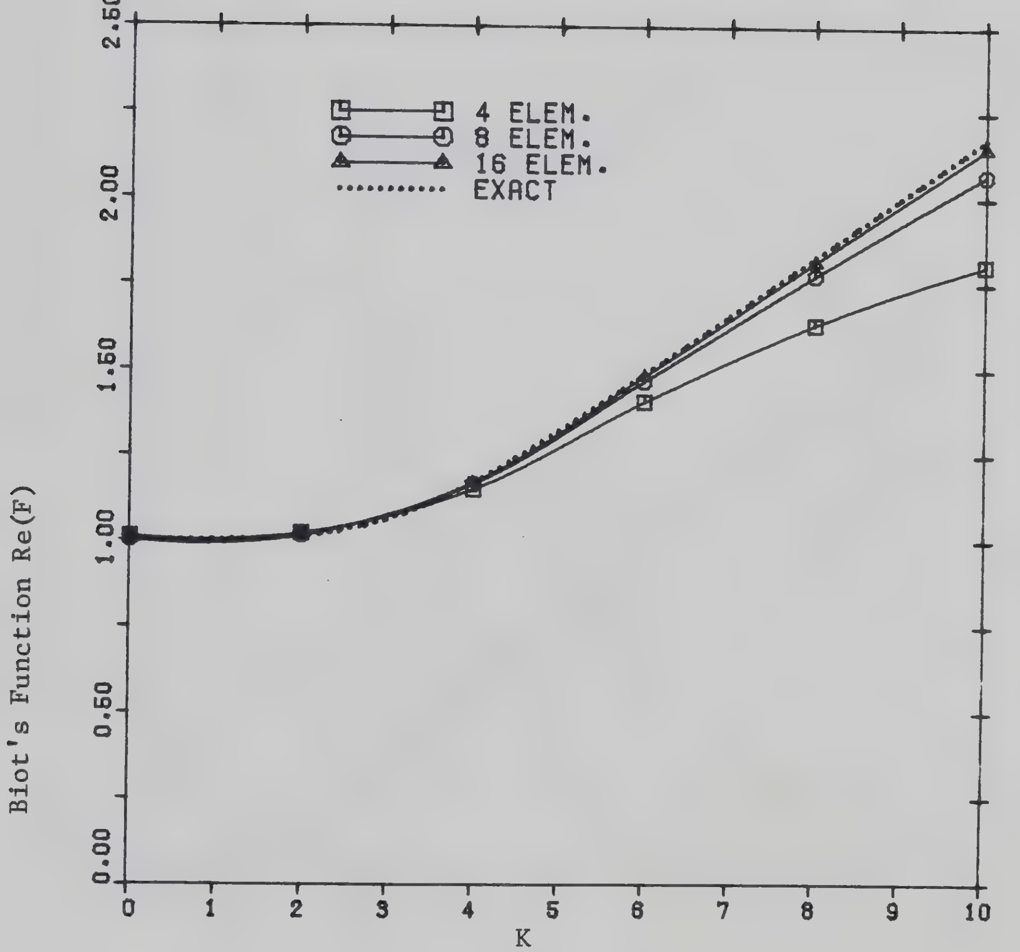

Figure 4.8 Real (F) vs. K.
For circle using various uniform grids in arc.

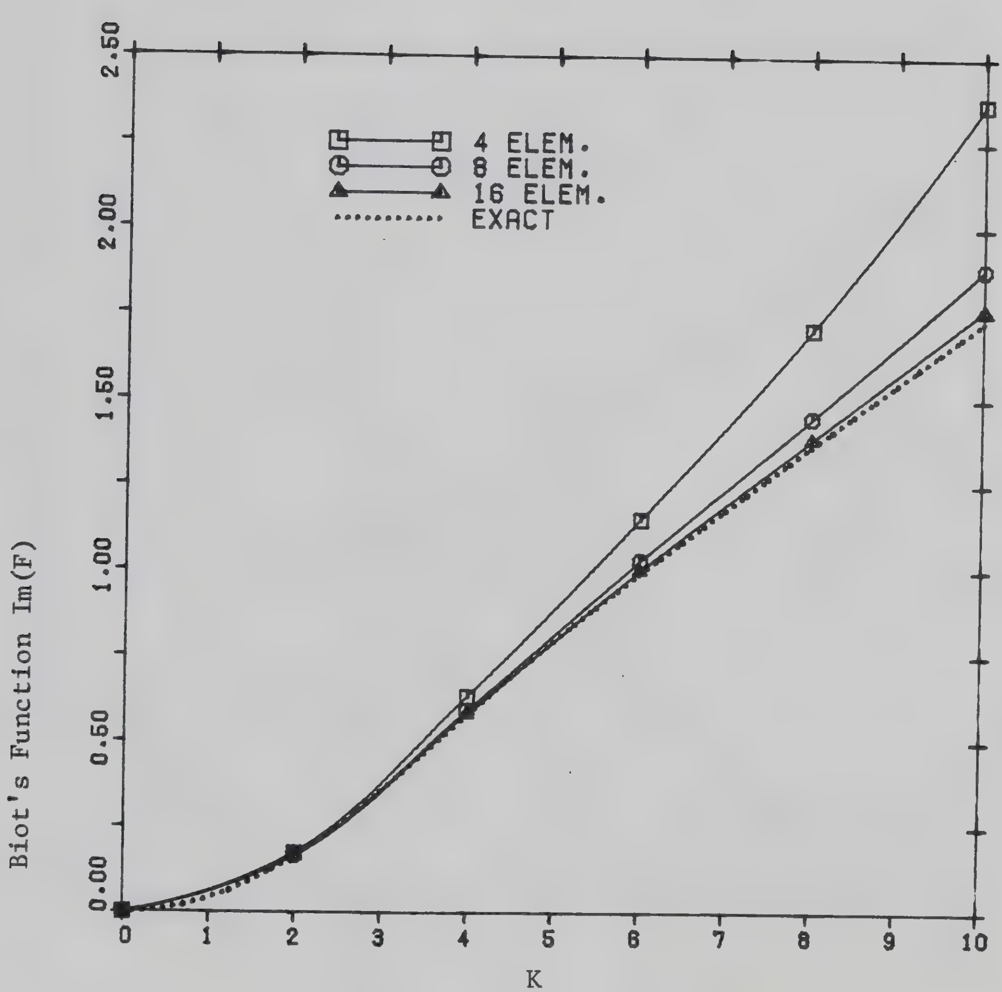

Figure 4.9 Imaginary (F) vs. K.
For circle using various uniform grids in arc.

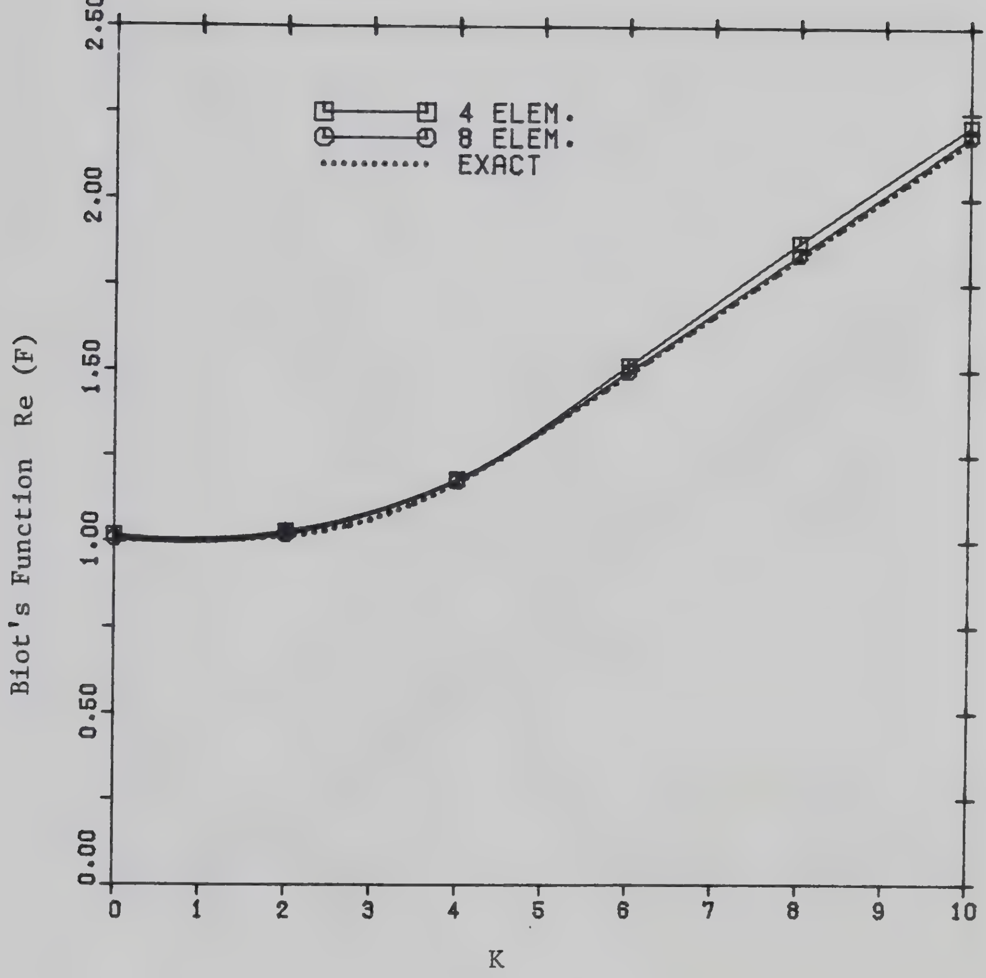

Figure 4.10 Real (F) vs. K.
For circle using improved grids.

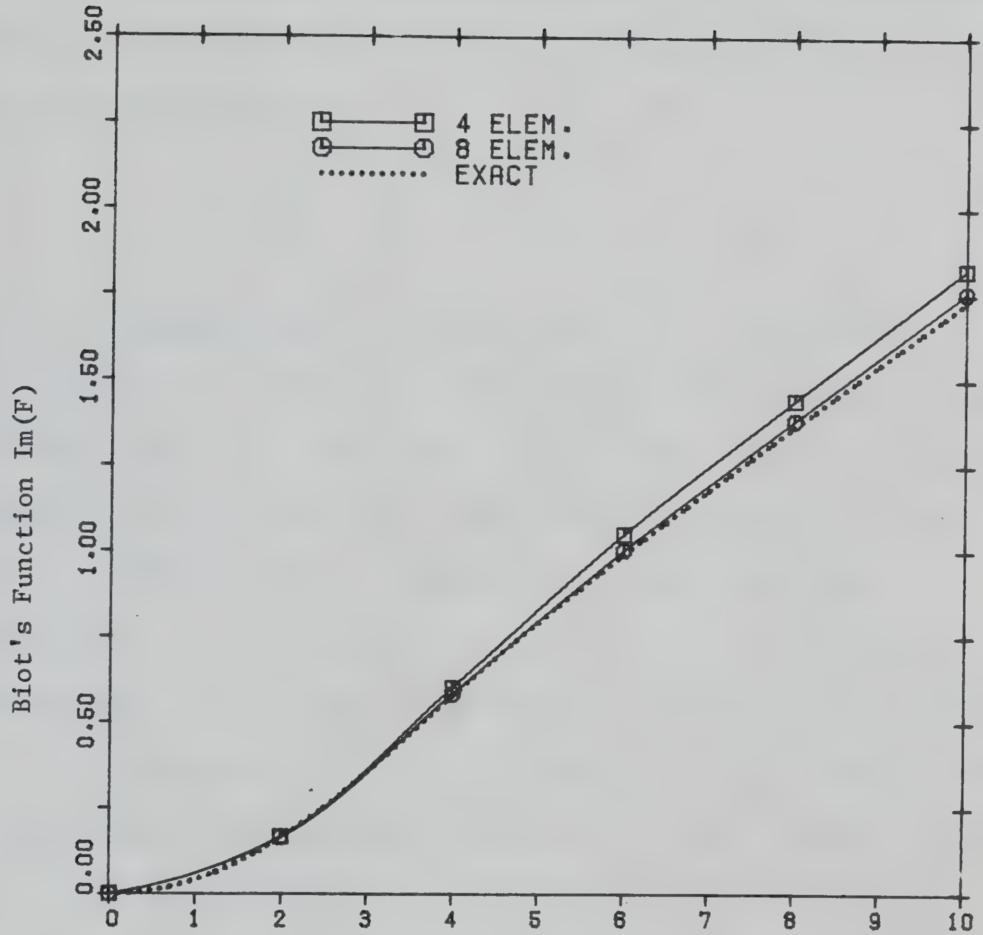

Figure 4.11 Imaginary (F) vs. K.
For circle using improved grids.

5. Shear Stresses

In the derivation of the matrix equations in chapter 2 it was shown how the forces the fluid exerts on the pipe walls could be found. The conventional way of studying the forces or stresses would be to use Newton's law[1] of viscosity as given by

$$\tau = \frac{\partial u}{\partial \hat{n}} \qquad 5.1$$

where $\hat{n}$ is perpendicular to the wall. It is difficult to use this equation in this application unless the element meshes are chosen such that near the walls there are lines of nodes perpendicular to the walls. Even with this type of grid, which is inconvenient to generate, errors would be introduced in the process of taking the derivatives of velocity. So it is clearly better to use the shear force matrix equations as derived in chapter 2. The results that this equation produces are the forces in the region of each node required to maintain equilibrium in the system.

A weighting system must be applied to the force at a particular node to determine the average shear stress around that point. This weighting function depends on the spacing of the nodes next to the point of interest and the interpolation function used in deriving the element. In the results presented the interpolation functions assume linear variation between nodes of all properties, including shear.

----

[1]For Newtonian fluids only.

Figure 5.1 and Figure 5.2 are for the case of a circular pipe to show the typical characteristics of the shear force F as K is varied. The pressure gradient is a constant. Figure 5.1 shows how the shear force on one node, at time t=0, varies with K. The value of F is proportional to the pressure gradient and the area of the pipe. The force per node is inversely proportional to the number of nodes used to represent the circular pipe. For example, if the area of the pipe is unity and a simple arc of 45° is used to model the circle(i.e., there are effectively 8 nodes on the circumference), the force on each node, at K=0, is 1/8 of the product of the pressure gradient and the pipe area.

As K increases the force at t=0 drops quickly at K=2 but at K=4 it seems to be decreasing asymptotically to zero. Figure 5.1 also shows the same example with $\omega t=90°$. As K approaches zero obviously the shear force approach zero. Its behavior is very interesting after K=2. It reaches a peak near the value of the force at t=0 at about K=2.5 and begins decreasing identically to the force at t=0.

Figure 5.2 shows how the magnitude of the shear force |Fs| defined as

$$|Fs| = (Fsr^2 + Fsi^2)^{1/2} \qquad 5.2$$

varies with K.

The mesh of Figure 5.3 is included to provide a better understanding of the following results. The symmetry of the

triangle and the square are used to the fullest.

Figure 5.4 to Figure 5.15 show the shear stress the fluid exerts along the pipes at various frequencies. Figure 5.3 shows the mesh used to obtain the final results of the triangular and square pipes. It is the same mesh as that of Figure 4.21. The only difference in modelling the two types of configurations, as far as programing is concerned, is which sides of the pipe are constrained and the difference of scale to make the pipe have the desired hydraulic radius. For example, to model the triangle of hydraulic radius 1 the dimensions of the mesh in Figure 5.3 is used with the nodes labelled A to U constrained. To model the square of hydraulic radius 1 the scale of Figure 5.3 is reduced by 2.414 and only the nodes Q to U are constrained.

In Figures 5.4 to 5.15 each data point on the graphs represents an average shear stress in the area of a node. The data points are labelled to show data points corresponding to each node in Figure 5.3.

For Figures 5.4 to 5.15 the vertical axis is shear stress for the pipes with hydraulic radius of unity and pressure gradient of unity. For Figures 5.4 to 5.9 the horizontal axis is the distance along the perimeter of the pipe beginning at the corner of the square pipe and ending at half the width. See points Q to U of Figure 5.3. For Figures 5.10 to 5.15 the horizontal axis is the distance along the perimeter of the isoceles triangle beginning at the right angle corner and ending at the midpoint of the

opposite side of the triangle. The distance from A to U is the sum of A to Q and Q to U. Again, by symmetry, information of the variable is completely shown by these cases.

The case of K=0 is worth some extra comment. When the frequency is zero the governing momentum equation reduces to

$$\frac{\partial P}{\partial X} = \mu \nabla^2 U \qquad 5.3$$

which is of the same form as Prandtl's torsion function for prismatic bars from the field of elasticity. (see Sokolnikoff [17] or Timoshenko [18]) It can be shown that the shear stresses of the steady state fluid flow are analogous to the stresses of a bar in torsion. The largest stresses occur at the perimeter of the configuration in both cases.

It may appear as an obvious flaw that in these figures, at K=0, the shear stress is not zero in the corners. Since the matrix equation produces the shear force in the area of the node and dividing by the area represented by the node only gives average shear stress it is not possible to define the stress in the corner. A finer grid along the perimeter of the pipe will produce more accurate shear stress results.

From these results, however, some general observations may be made. At low frequencies the shear stress is nearly parabolic along the flat edges of both the triangular and

square pipes. As the frequency increases the profiles flatten and the magnitude decreases. In all cases the stress approaches zero in the corners of the pipes.

The primary use of the shear force matrix equation is to find the average shear stress on the pipe in order to calculate the Biot curves. The average shear stress is found by summing the shear forces supplied by the matrix equation and dividing by the length of perimeter they act on. This procedure should be more accurate than calculating a number of shear stresses around the pipe and averaging them because of errors introduced in finding derivatives of the velocity numerically.

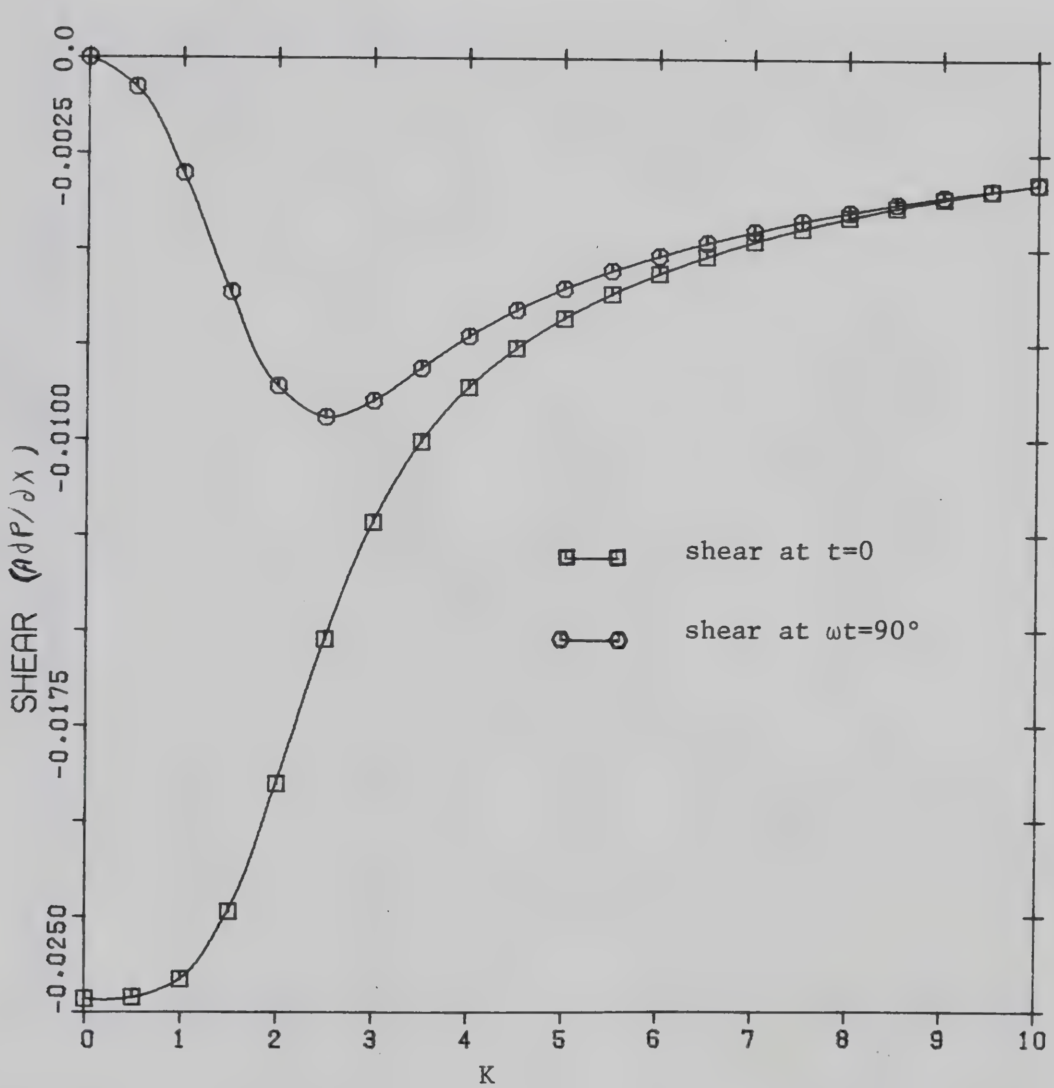

Figure 5.1 Shear vs. K for circular pipe at two times in the cycle

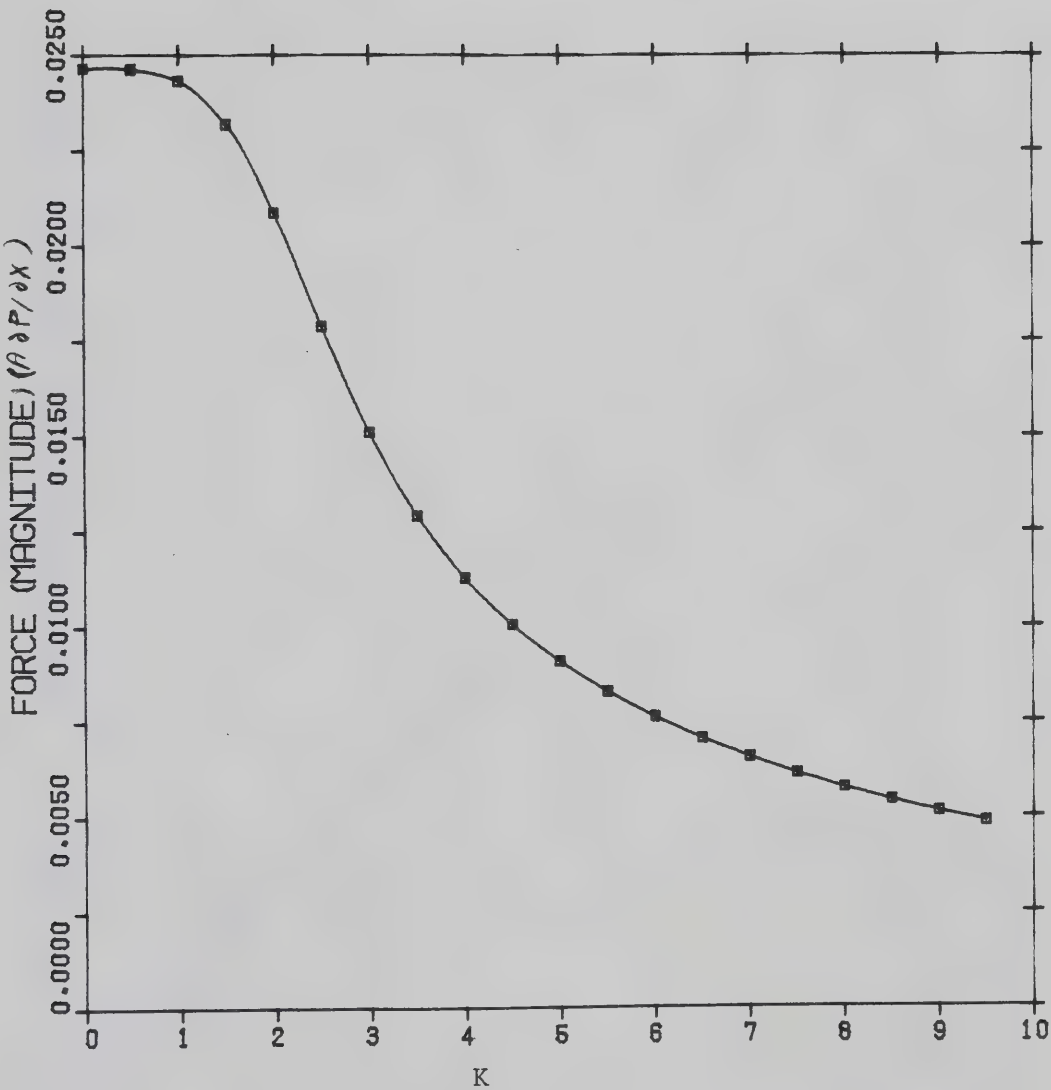

Figure 5.2 Magnitude of shear force vs. K for circular pipe.

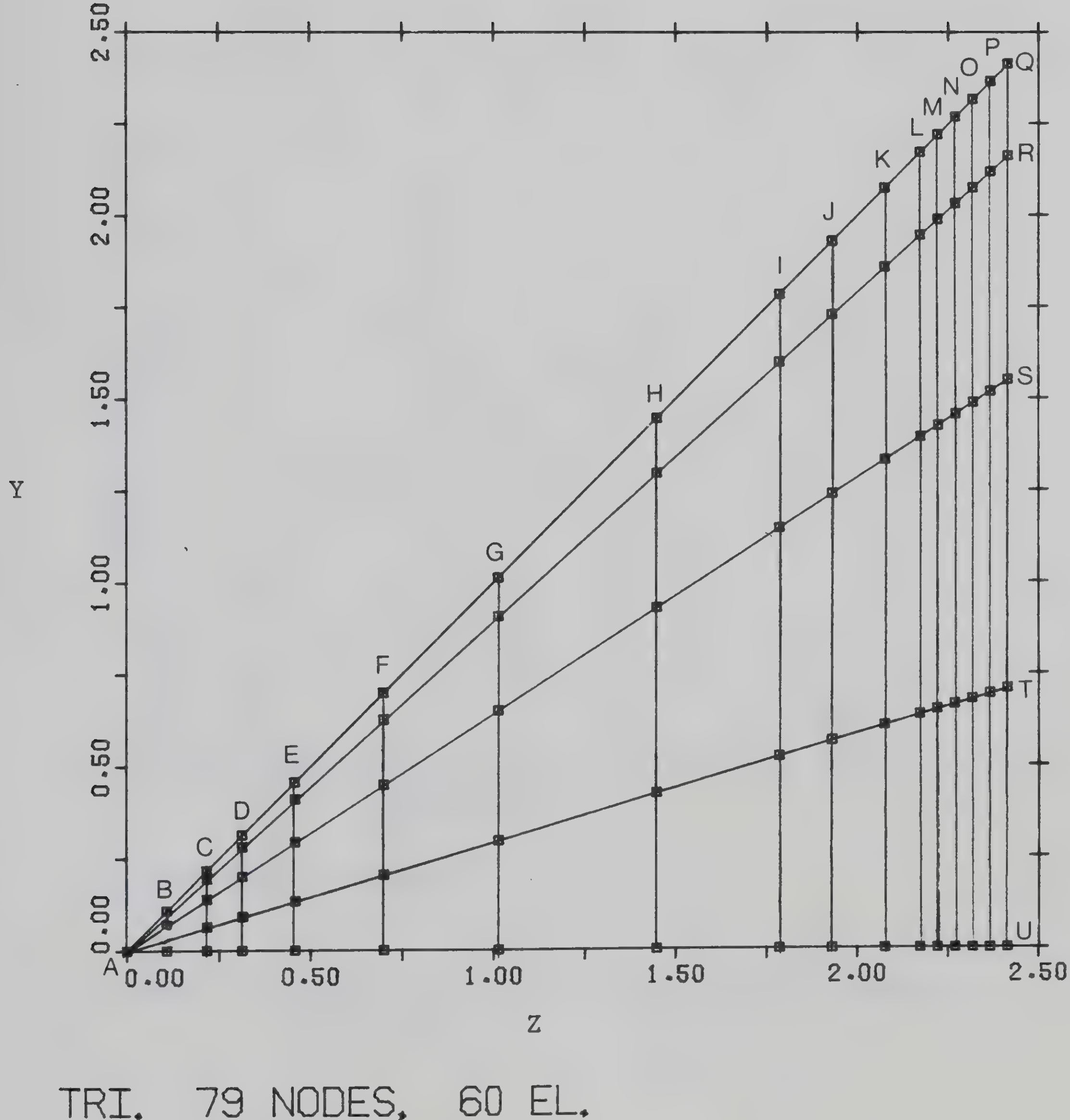

Figure 5.3 79 node grid to model triangle and square.

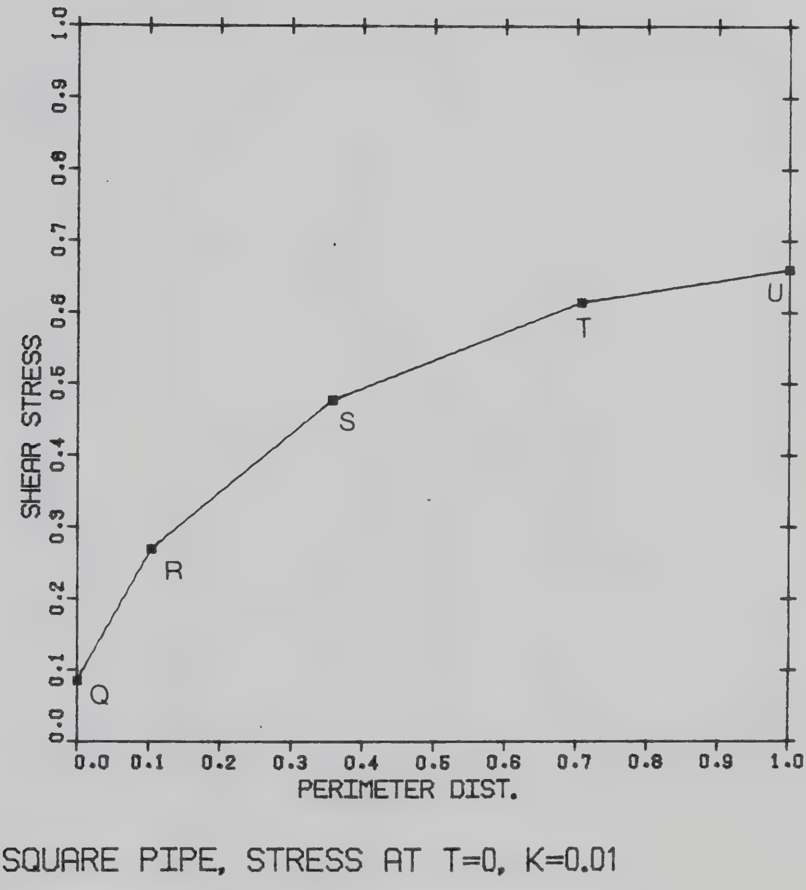

Figure 5.4 Shear stress for square pipe.Lettered values correspond to nodes of Figure 5.3.

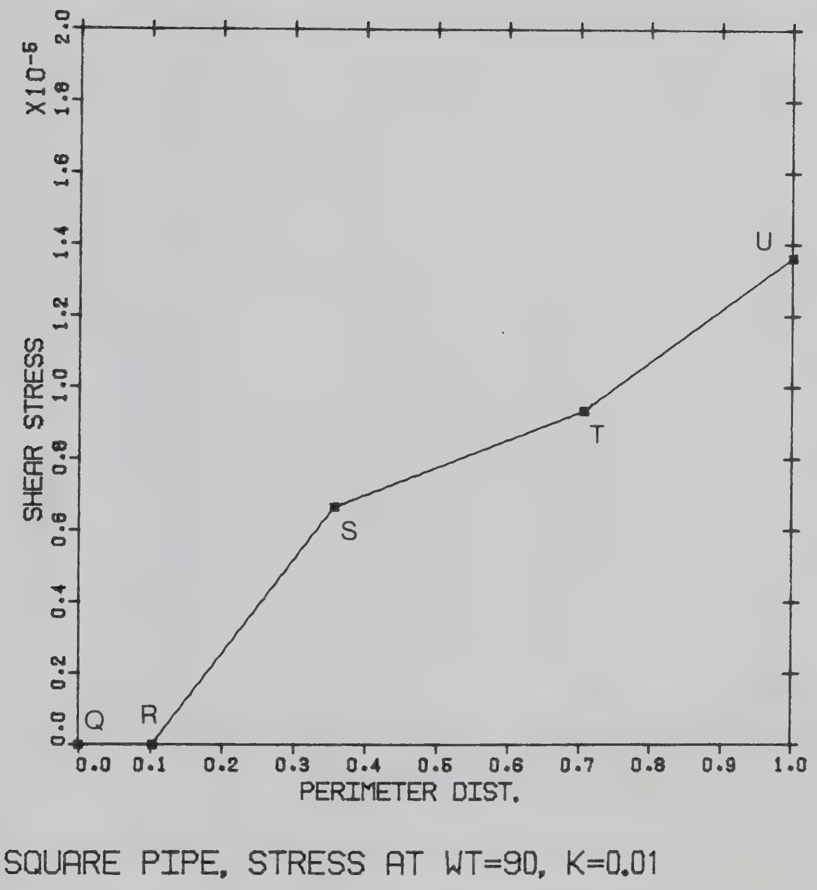

Figure 5.5 Shear stress for square pipe. Lettered values correspond to nodes of Figure 5.3.

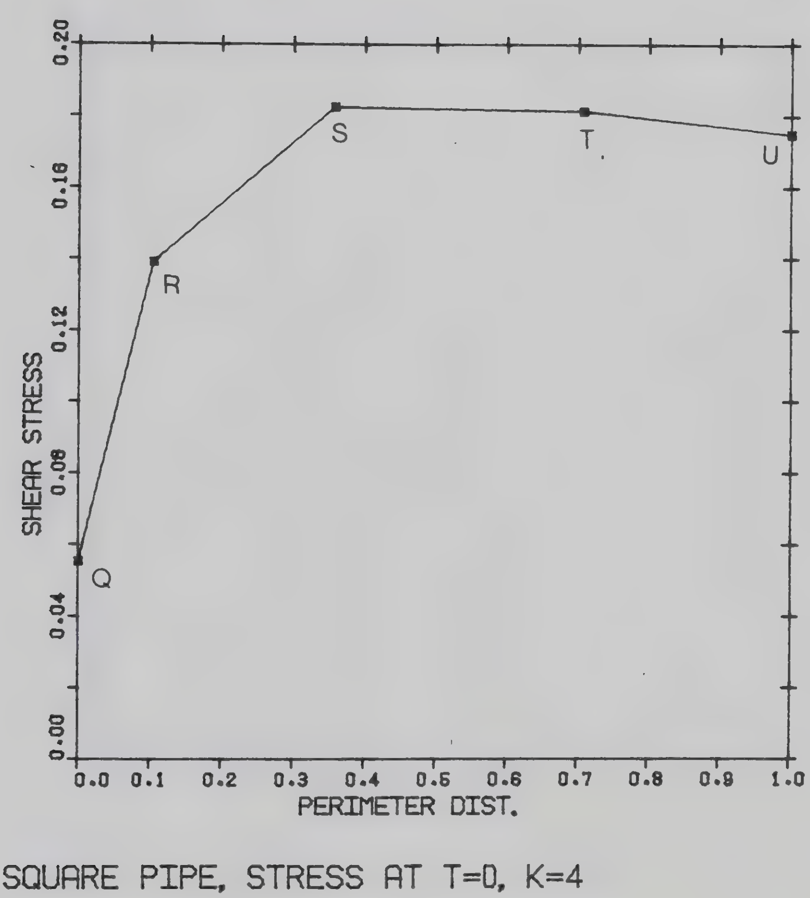

Figure 5.6 Shear stress for square pipe. Lettered values correspond to nodes of Figure 5.3.

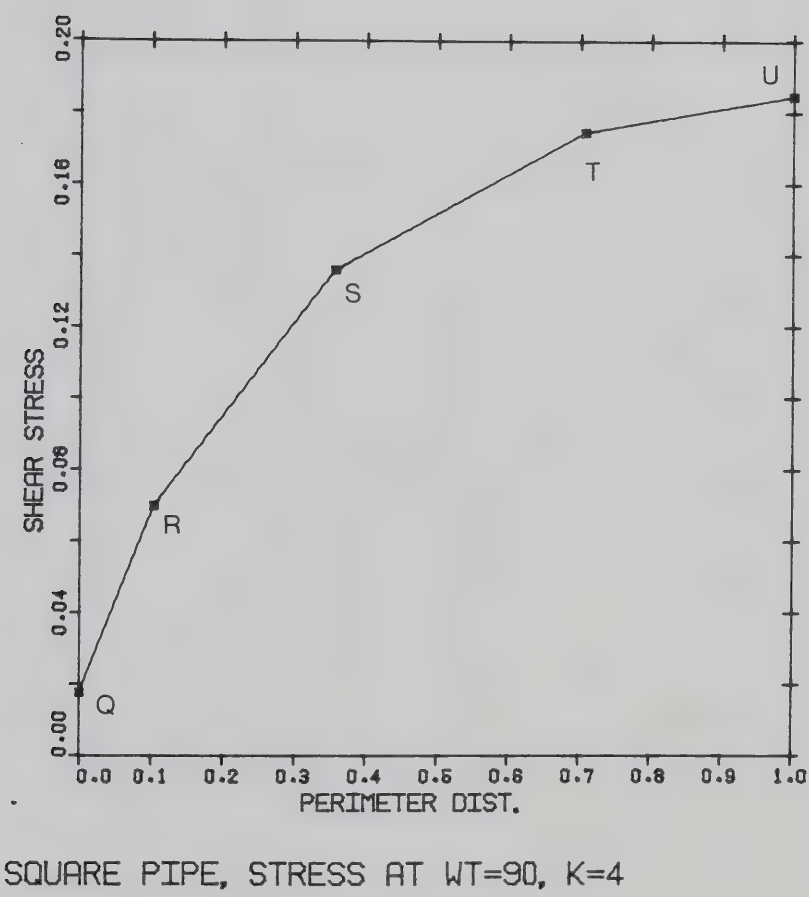

Figure 5.7 Shear stress for square pipe. Lettered values correspond to nodes of Figure 5.3.

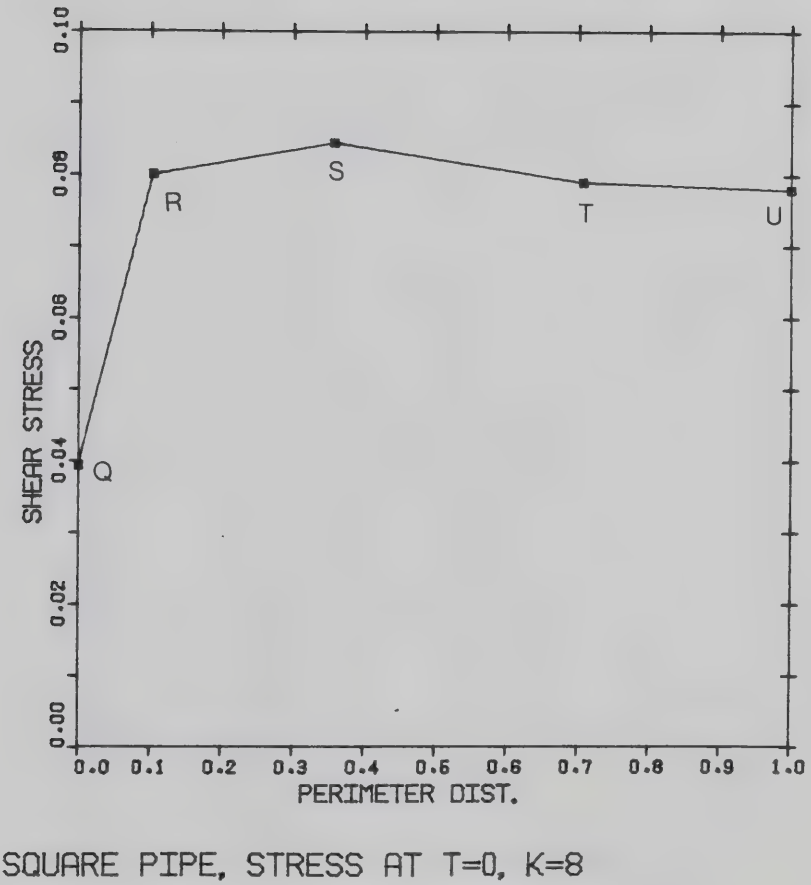

Figure 5.8 Shear stress for square pipe. Lettered values correspond to nodes of Figure 5.3.

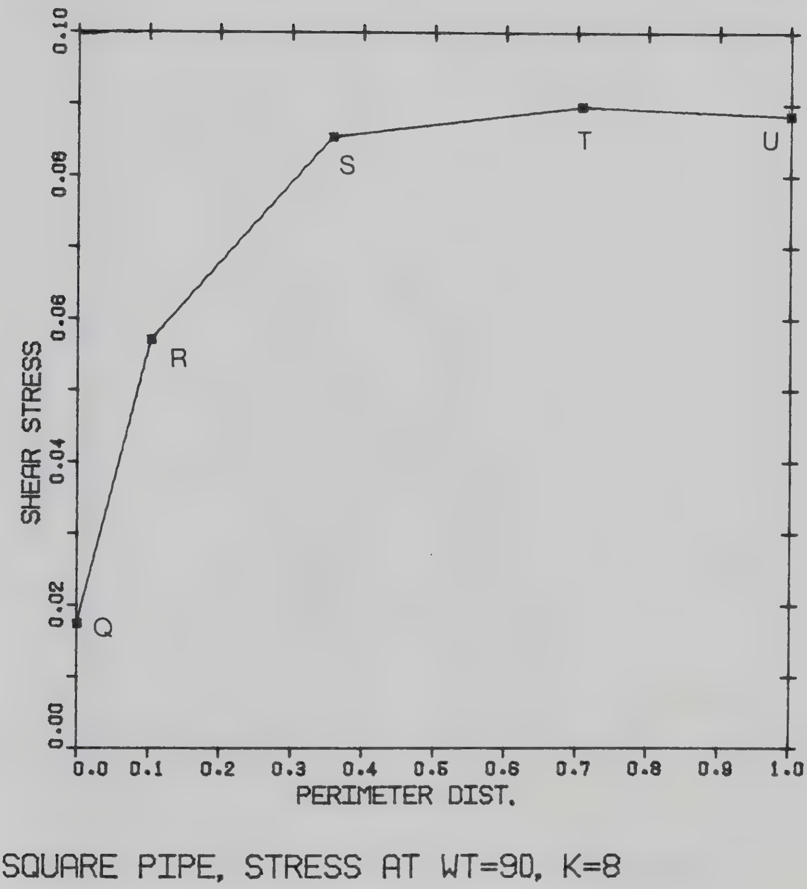

Figure 5.9 Shear stress for square pipe. Lettered values correspond to nodes of Figure 5.3.

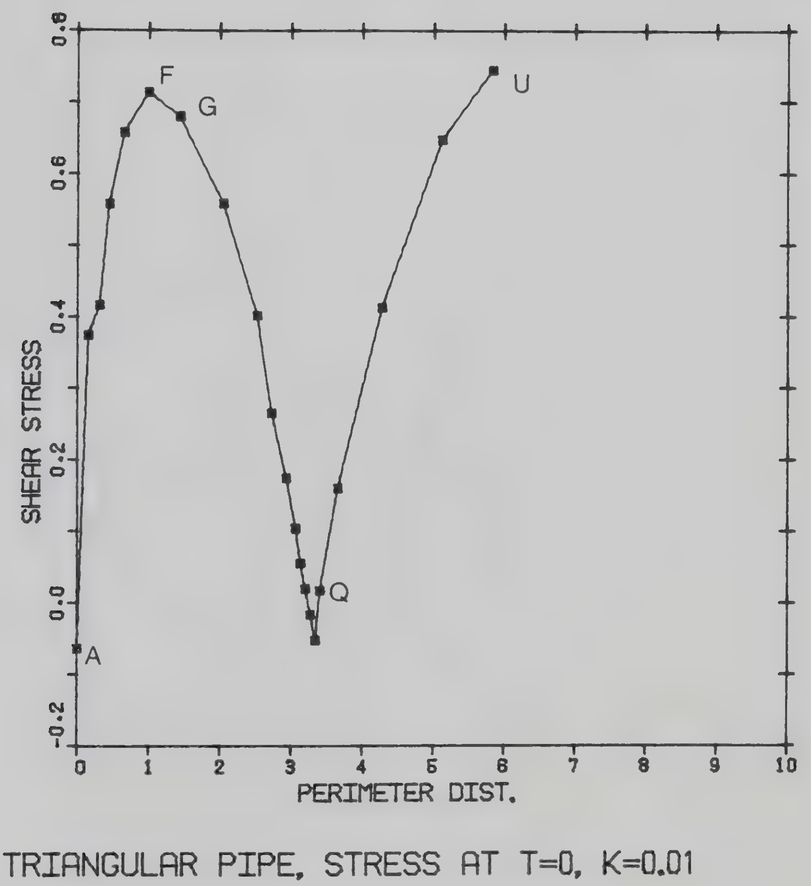

Figure 5.10 Shear stress for triangular pipe. Values correspond to lettered nodes of Figure 5.3.

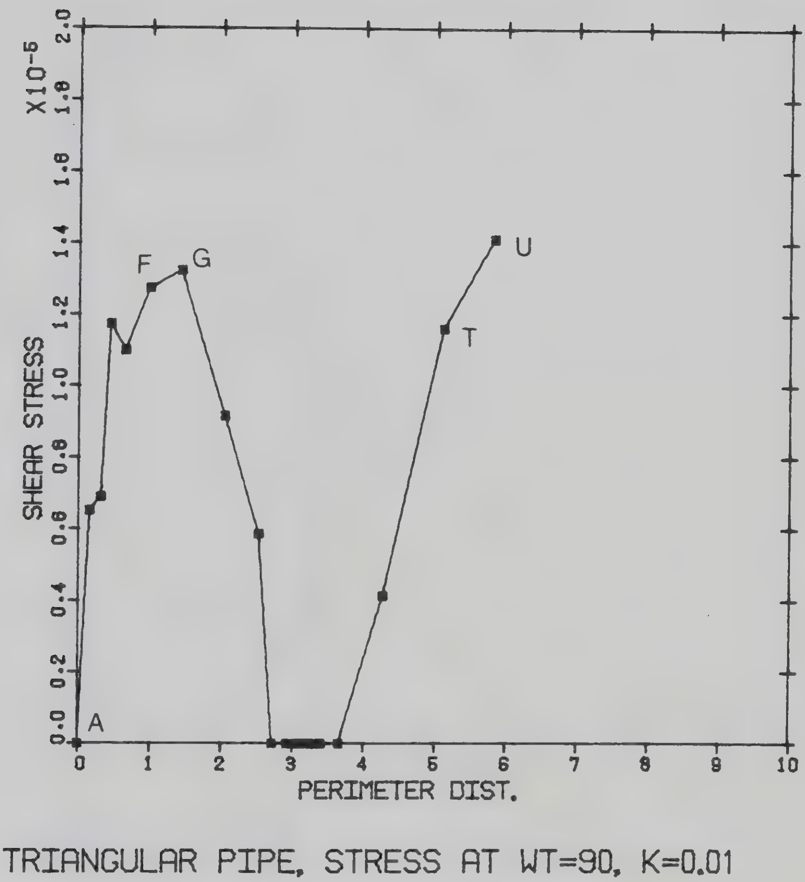

Figure 5.11 Shear stress for triangular pipe. Values correspond to lettered nodes of Figure 5.3.

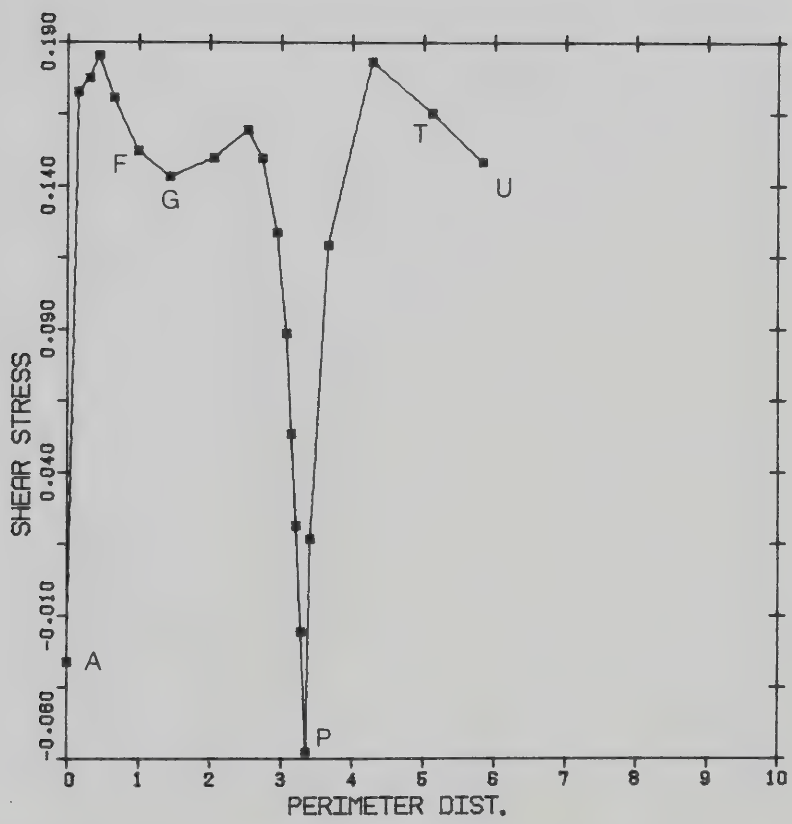

Figure 5.12 Shear stress for triangular pipe. Values correspond to lettered nodes of Figure 5.3.

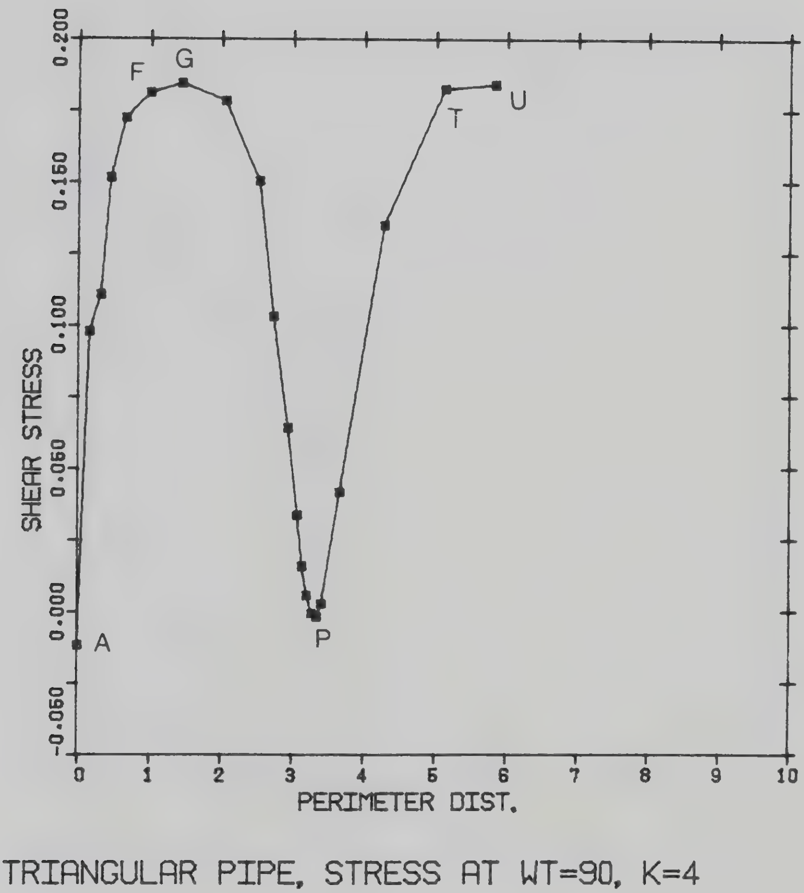

Figure 5.13 Shear stress for triangular pipe. Values correspond to lettered nodes of Figure 5.3.

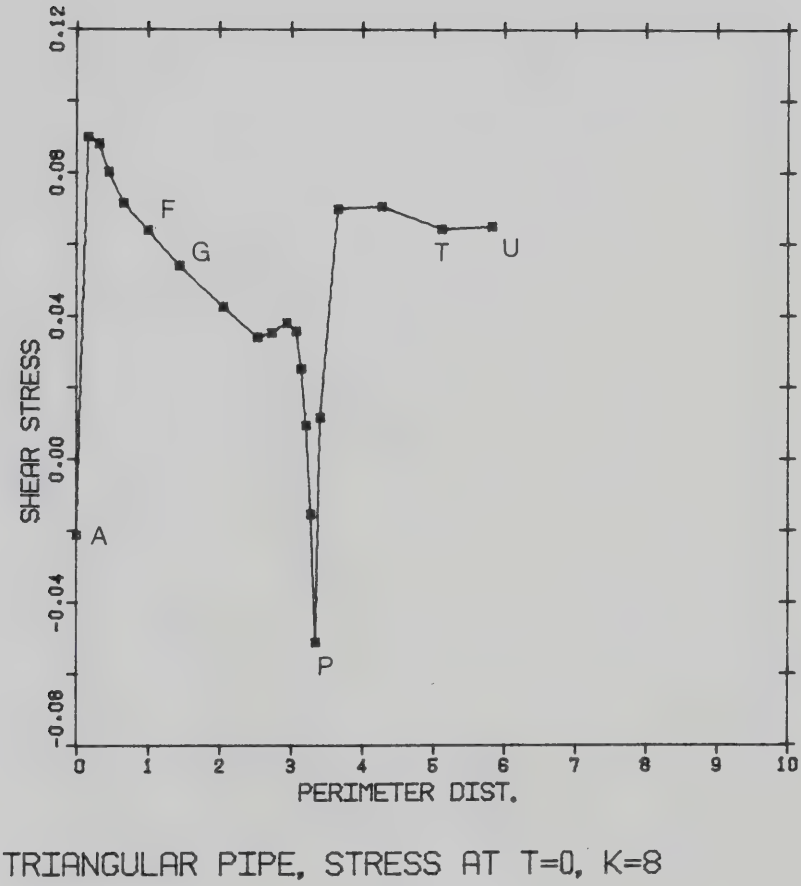

Figure 5.14 Shear stress for triangular pipe. Values correspond to lettered nodes of Figure 5.3.

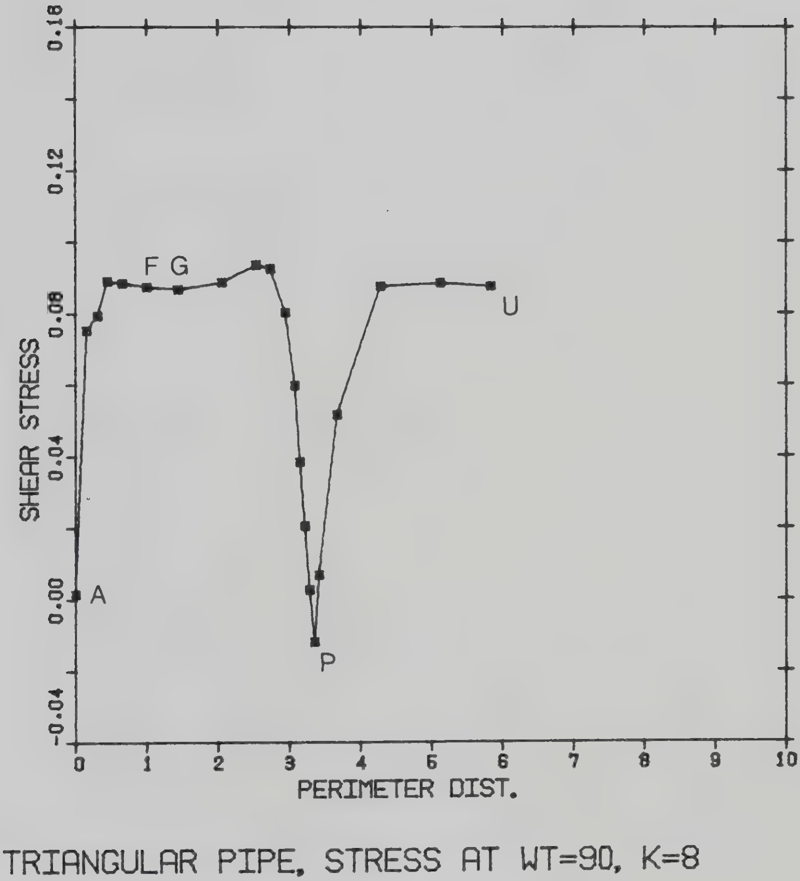

Figure 5.15 Shear stress for triangular pipe. Values correspond to lettered nodes of Figure 5.3.

6. Pipe Acoustic Properties

6.1 Resistivity and Effective Density

This analysis began with a simplification of the Navier-Stokes equations

$$\frac{\partial P}{\partial X} = - \rho_o \frac{\partial u}{\partial t} + \mu \nabla^2 U \qquad 6.1$$

from which are found the velocity distributions in the pipe. Now using only the mean velocities

$$\overline{U} = (\int U_r \, dA + j \int U_i \, dA) \frac{1}{A} \qquad 6.2$$

and writing the above force balance as

$$\frac{\partial P}{\partial X} = (\rho_e \, j \, \omega + R) \, \overline{U} \qquad 6.3$$

where R is the resistivity per unit length (Rayls/m in MKS), ρ_e is the effective density. Rearranging the above equation results in

$$\rho_e \, j \, \omega + R = \frac{1}{\overline{U}} \frac{\partial P}{\partial X} \qquad 6.4$$

Thus

$$R = \mathrm{Re}\left(\frac{1}{\overline{U}} \frac{\partial P}{\partial X} \right) \qquad 6.5$$

$$\rho_e \, \omega = \mathrm{Im} \left(\frac{1}{U} \frac{\partial P}{\partial X}\right) \qquad 6.6$$

It is known from flow dynamics that for steady state flow (K=0) in a narrow slit of width b

$$R = 12\mu/b^2 \qquad 6.7$$

and in a circular pipe of radius a

$$R = 8\mu/a^2 \qquad 6.8$$

where μ is the dynamic viscosity. The results of the model match these values very well.

This information is very important to the application of the results. To determine the resistivity for any pipe at any frequency the following steps should be taken. Determine which of the example shapes best approximates the shape of the new pipe. Calculate the hydraulic radius of the new pipe. Calculate the K from the hydraulic radius, the fluid properties and the circular frequency of interest. At this K find from Figure 6.1 the R value. Multiply it by the dynamic viscosity and divide by the square of the hydraulic radius.

With a slight variation of the above procedure it might be within reason to find approximately the resistivity for a

porous material. The following has not been verified, however. The first step is to experimentally find the resistivity of a sample of the material. This is done by finding the pressure drop across a sample of material (in a pipe where the sample seals a portion of the pipe) given a known steady flow of air through the sample. This information is used in equation 6.5 . Since the frequency is zero

$$R=-1/\bar{U}(dP/dX) \qquad 6.9$$

Using Lord Rayleigh's [15] assumption that a porous material can be approximated by a matrix of parallel channels then from equation 6.7 a typical pore dimension can be determined. With this information the K can be determined at whatever frequency is of interest and R can be scaled as described above.

As mentioned the extension to porous materials needs testing. A simple test with a few samples could be done to see if there is good correlation to pipe flow. One difference could already be predicted and that is the position of the peaks of absorption if an impedence tube is used. The path length in a porous material is greater than simply its width so the peaks would be shifted to the lower frequencies. Nonetheless the procedure would be very useful.

For very high frequencies Zwikker and Kosten [19] have shown that

$$R = 1/r \sqrt{2\mu\omega\rho_o} \qquad 6.10$$

$$\text{or } R = K \mu \sqrt{2}/r^2 \qquad 6.11$$

The finite element results approach these values for the circular pipe.

Crandall [3] has shown that as the frequency approaches zero, the effective density in a circular pipe approaches four thirds the static density. Again this is the behavior of the numerical results. As the frequency increases the effective density approaches static density for all geometries of pipe. The value of the density is dependent only on K. Unlike the resistivity no scaling is needed.

Figure 6.1 shows the resistivity, R, for various geometries of pipe. The viscosity used is unity. In each case the hydraulic radius is also unity. Figure 6.5 shows the relative size of these configurations, each with hydraulic radius of unity.

Figure 6.2 shows the ratio of effective density to static density under the same conditions as noted above.

To note the sensitivity to the grid type Figure 6.3 and Figure 6.4 are included showing the results of the same variables. The rectangle's grid in Figure 6.3 and Figure 6.4 is uniform whereas in Figure 6.1 and Figure 6.2 the exponential transformation, similar to equation 4.4, is applied to concentrate the nodes near the walls and corners of the pipe. In Figure 6.1 and Figure 6.2 the grids for the trangular and square pipes have approximately twice as many

elements. In both cases the type of spacing of the nodes is the same i.e. the elements are relatively finer to the same degree near the edges.

This indicates, first of all, that the density term is not greatly affected by varying the grid. Second, and more importantly, the resistivity is significantly raised at high frequencies by using a better grid. Thus it should be noted that even though from Figure 6.1 it seems there is satisfactory convergence the program does yield a lower bound to the actual resistivity.

It is interesting to note the ordering of the curves. The order of the resistivity curves is reversed compared to the effective density curves. In addition the order is unrelated to the order of the Biot curves.

6.2 Impedence via Exact Equation

In order to completely specify the acoustic characteristics of a material two independent functions are required. In the previous section these were the resistivity and effective density. A more common method to describe the characteristics is with the complex impedance Z.

The impedance is based on the particle velocity generated by a given sound pressure at the surface of the absorbing material and is defined by

$$Z = P / U \,\big|_{surface} \qquad 6.12$$

In this case the absorbing material is the matrix of parallel pipes and the "surface" is at the open end of the pipes. The other end is assumed to have a rigid terminus to simulate the specimen being mounted against a hard wall.

Appendix A derives the relation between the impedence and the absorption coefficient α as being

$$\alpha = 4\mathrm{Real}(Z) / (|Z|^2 + 2\mathrm{Real}(Z) + 1) \qquad 6.13$$

Lines of constant absorption are shown in Figure 6.6 . When Zr is unity and Zi is zero complete absorption occurs.

Appendix A also contains the derivation of the impedence in terms of the resistivity and effective density. The result is

$$Z = Zo \coth(j\beta L) \qquad 6.14$$

$$Zo = P/U = \left(\frac{\rho_o C^2}{\omega}\right) \quad \beta = \rho_o C\left(\frac{\rho_e}{\rho_o} - j\ R/\rho_o\omega\right)^{1/2} \qquad 6.15$$

This is the exact answer assuming the pipe is of constant cross-section along its length. Figure 6.7 shows the impedence curve using the above exact equation for an isoceles right triangle with hydraulic radius of 0.00023 m.

6.3 Impedence via Acoustic Finite Element

A second finite element program was developed which approximates the pressure distribution along a pipe given the resistivity, effective density, the frequency and the input velocity.

This is done in such a way as to give us the ability to model the pressure distribution in a pipe which varys in area along its axis. This is of some advantage over using the exact equation of the previous section because a pipe of varying area may more closely model a porous material. This is suggested for further work.

The derivation of this program is based on Galerkin's method also. Craggs [2] derives a similar element from variational principles.

The initial equations are the force balance and continuity, respectively

$$- \text{grad } P = (j\, \rho_e \omega + R)\, U \qquad 6.16$$

$$- \frac{j\omega}{\rho C^2} P = \text{div } U \qquad 6.17$$

In matrix form the final equation is

$$\begin{bmatrix} [s] - k^2 \dfrac{\rho_e}{\rho_o} [P] & - k \dfrac{R}{\rho_o C} [P] \\ k \dfrac{R}{\rho_o C} [P] & [s] - k^2 \dfrac{\rho_e}{\rho_o} [P] \end{bmatrix} \begin{Bmatrix} \{P_r\} \\ \{P_i\} \end{Bmatrix} = \frac{1}{\rho_o C} \begin{Bmatrix} \{Q_r\} \\ \{Q_i\} \end{Bmatrix} \qquad 6.18$$

where {Qr} is found from R, the interpolation functions and

the input velocity at the open end of the pipe. The array {Qi} is similar but in the place of R is the product of the effective density and circular frequency. [P] is referred to as the acoustic mass matrix and [S] is the acoustic stiffness matrix.

Appendix D contains the derivation of the above matrices and matrix equation. At first [P] and [S] are derived using only the above equations. However, the varying area can be taken into the calculation of these matrices by introducing the horn wave equation, which is

$$\frac{\partial^2 P}{\partial t^2} = \frac{1}{C^2}\frac{1}{A(x)}\frac{\partial}{\partial X}\left\{\left(\frac{\partial P}{\partial X}\right) A(x)\right\} \qquad 6.19$$

This equation leads to

$$[s] = \int_0^L A_{(x)} \left(\frac{\partial P}{\partial X}\right)^2 dX \qquad 6.20$$

$$[P] = \int_0^L A_{(x)} (P \quad)^2 \ dX \qquad 6.21$$

where L is the element length.

This program was tested with interpolation functions that assume linear variations of the area and pressure between the ends of the elements, for example

$$P(x) = P_1(1 - x/L) + P_2\ x/L \qquad 6.22$$

P_1 is the pressure at the node at x=0 and P_2 is the pressure at the node at x=L.

These interpolation functions resulted in

$$[s] = \frac{A_1+A_2}{12}\begin{bmatrix} 1 & -1 \\ -1 & 1 \end{bmatrix} \qquad 6.23$$

$$[P] = \frac{L}{12}\begin{bmatrix} 3A_1+A_2 & A_1+A_2 \\ A_1+A_2 & A_1+3A_2 \end{bmatrix} \qquad 6.24$$

It is suggested that since the advantage of this program is in modelling porous materials a higher order variation should be used thus eliminating at least the discontinuities of the derivatives of the area. For now it is sufficient to use the linearly varying acoustic elements since the exact equation (used for verification) is only valid for constant area pipe system.

6.4 Results

The results of the acoustic finite element model are compared to the results from the exact equation in Figure 6.7 . In both cases the calculations are based on the case of a triangular pipe of hydraulic radius of 0.23 mm.

The prediction of the model follows the trend of the exact equation less than expected. Craggs [2] derived a similar element but obtained better correlation.

The acoustic finite element (AFE) results are all closer to the point (Zr=1,Zi=0) (at which complete absorption occurs, see Fig. 6.6) than the exact equation.

Comparing Figure 6.7 Figure 6.8 shows that doubling the number of elements does not significantly improve the results. The solution appears to have converged. Better results were expected because Craggs [2] with a similar element (in a slightly different use) obtained good results. Thus the predicted absorption is greater than that of the exact equation.

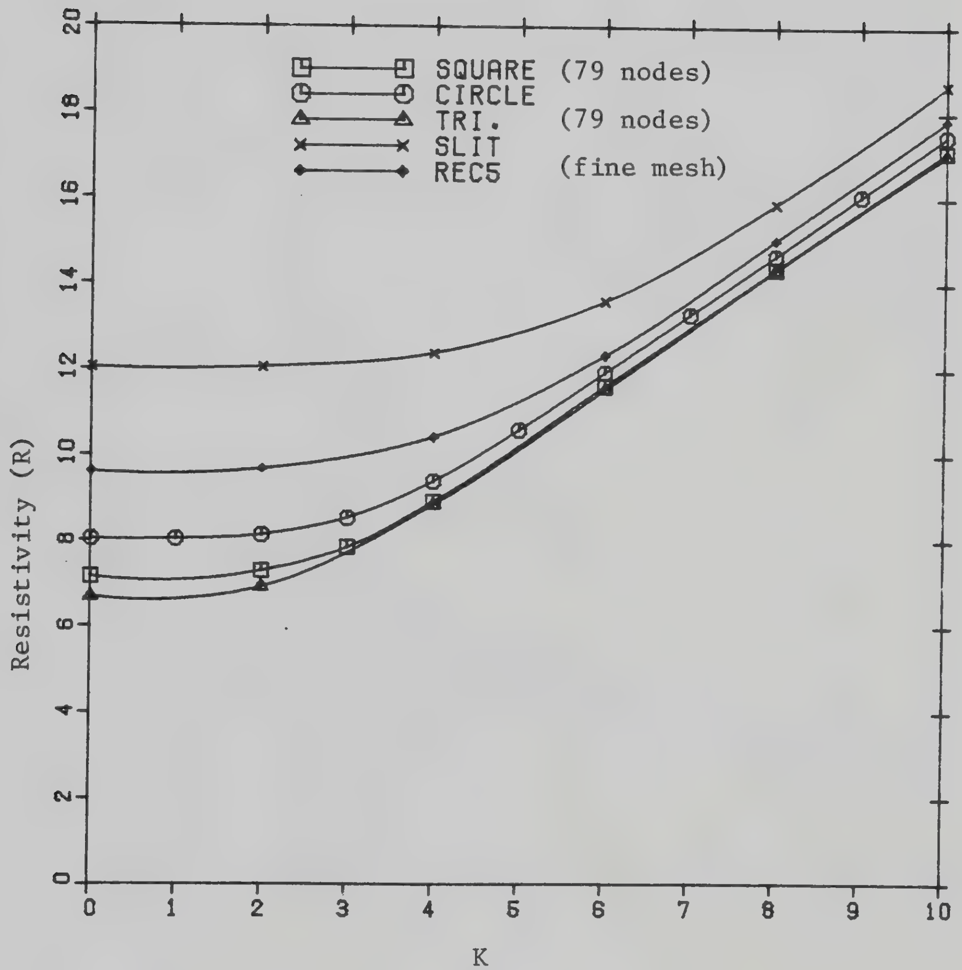

Figure 6.1 Resistivity for various geometries using best meshes. Hydraulic radius is unity for each case.

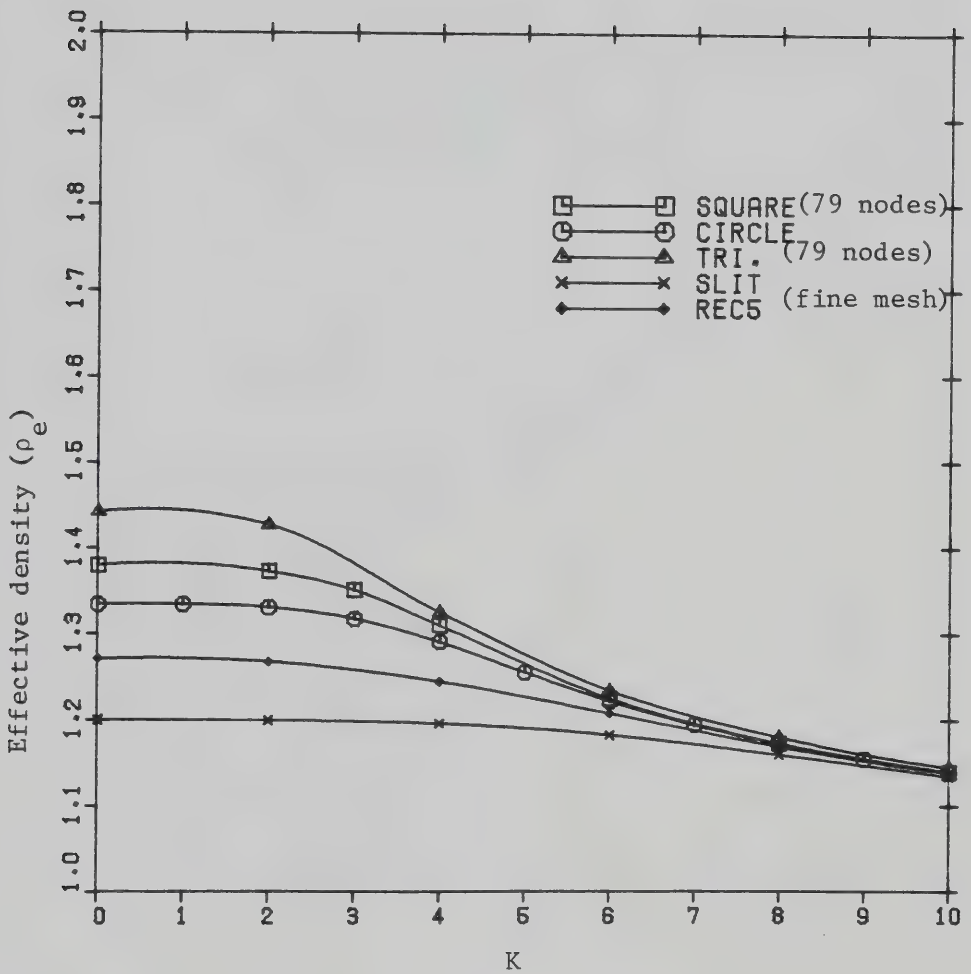

Figure 6.2 Effective density for various geometries using best meshes.

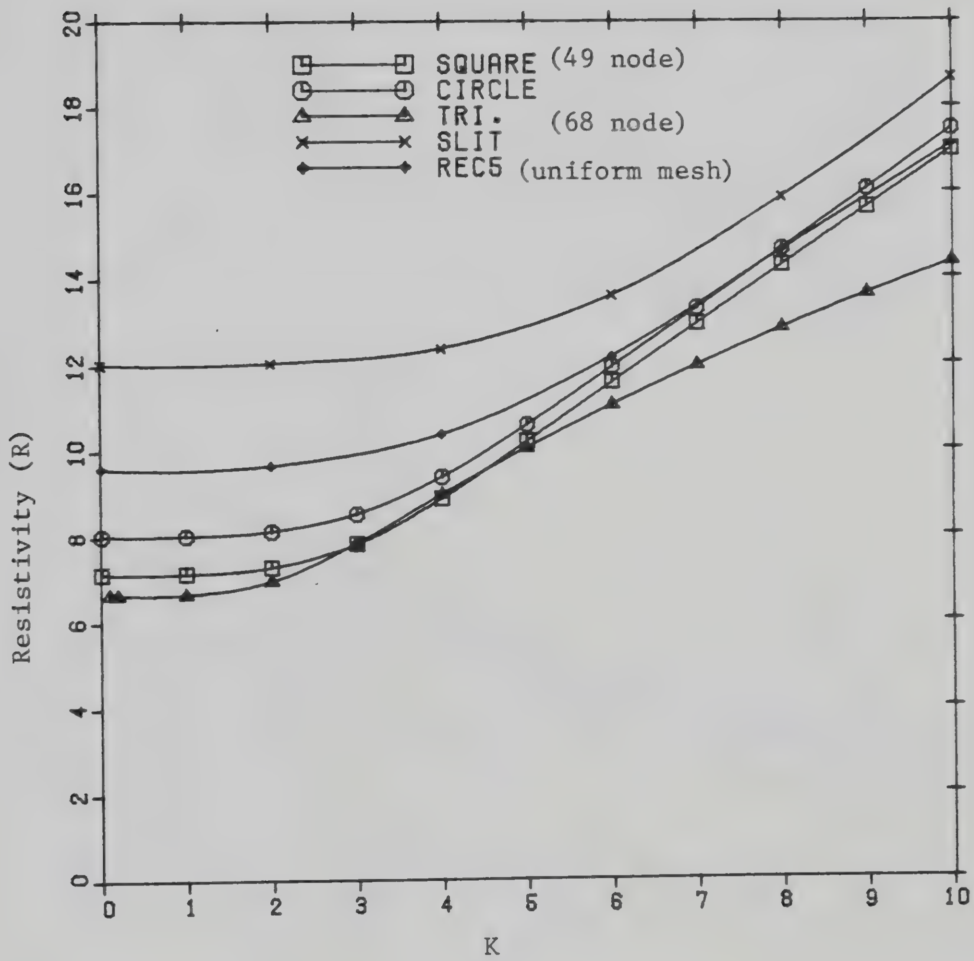

Figure 6.3 Resistivity for various geometries using second best meshes. Hydraulic radius is unity for each case.

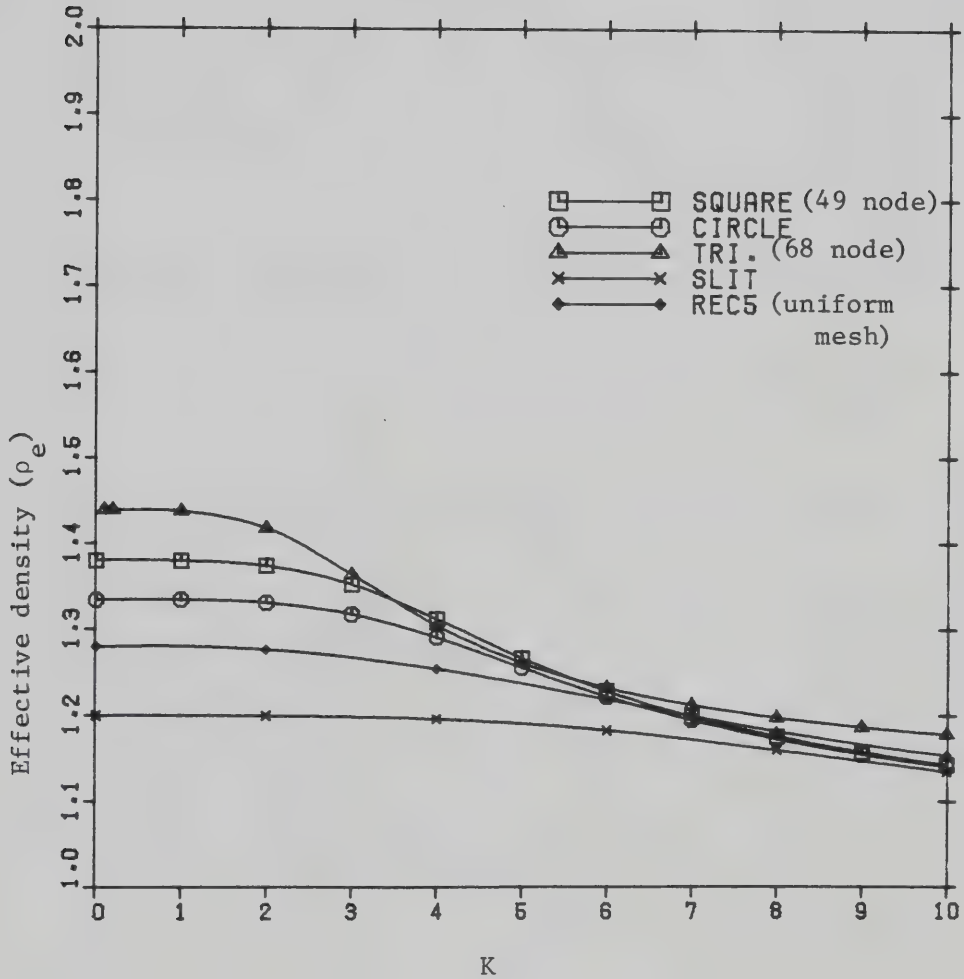

Figure 6.4 Effective density for various meshes using second best meshes.

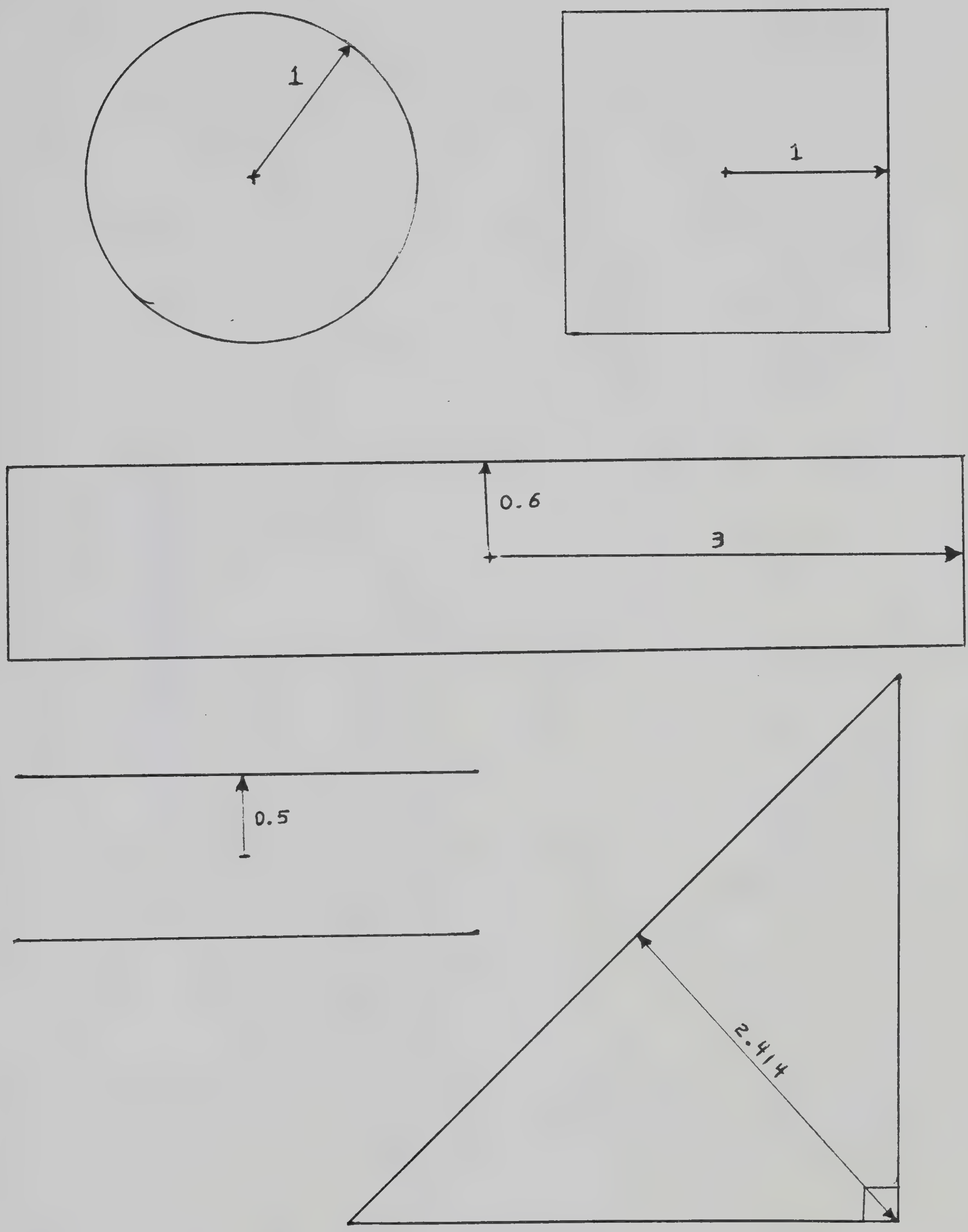

Figure 6.5 Pipe cross-sections scaledto same hydraulic radius.

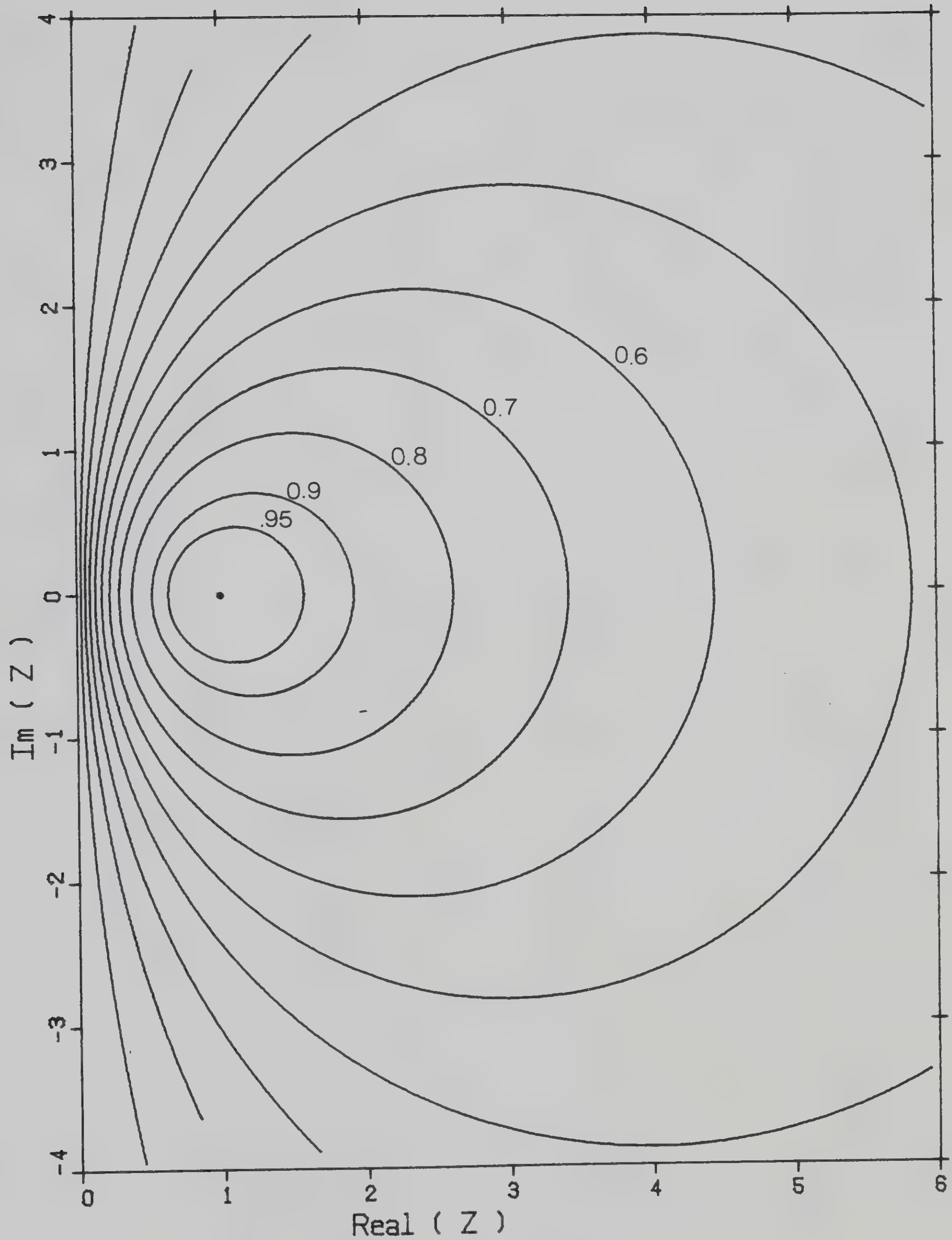

Figure 6.6. Lines of Constant α

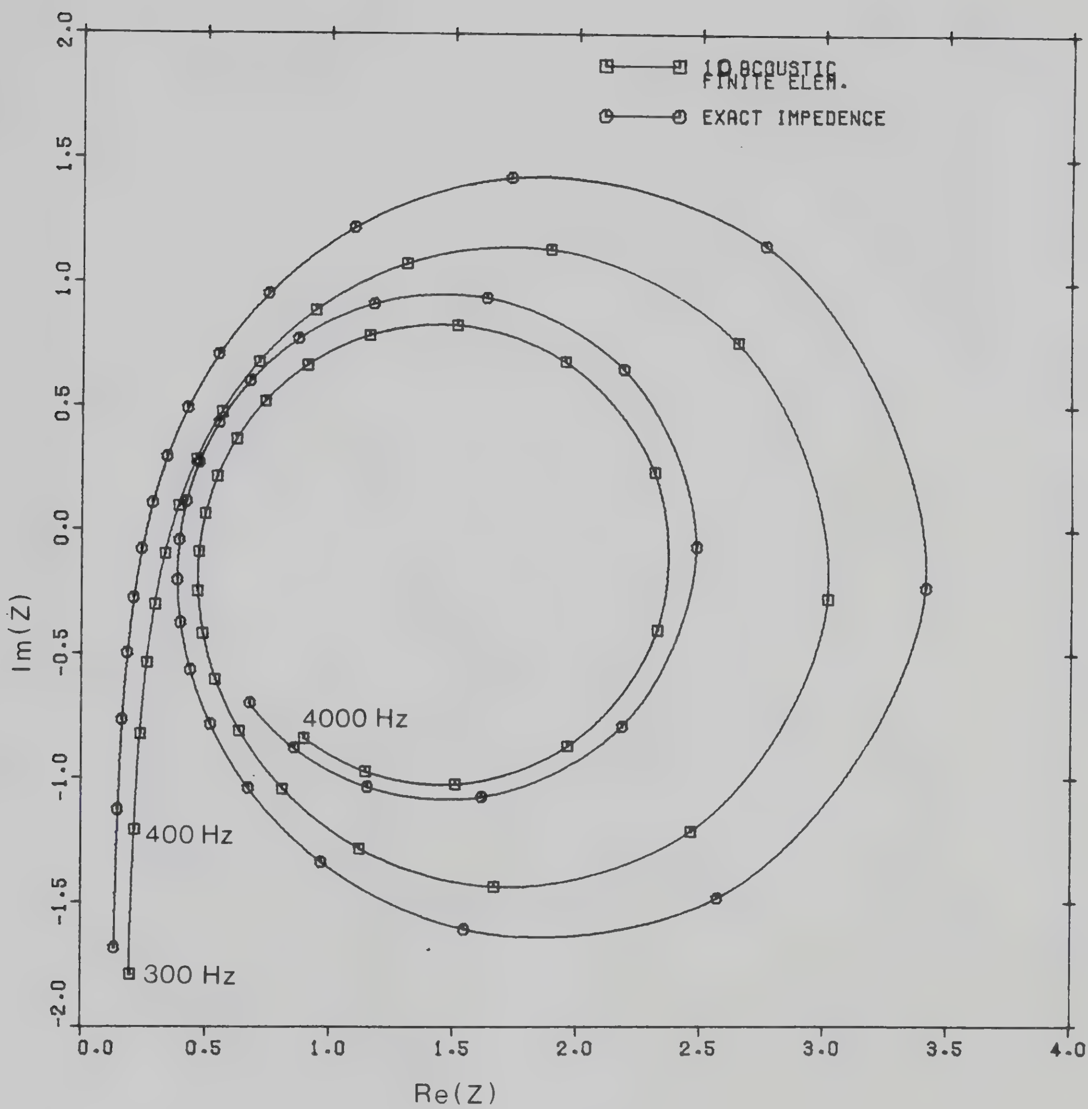

Figure 6.7 Impedence for triangular pipe
(Length = 0.076 m, r_h = 0.0023m)
Calculated via exact equation and acoustic finite elements (10 elements).

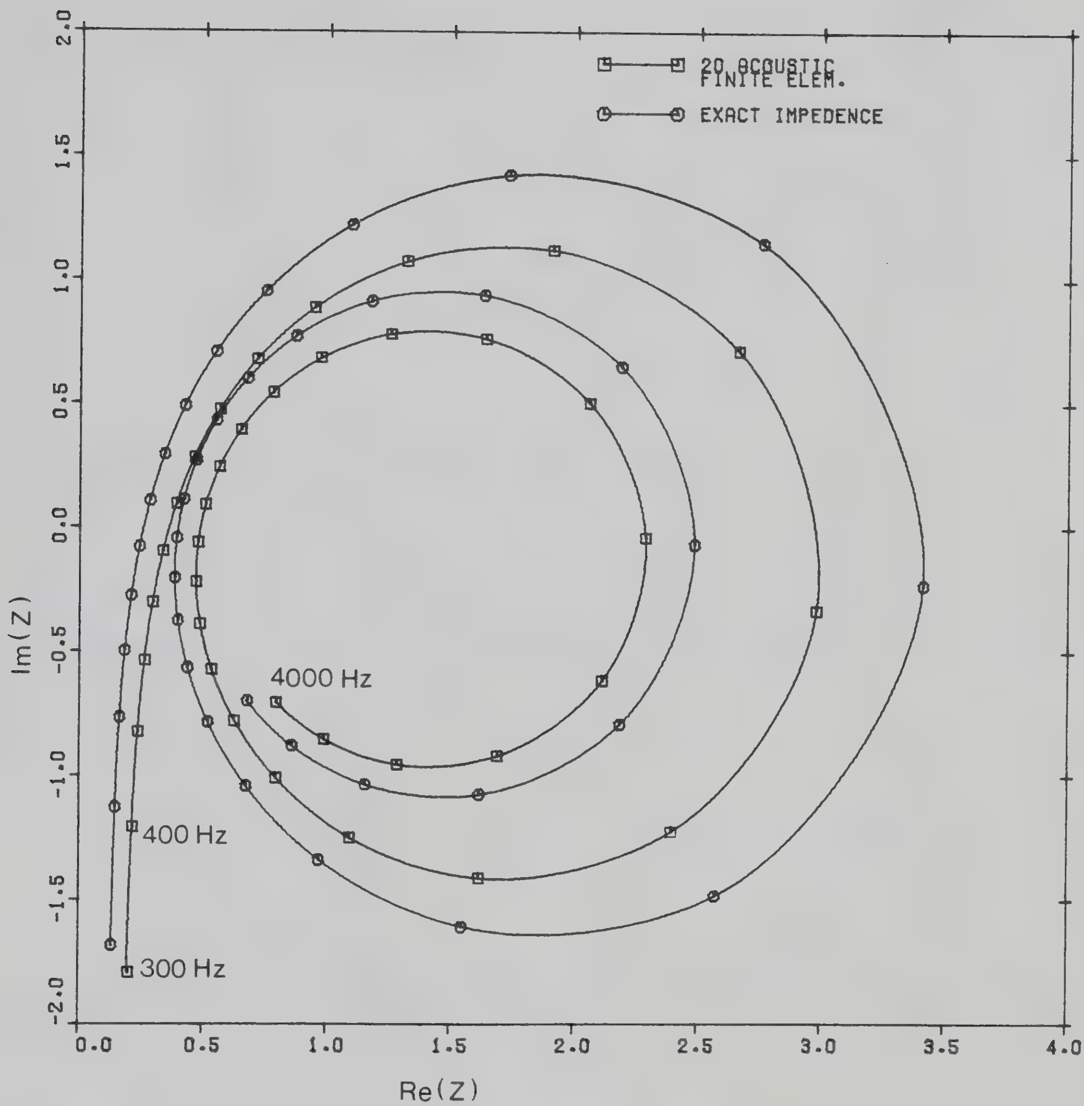

Figure 6.8 Impedence for triangular pipe
(Length = 0.076 m, r_h = 0.0023m)
Calculated via exact equation and acoustic
finite elements (20 elements).

7. Absorption, Theoretical and Experimental

Most of the results obtained by the computer model are not easily verified by experiment, eg. the velocity distribution in a non-circular pipe. There is fortunately a simple, easily repeatable experiment with which to find the impedance and absorption for a porous absorbing material. That is the impedance tube experiment.

7.1 Absorption from the Numerical Model

Our numerical model so far has led to the specific impedance, Z , of a pipe given its length and dimensions of its cross-section. From the specific impedance can be found the absorption (see also Appendix A) via

$$\alpha = 4\,\mathrm{Real}(Z) / (|Z|^2 + 2\mathrm{Real}(Z) + 1) \quad 7.1$$

These results can be compared to the experimental measurement of absorption by a mesh of triangular pipes.

7.2 The Experiment

The apparatus involved in the impedance test is seen in Fig. 7.1(a) and drawn schematically in Figure 7.1(b) .

A plane sound wave, generated by the loud speaker, is reflected by the specimen at the opposite end of the tube. A partial standing wave results in the tube. A microphone attached to a moveable probe finds the maximum

and minimum pressures of the standing wave. From this the absorption can be found, as derived by Kuttruff[12] (and summarized in Appendix A). The absorption α is

$$\alpha = 4(PmaxPmin) / (Pmax+Pmin)^2 \qquad 7.2$$

The distance between the specimen's surface and the first pressure minimum is required to find the phase angle in the reflection factor. Denote this distance by Xmin. The phase angle is

$$\beta = 1 - 4 \frac{X_{min}}{\lambda} \qquad 7.3$$

where λ is the wavelength.

The reflection factor Rf is defined as

$$R_f = |R_f| \exp(j\omega\beta) \qquad 7.4$$

The absolute value of the reflection factor can be found from the maximum and minimum pressure also

$$|Rf| = (Pmax - Pmin) / (Pmax + Pmin) \quad 7.5$$

To find the specific impedence

$$Z = (1 + Rf) / (1 - Rf) \qquad 7.6$$

The dimensions of the impedence tube fix limits on the range of frequencies which can be reliably tested. The

length of the tube must be long enough to permit the formation of at least one maximum and one minimum of the pressure distribution at the lowest frequency of interest. For the following results a tube of approximately 1 meter was used. This set the lower limit around 200 Hz. Actually the results between 0 and 400 Hz are interpolated (at f=0 attenuation is zero). The diameter of the tube set an upper limit on the frequency. For circular tubes the diameter must be less than 0.586 times the wavelength (see Kuttruff [12]). In obtaining the following results a tube with a diameter of 0.05 m was used. This set the upper limit at 4000 Hz.

Kuttruff [12] mentions that since loudspeakers are not generally free from distortion and therefore higher harmonics of the measuring frequency are produced, causing errors, it is recommended to use octave filters to remove the frequencies not desired. This advice was followed.

7.3 The Specimen

The sample used to obtain the experimental results was provided by General Motors Corp.

The specimen is made by laying a sheet of finely corrugated foil on a layer of plane foil and rolling up the two layers. The result is essentially a matrix of parallel, nearly triangular, tubes. See Figures 7.2(a), 7.2(b) and 7.3 . These pipes are described as "nearly triangular" because it is not possible to bend the foil in precisely 90°

corners. There will always be a non-zero radius of curvature at the corners. It is assumed that a typical pipe in the specimen can be modelled by an isoceles right triangle with a hypotenuse of 1.1 mm. This means its hydraulic radius is 0.23 mm. The specimen of Figure 7.2(a) is 76 mm in length and 51 mm in diameter.

For this sample in air the 4000 Hz limit of the test equipment translates to a K of 9.2 in the triangular pipes.

7.4 Results

General Motors Corp. also supplied their own test results for the specimen. Figure 7.4 compares present test results with those supplied. Since the curves are very close to each other it is reasonable to conclude that the repeatability of the impedance tube method is good. In the remaining figures the experimental data is from our test.

Figure 7.5 and Figure 7.6 compare the experimental results to the absorption obtained using the impedance of the exact equation. The only difference between the results of the model is the speed of sound used. The values used are C=290 m/s and C=343 m/s respectively.

The experimental and predicted results compare very well. The slight discrepencies between the results can be broken into two categories; the height difference of the curves and the frequency at which the peak absorption occur. The height difference depends on the length and area of the

pipe, the limitations of the assumtions made on the fluid behavior and the limitations of the numerical calculations. The frequency at which the peaks occur depends on the length of the pipes and the speed of sound in the pipes.

To model the corrugated foil specimen it was assumed that the pipes were similar and could be represented by an isoceles triangle with a hydraulic radius of 0.23 mm. A small error in measuring the hydraulic radius of the pipe would cause an error in the absorption of the same order of magnitude.

In deriving the model of the fluid motion an assumption is made in neglecting the temperature changes so as to allow the use of a constant viscosity. The assumption is that the wall of the pipe maintains a constant temperature and the heat conductivity of the fluid to the wall is perfect, this means isothermal compression and expansion. It can be reasoned that this is closest to the truth at low values of K. At higher values of K the process becomes adiabatic. Increasing K can be thought of as increasing the radius of the pipe, this means the fluid in the center of the pipe can less easily transfer its heat to the wall. With less heat transfer the process becomes adiabatic.

If the compression is isothermal the speed of sound in the pipe is C=290 m/s. The first absorption peak of the numerical model for C=290 m/s is at the same frequency as the experimental data. It can be shown that the frequency at which the peak occurs is proportional to the ratio of the

speed of sound in the pipe and the length of the pipe. Therefore since only the first peak matches with the experimental result this is confirmation that C=290 m/s at low frequencies and the compression is isothermal as assumed. The second peak of the numerical result in Figure 7.5 is left of the experimental peak. This move to the right of the experimental results means the speed of sound is increasing. Figure 7.6 shows the effect of using C=343 m/s for the model.

It is possible to improve the matching of the peaks of the absorption curve by using empirical relations to determine the speed of sound at various frequencies. For this sample this would become more important at frequencies above about 3000 Hz.

Lamb [13], in a proof which is a variation of that given by Lord Rayleigh [15], derives the decay of a wave in a circular pipe considering viscous effects only. He mentions that a more complete investigation was provided by Kirchhoff [11] in which thermal processes are considered, as well as viscosity. Lamb [13] compares the different results of decay and states that the decay is increased by considering thermal processes but remains of the same order of magnitude.

No consideration is made in this model to account for dissipation due to thermal effects or the viscosity changes either across the pipe or with respect to the cycle. These considerations are neglected by the assumption of constant

temperature at all time. This assumption is likely the largest single factor responsible for the deviation of the absorption of the model from experimental results. The assumption, as mentioned, is best at low K as evidenced by the experimental absorption increasing faster with frequency than the absorption of the model.

Another factor to consider is the limitation of the numerical technique. When comparing the resistivity curves of a particular pipe modelled with different grids, in chapter 6, it was noted that the model produces a lower bound on the resistivity. In addition the accuracy decreased with frequency producing a much lower bound in the case of a crude mesh. Thus the calculated absorption will be a lower bound and will be further from the experimental data at higher frequencies.

At higher frequencies there are two factors causing drift in the same direction, the lack of thermal effects and the limitations of the mesh. A number of meshes were compared and the one used to generate the final data seemed to be very close to a converged answer. Therefore it is felt that most of the error, albeit small, is due to the lack of consideration of thermal effects.

A point of discussion on the absorption obtained from the model is why the height of the absorption curve is greater for C=290 m/s than for C=343 m/s. From the theory, the only influence the speed of sound has is on the location of the peaks, rather than the value of the absorption.

In conclusion, from these comparisons with the results of the experiment it seems the integrity of the analysis is very good.

(a) Testing Equipment.

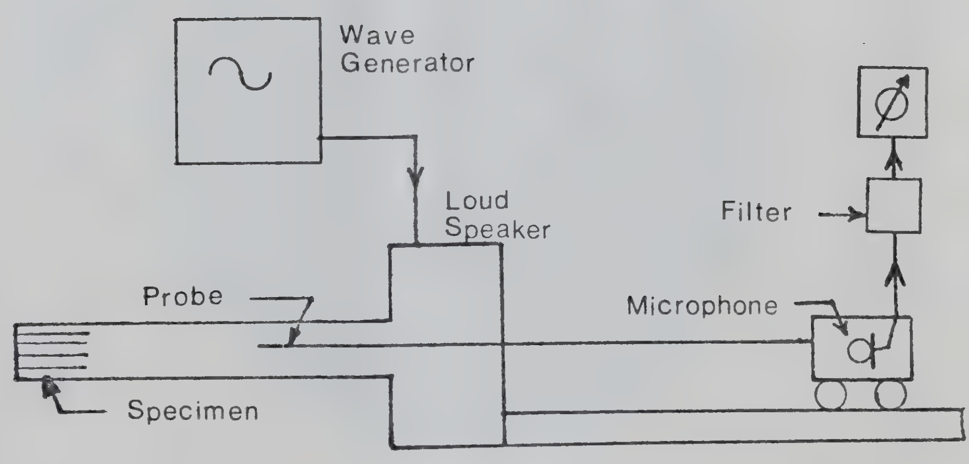

(b) Schematic of Testing Equipment

Figure 7.1 Testing Equipment

a) Scale 4:5

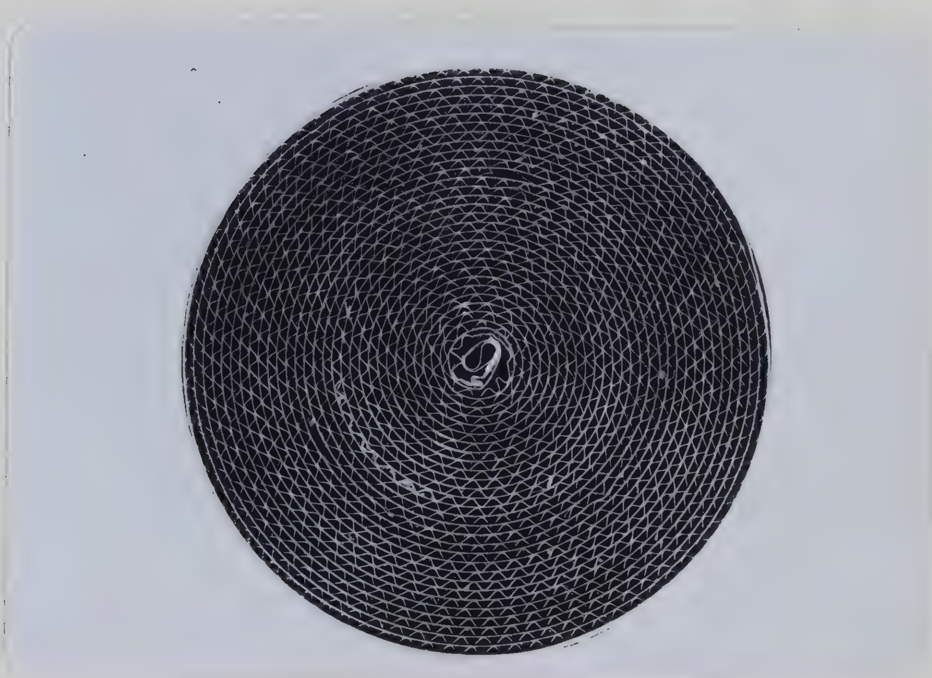

b) Scale 3:2

Figure 7.2 Specimen

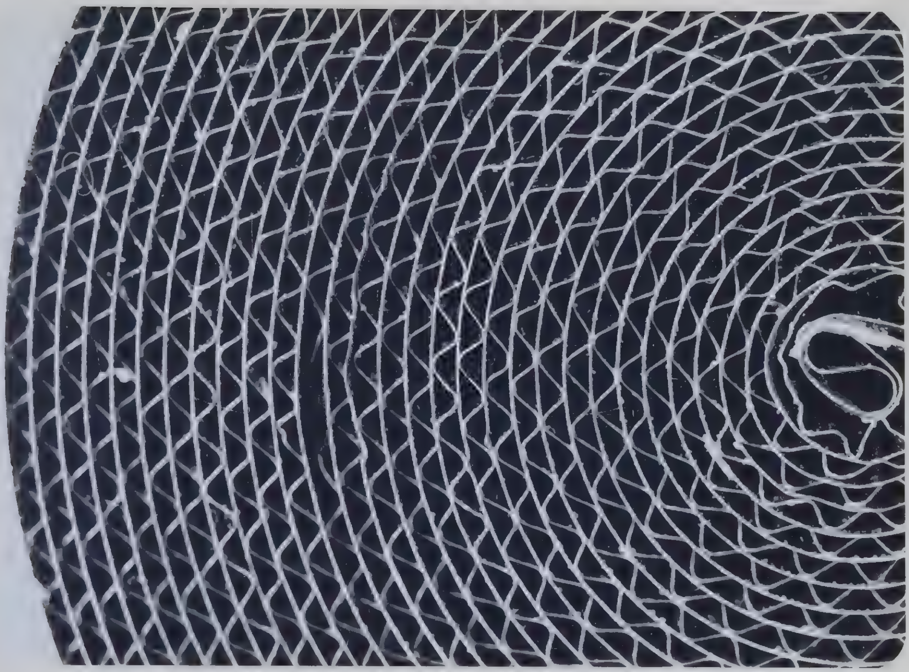

Figure 7.3 Specimen Scale 2.25

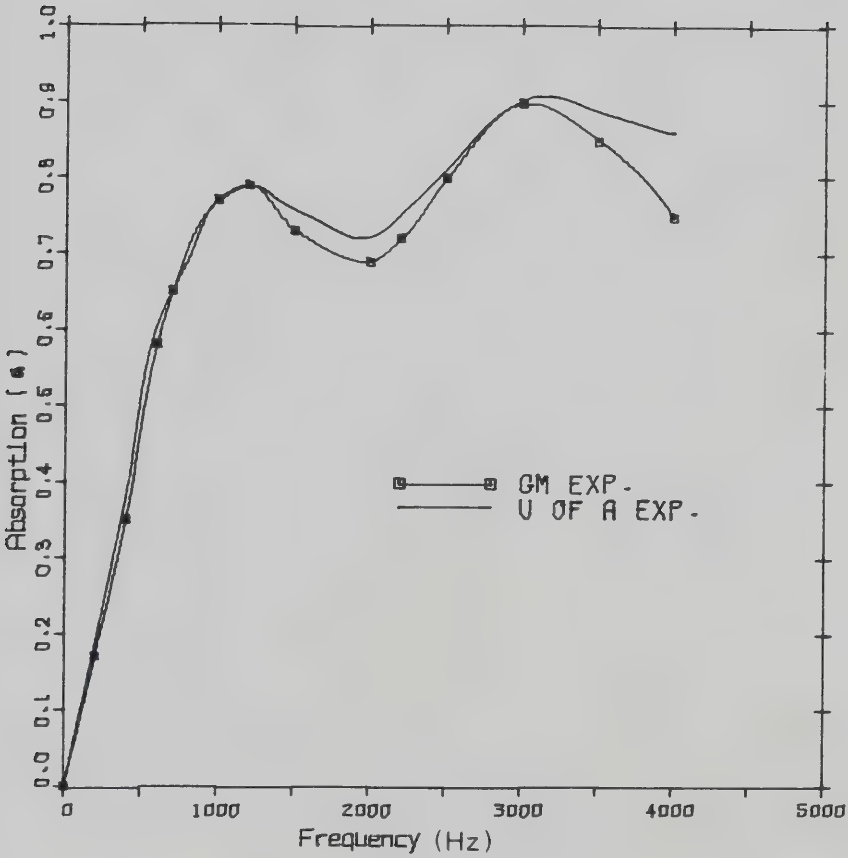

Figure 7.4 Absorption (exp.)

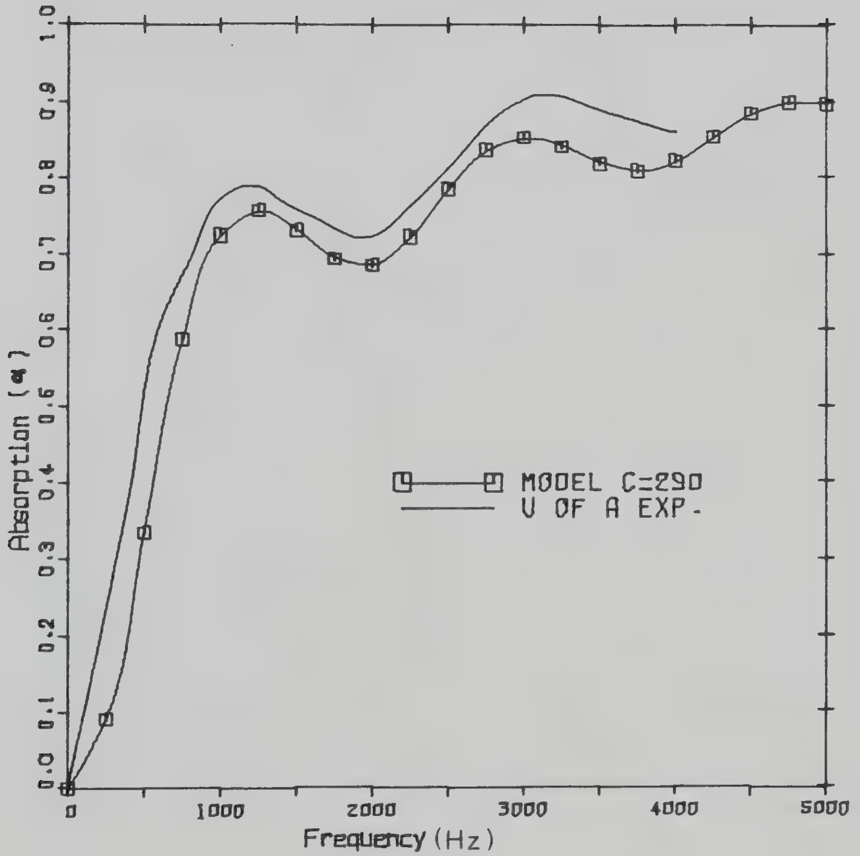

Figure 7.5 Absorption

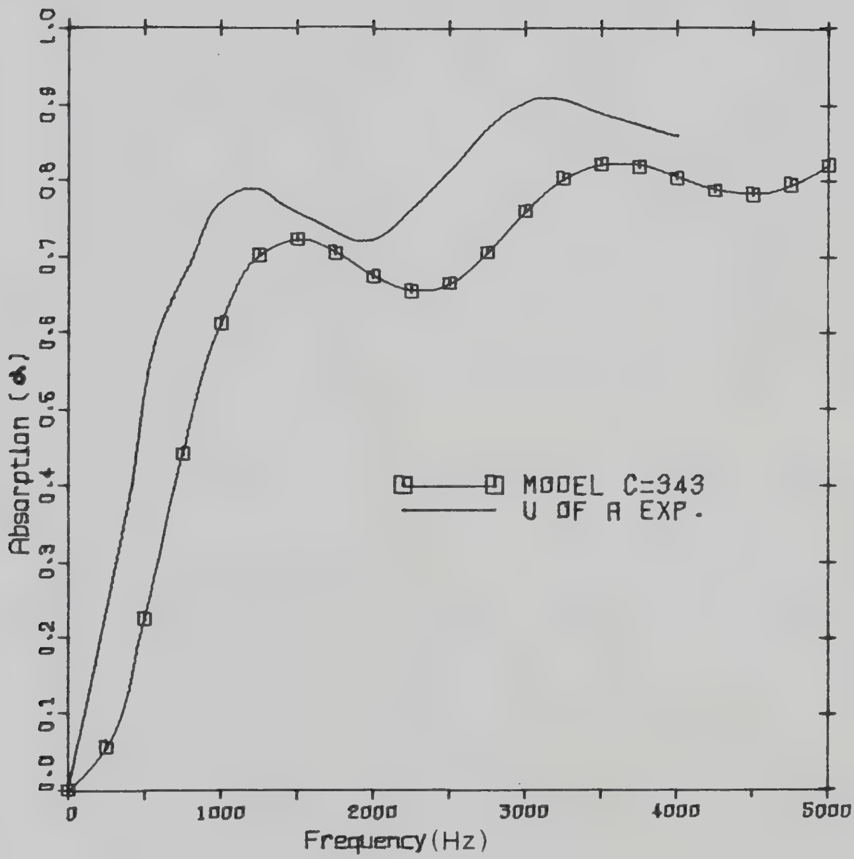

Figure 7.6 Absorption

8. Discussion and Summary

8.1 Method of Solution

In defining the problem, necessary assumptions are made to reduce the problem to a manageable form. The Finite Element Method was chosen to solve the defined problem. This method is relatively new to the solution of fluid motion problems. Most of its use is in the field of solid mechanics. The terms 'stiffness matrix' and 'mass matrix' originating in solid mechanics have been adopted here because of the analogous use and behavior of the fluid motion to structural motion.

The method of solution initially had the requirement that it must be able to handle any shape of domain. It was later found that for efficiency it also must possess the flexibility of concentrating on the solution near the edges of the domain. The Finite Element Method is thus particularly applicable to this problem. Fairly good results can be easily obtained on existing computing systems.

In defining the problem an assumption is made about the form of the pressure wave being harmonic. This assumption is of convenience, not necessity. Even with this assumption the solution for an arbitrary input pressure function could be found by adding the solutions of its component frequencies and amplitudes similar to Fourier series of wave forms because the governing equation is linear. If for some reason

this procedure is not desired it is valid to begin with the differential equation (Equation 2.2) and define interpolation functions with a dimension in time i.e., Ni=Ni(y,z,t) and input nodal pressure gradients as a function of time. This might be the best way to find the velocity distribution due to a pressure gradient which is, for example, triangular with time.

Galerkin's method is used to derive the matrix equations. This method of approximation is powerful, relatively simple and can be applied to any linear or non-linear governing equation. The equations resulting from the Galerkin's method are the same as those from the variational principle. [1]

Galerkin's method was chosen first to benefit from its advantages but also in order to become familiar with a technique which is readily applicable to many problems.

This analysis produces an approximate solution to the velocity profile in any shaped pipe at any reasonable frequency and at any time in the cycle of the periodic pressure gradient. These results can be directly and easily used to find the shear forces on the pipe wall, the stress state of a bar in torsion, as well as the acoustic properties. These properties include the resistivity and

----

[1] Galerkin's method would produce different equations, though still valid, from Lagrange's equations if the original equation had been multiplied throughout by an arbitrary factor. However, in mechanical problems there is an optimum way of applying Galerkin's method which renders it equivalent to the use of Lagrange's equation(See Ref 6).

effective density, and, given the pipe length, the impedance and absortion.

8.2 Conclusions

The major points to be noted are:

1) The principle of similarity can be applied to the resistivity results so that the acoustic properties of most configurations and any size of pipe can be determined from the information presented. The effective density results do not require scaling.
2) The correlation of the experimental data to the finite element data is very good.
3) For the cases of resistivity and absorption the program gives a lower bound to the solution. This is most relevant when using results from a relatively crude mesh.
4) At K=0, the solution is applicable to finding the stress state in prismatic bars subjected to torsion.
5) Accuracy is most dependent on concentration of nodes near the pipe wall.
6) The Acoustic Finite Element can be used to model impedance of a pipe with varying area along the axis.
7) The analysis and method of solution have been verified by experiment. Problems with similar assumptions, governing equation and boundary conditions can be solved with confidence via this method.

8) Some improvement could be made in the model by accounting for the influence of thermal processes in the decay of the wave.

References

1) BIOT, M.A., "Theory of Propagation of Elastic Waves in a Fluid-Saturated Porous Solid . II Higher Frequency Range", J. Acoustical Society of America, vol 28, no.2, 1956.

2) CRAGGS, A., "A Finite Element Model for Rigid Porous Materials", J. Sound and Vibrations, 61(1), 101-111, 1978.

3) CRANDALL, I.B., "Theory of Vibrating Systems and Sound", D. Van Nostrand Inc., NY, 1926.

4) CREMER,L."Die Wissenschaftlichen Grundlagen der Raumakustik", Vol.III, Section 45, Leipzig, 1950

5) DINNIK, A.N., "Galerkin's Method for Determining the Critical Strengths and Frequencies of Vibrations", Aeronautical Engineering USSR, vol 9, no 5, p99, 1935.

6) DUNCAN, W.J., "Galerkin's Method in Mechanics and Differential Equations", R & M 1798, 1935.

7) FRAZER, R.A., DUNCAN, W.J., and COLLAR, A.R., "Elementary Matrices", Cambridge, 1963.

8) FRAZER, R.A., JONES, W.P., and SKAN, S.W., "Approximations to Functions and to the Solutions of Differential Equations", R & M 1799, 1938.

9) GROSSMAN, E.P., "The Twist of a Monoplane Wing", Transactions of the Central Aero-Hydrodynamical Institute, Moscow, No 253, 1936.

10) HUEBNER, K.H., "The Finite Element Method for Engineers", John Wiley & Sons Inc., NY, 1975.

11) KIRCHHOFF Pogg. Ann. Vol CXXXXIV., p177, 1868

12) KUTTRUFF, H., "Room Acoustics", Applied Science Publishers Ltd., London, 1973.

13) LAMB, H., "The Dynamical Theory of Sound", 2nd ed., Dover Publications, Inc., NY, 1960. (Edward Arnold Ltd., London, 1925).

14) McDONALD, D.A., "Blood Flow in Arteries", Edward Arnold Ltd., London, 1974.

15) RAYLEIGH, J.W.S., "The Theory of Sound", vol 2, Dover Publications Inc.,1945.

16) SCHLICHTING, H., "Boundary Layer Theory", McGraw-Hill, NY, 1968.

17) SOKOLNIKOFF, I.S., "Mathematical Theory of Elasticity", McGraw-Hill, NY, 1956.

18) TIMOSHENKO, S., and GOODIER, J.N., "Theory of Elasticity", McGraw-Hill, NY, 1951.

19) ZWIKKER, C. and KOSTEN, C.W., "Sound Absorbing Materials", Elsevier Publishing Co. Inc., NY, 1949.

Appendix A, Acoustic Properties Equations

This section will show the steps for deriving the absorption of a wall in terms of the specific impedance and in terms of the maximum and minimum pressures(to be used for the impedance tube experiment).

Assume that the wall is at x=0, the wave is travelling parallel to the X axis and the wave direction is normal to the wall. If the incident wave is coming from the negative X direction its sound pressure is

$$Pi(x,t)=\hat{P}o.\exp[j(\omega t-kx)] \qquad A.1$$

For a plane wave moving in the positive X direction

$$\frac{\partial P}{\partial X} = -\rho\frac{\partial U}{\partial t} \qquad A.2$$

Therefore, the particle velocity of the wave is given by

$$\vec{U}_{(x,t)} = \frac{\hat{P}_o}{\rho_o C}\exp\{j(\omega t-kX)\} \qquad A.3$$

For the reflected waves

$$P_{(x,t)} = R_f\ \hat{P}_o\ \exp\{j(\omega t + kX)\} \qquad A.4$$

where Rf is the reflection factor,

$$\overleftarrow{U}_{(x,t)} = -R_f\frac{\hat{P}_o}{\rho_c}\ \exp\{j(\omega t + kX)\} \qquad A.5$$

$$R_f = |R_f| \exp(j\beta) \qquad \text{A.6}$$

Both $|Rf|$ and β can be found from the impedance tube as described near the end of this section. The reflection factor is a property of the wall and describes both the attenuation and phase change of the reflected wave.

The total sound pressure and particle velocity in the plane of the wall are obtained by simply adding the expressions for the incident and the reflected waves and setting x=0

$$P_{(o,t)} = \hat{P}_o(1 + R_f) \exp(j\omega t \qquad \text{A.7}$$

$$U_{(o,t)} = \frac{\hat{P}_o}{\rho_o C} (1 - R_f) \exp(j\omega t) \qquad \text{A.8}$$

P(0,t) divided by u(0,t) gives the impedance

$$\rho_o C\ Z = \frac{P_{(o,t)}}{U_{(o,t)}} = \rho_o C \quad \frac{1 + R_f}{1 - R_f} \qquad \text{A.9}$$

Conversely

$$R_f = \frac{Z - 1}{Z + 1} \qquad \text{A.10}$$

where Z is the specific acoustic impedance.

Since the intensity of a wave is proportional to the square of the pressure amplitude and the absorption coefficient α is the loss of incident intensity on reflection it follows that

$$\alpha = 1 - |R_f|^2 \qquad \text{A.11}$$

Substituting eqn A10 into eqn A11 gives

$$\alpha = \frac{4\ \mathrm{Re}(Z)}{|Z|^2 + 2\ \mathrm{Re}(Z) + 1} \qquad \text{A.12}$$

The relation between the absorption coefficent and the specific impedance can be seen in Fig. 6.6.

The distribution of the sound pressure in the standing wave due to the wall is found by adding eqn 1 and eqn 4 and taking the absolute value

$$P_{(X)} = \hat{P}_o\{1 + |R_f|^2 + 2|R_f| \cos(2kX + \beta)\}^{1/2} \qquad \text{A.13}$$

The pressure amplitude varies periodically between

$$P_{max} = \hat{P}_o(1 + |R_f|) \qquad \text{A.14}$$

and

$$P_{min} = \hat{P}_o(1 - |R_f|) \qquad \text{A.15}$$

The distance between maxima is half the wavelength.

From equations A11, A14 and A15,

$$|R_f|^2 = \frac{P_{max} - P_{min}}{P_{max} + P_{min}} \qquad \text{A.16}$$

$$\alpha = \frac{4\ P_{max} - P_{min}}{(P_{max} + P_{min})^2} \qquad \text{A.17}$$

In the impedance tube it is easy to measure the minimum and maximum pressures as well as the distance between the surface of the test specimen and the first pressure minimum. This is all the informatiom necessary to determine the wall impedance.

From eqn 13 the first minimum occurs when $\cos(2kx+r)=-1$. Denoting the minimum distance which satisfies this condition by Xmin the phase angle β (of eqnA6) is found from

$$\beta = (1 - 4\,\frac{X_{min}}{\lambda}) \qquad \text{A.18}$$

where lamda,λ,is the wavelength=c/(frequency)
Thus the absorption, reflection factor and the impedence of the sample can be obtained from the impedence tube. The following, from Craggs [2], shows how the impedence can be derived in terms of the resistivity and effective density.

The exact solution for the input impedance, Z, of a column of absorption material of length l with a rigid termination is given by Zwikker and Kosten(19) as $Z=Zo.\coth(jlk)$, where Zo is the characteristic impedance and

k is the complex propagation constant. The quantities Zo and k may be obtained considering the one dimensional form of the equilibrium and continuity equations, as shown by Kuttruff(12)

$$-\frac{\partial P}{\partial X} = \rho_e \dot{\overline{U}} + R\,\overline{U} \qquad \text{A.19}$$

$$\frac{-1}{C^2 \rho_o} \frac{\partial P}{\partial t} = \frac{\partial U}{\partial X} \qquad \text{A.20}$$

and then substituting the following relationships for a plane harmonic progressive wave

$$jK\hat{P} - (j\omega\rho_e + R)\,\hat{U} = 0 \qquad \text{A.21}$$

$$-\left(\frac{j\omega}{\rho_o C^2}\right)\hat{P} + j\,K\,\hat{U} = 0 \qquad \text{A.22}$$

For a non-trivial solution the determinent must be zero.

$$\begin{vmatrix} jK & -(j\omega\rho_e + R) \\ -\dfrac{j\omega}{\rho_o C^2} & jK \end{vmatrix} = 0 \qquad \text{A.23}$$

This gives

$$K = \frac{\omega}{C}\left(\frac{\rho_e}{\rho_o} - \frac{jR}{\rho_o \omega}\right)^{1/2} \qquad \text{A.24}$$

and

$$Z_o = P/U = \frac{\rho_o C^2}{\omega} K = \rho_o C\left(\frac{\rho_e}{\rho_o} - \frac{jR}{\rho_o \omega}\right)^{1/2} \qquad \text{A.25}$$

Appendix B, Fluid Finite Elements

This appendix is to provide the discussion of the steps necessary to reproduce the finite element solutions or provide a basis on which to build extensions of the analysis.

The momentum balance governing equation is

$$-\frac{\partial P}{\partial X} = \rho \ \frac{\partial U}{\partial t} - \nabla^2 U \qquad \text{B.1}$$

From the wave equation we find the satisfactory form of a harmonic wave

$$P = \hat{P}.\exp(j(wt-kx)) \qquad \text{B.2}$$

Substituting a velocity of this same form into eqn B1 gives

$$-\frac{\partial P}{\partial X} = j\rho\omega U - \nabla^2 U$$

Applying the method of weighted residuals we approximate U by $\tilde{U}$. The error introduced by this approximation is the residual, ε

$$\frac{\partial P}{\partial X} + j\rho\omega \tilde{U} - \nabla^2 \tilde{U} = \varepsilon \qquad \text{B.3}$$

Let us assume $\tilde{U}$ to be in the form

$$U \simeq \tilde{U} = \sum_{i=1}^{r} NiCi \qquad B.4$$

Ni are interpolation functions, Ci are the unknown field variables to be found. Ci are velocities at the r points in the domain if linear interpolation functions are used.

If the order of the interpolation functions is increased, Ci must include derivatives of the field variable. In the following solution let Ci=Ui.

To make the residual small in some sense we may set the total error to zero, i.e.

$$\int \varepsilon \, dA = 0 \qquad B.5$$

But to solve for the r unknowns we use r independent weighting functions in the above integral, i.e.

$$\int \varepsilon \, Wi \, dA = 0 \qquad B.6$$

Galerkin's criterion specifies that the weighting functions should be the same as the interpolation functions. Therefore, applying this to our governing equation (B2) Galerkin criterion gives

$$\int Ni \left\{ \frac{\partial P}{\partial X} + \rho_o \, \omega \, j \, \tilde{U} - \nabla^2 \tilde{U} \right\} dA = 0 \qquad B.7$$

Integrating term by term we define {P} and [M] by

$$\int \frac{\partial P}{\partial X} \{N\} \, dA = \{P\} \qquad \text{B.8}$$

$$\rho_0 \omega \int \{N\} \lfloor N \rfloor \, dA \, \{U\} = \rho_0 \omega [M] \{U\} \qquad \text{B.9}$$

The method of weighted residuals requires that the order of the interpolation functions must be the same as the highest order in the equation to be solved. Thus to reduce the order of our equation we integrate the Laplacian on $\tilde{U}$ by parts. This, in most cases, conveniently introduces the boundary conditions as well as reduces the required order of the interpolation so that linear variation between unknowns may be assumed.

$$-\mu \int Ni \nabla^2 U \, dA = -\mu \int \left(Ni \frac{\partial^2 U}{\partial Z^2} + Ni \frac{\partial^2 U}{\partial Y^2}\right) dA$$

$$= -\mu \oint \left(Ni \frac{\partial U}{\partial Z} n_z + Ni \frac{\partial U}{\partial Y} n_y\right) dS \qquad \text{B.10}$$

$$-\mu \int \left(\frac{\partial Ni}{\partial Z} \frac{\partial U}{\partial Z} + \frac{\partial Ni}{\partial Y} \frac{\partial U}{\partial Y}\right) dA$$

$$= -\mu \int \left(\left\{\frac{\partial N}{\partial Z}\right\} \left\lfloor \frac{\partial N}{\partial Z} \right\rfloor + \left\{\frac{\partial N}{\partial Y}\right\} \left\lfloor \frac{\partial N}{\partial Y} \right\rfloor\right) dA \, \{U\}$$

The surface integrals become zero since the boundary condition requires U=0 on the boundary of the pipe. For convenience let

$$\mu \int [\{\frac{\partial N}{\partial Z}\} \lfloor \frac{\partial N}{\partial Z} \rfloor + \{\frac{\partial N}{\partial Y}\} \lfloor \frac{\partial N}{\partial Y} \rfloor]\, dA\, \{U\} = \mu [D]\, \{U\} \qquad B.11$$

Now in the condensed notation we may write

$$\{P\} = (\mu[D] + j\rho_o\omega\, [M])\, \{U\} \qquad B.12$$

and taking on the notation of chapter 2

$$\begin{Bmatrix} \{P\} \\ \\ \{F\} \end{Bmatrix} = \left(\mu \begin{bmatrix} [D_{ff}] & \vdots \\ \cdots & + \\ [D_{cf}] & \vdots \end{bmatrix} + j\rho_o\omega \begin{bmatrix} [M_{ff}] & \vdots \\ \cdots & + \\ [M_{cf}] & \vdots \end{bmatrix} \right) \begin{Bmatrix} \{U\} \\ \\ \{U_o\} \end{Bmatrix} \qquad B.13$$

The solution of U now involves solving the above complex matrix equation. The variables {P}, {F} and {U} are complex as well as the term in the round brackets.

Some computing facilities cannot easily solve for variables comprised of real and imaginary values. In order to solve for variables with only real parts we take the example of solving for U in the above equation

$$\{P\} = (\mu[D_{ff}] + j\rho_o\omega\, [M_{ff}])\{U\} \qquad B.14$$

Breaking the variables into

$$\{P\} = \{P_r + jPi\} \qquad B.15$$

$$\{U\} = \{U_r + jUi\} \qquad B.16$$

and substituting this into equation (B.) yields

$$\{Pr + jPi\} = (\mu[D_{ff}] + j\ \rho\omega[M_{ff}])\ \{Ur + jUi\} \qquad B.17$$

Multiplying term by term and separating the real terms into one equation, the imaginary terms into another gives, respectively

$$\{Pr\} = \mu[D_{ff}]\{Ur\} - \rho_o\omega[M_{ff}]\{Ui\} \qquad B.18$$

$$\{Pi\} = \rho_o\omega[M_{cf}]\{Ur\} + \mu[D_{cf}]\{Ui\} \qquad B.19$$

This is the equivalent of

$$\begin{Bmatrix} Pr \\ Pi \end{Bmatrix} = \begin{bmatrix} \mu[D_{ff}] & -\rho_o\omega[M_{ff}] \\ \rho_o\omega[M_{ff}] & \mu[D_{ff}] \end{bmatrix} \begin{Bmatrix} Ur \\ Ui \end{Bmatrix} \qquad B.20$$

and we have eliminated j from the equations. Treating the shear force portion of equation (B.13) similarly gives

$$\begin{Bmatrix} Fi \\ Fi \end{Bmatrix} = \begin{bmatrix} \mu[D_{cf}] & -\rho_o\omega[M_{cf}] \\ \rho_o\omega[M_{cf}] & \mu[D_{cf}] \end{bmatrix} \begin{Bmatrix} Ur \\ Ui \end{Bmatrix}$$

At this point it is necessary to choose interpolation functions to solve for [M], [D] and {P}. For this work the

chosen interpolation functions assume linear variation of the dependent variable between nodes. This means that the only unknowns at each node is the velocity i.e. consideration of derivatives is not required.

Generalized coordinates were tried but this system does not work for some orientations of the elements. This problem was circumvented by adopting a natural coordinate system. See Huebner [2] for details.

On comparing the results of the two methods it was noticed that for most elements the elemental matrices produced by one method are entirely different from those of the second method. Only for elements that are square in the YZ plane are the elemental matrices identical. In spite of the different elemental results the two methods produced identical velocity profiles.

Appendix C, Biot Equation

The following is a summary of the work done by M.A. Biot [1].

Biot [1] considers the case of two parallel plates as well as a pipe of circular crosssection. This summary contains only the case of a circular pipe.

Consider only the two-dimensional motion and neglect all pressure gradients and velocity components normal to the boundaries. The x direction is parallel to the boundaries and the r direction is normal to it with the boundaries being r=a. Let the walls be rigid and stationary. The X component of the velocity is u(r).

The equation of motion is

$$\frac{\partial P}{\partial X} = - \rho_o \frac{\partial U}{\partial t} + \mu \nabla^2 U \qquad \text{C.1}$$

where ρ is the fluid density and ∇^2 is the Laplacian operator. The operator in this case reduces to

$$\nabla^2 = \frac{\partial^2}{\partial r^2} + \frac{1}{r} \frac{\partial}{\partial r} \qquad \text{C.2}$$

Thus the above equation becomes

$$\frac{\partial P}{\partial X} = - \rho_o \frac{\partial u}{\partial t} + \mu \left(\frac{\partial^2 u}{\partial r^2} + \frac{1}{r} \frac{\partial u}{\partial r} \right) \qquad \text{C.3}$$

All quantities are sinusoidal function of time containing a

factor $e^{j\omega t}$. Rewriting C.3 without this factor,

$$\frac{\partial P}{\partial X} = - j\rho\omega U + \mu \frac{\partial^2 u}{\partial r^2} + \mu \frac{1}{r}\frac{\partial u}{\partial r} \qquad \text{C.4}$$

This is Bessels differential equation for U. The solution for U, remembering U is finite at r=0 and the boundary condition U=0 at r=a, is

$$U\left(\frac{j\omega}{\partial P/\partial X}\right) = 1 - \frac{J_o[j(\frac{j\omega\rho}{\mu})^{1/2}\ r\ ]}{J_o[j(\frac{j\rho\omega}{\mu})^{1/2}\ a]} \qquad \text{C.5}$$

Note that the acoustic Reynolds number $K=a(\frac{AU}{\mu})^{1/2}$ can be seen in the denominator.

Deriving the correction function requires the average velocity, which reduces to

$$U_{ave}\left(\frac{j\omega}{\partial P/\partial X}\right) = 1 - \frac{2(\text{ber}'\ K + j\ \text{bei}'\ K)}{jK(\text{ber}\ K + j\ \text{bei}\ K)} \qquad \text{C.6}$$

where

$$K = a\ \left(\frac{\rho\omega}{\mu}\right)^{1/2} \qquad \text{C.7}$$

$$\text{ber}'\ Z = \frac{\partial}{\partial Z}\ (\text{ber}\ Z) \qquad \text{C.8}$$

$$\text{bei}'\ Z = \frac{\partial}{\partial Z}\ (\text{bei}\ Z) \qquad \text{C.9}$$

In deriving the correction function also needed is the friction force on the wall. The stress (τ) at the wall is

$$\tau = - \mu \frac{\partial u}{\mu r}\Big|_{r=a} = \frac{\mu}{a}\ \left(\frac{\partial P/\partial X}{j\omega}\right)\ K\ T_{(K)} \qquad \text{C.10}$$

The total friction force is $2\ \pi r\tau$ and the ratio of this

force to the average velocity is

$$\frac{2\pi a \tau}{U_{ave}} = \frac{2\ \pi\ \mu\ KT_{(K)}}{1 - \frac{2}{jK}\ T_{(K)}} \qquad C.11$$

where

$$T_{(K)} = \frac{ber'\ K + j\ ber'\ K}{ber\ \ K + j\ bei\ \ K} \qquad C.12$$

and as K aproaches 0, ratio of A10 approaches $8\pi\mu$.

Biot now introduces the correction function

$$F_{(K)} = \frac{1}{4}\ \frac{KT_{(K)}}{1 - \frac{2}{jK}\ (T_{(K)})} \qquad C.13$$

such that F(0)=1 and

$$\frac{2\pi a\ \tau}{U_{ave}} = 8\ \pi\ \mu\ F_{(K)} \qquad C.14$$

As Biot also states, the function F(K) measures the deviation from Poiseulle flow friction as a function of the parameter K. For large values of K

$$F_{(K)} \rightarrow \frac{K}{4}\ (\ \frac{1 + j}{\sqrt{2}}\ ) \qquad C.15$$

Appendix D, Acoustic Finite Elements

It is implicitly assumed that the changes of density and pressure are small compared to the static values, furthermore, the particle veloctiy should be much smaller than the sound velocity of the medium.

Assuming the medium is an ideal gas

$$\frac{P}{P_o} = \gamma \frac{\rho}{\rho_o} = \frac{\gamma}{\gamma-1} \frac{\delta T}{T} \qquad \text{D.1}$$

where γ is the ratio of the specific heats for the gas. The speed of sound in a gas is $C = \gamma \frac{P_o}{\rho_o}$ D.1(a)

For free air the compressiblity and rarification of the wave occurs adiabatically and accordingly $\gamma = \frac{C_p}{C_v} = 1.4$, $C = 343$ m/s . In small pipes at low frequencies ($K \leq 4$) the compressibilty is closer to isothermal, thus decreasing the propagation speed $\gamma = 1$, $C = 290$ m/s .

From equation (D1) of course

$$\frac{\partial \rho}{\partial t} = \frac{\rho_o}{\gamma P_o} \frac{\partial P}{\partial t} = \frac{1}{C^2} \frac{\partial P}{\partial t} \qquad \text{D.2}$$

By continuity

$$-\frac{1}{\rho C} \frac{\partial P}{\partial t} = \frac{\partial U}{\partial X} \qquad \text{D.3}$$

Substituting (D2) into (D3) yields

$$\rho \frac{\partial U}{\partial X} = - \frac{1}{C^2} \frac{\partial P}{\partial t} \qquad D.4$$

Using again the harmonic variation in time of the variables and the mean velocity, the force balance is

$$\frac{\partial P}{\partial X} = (\rho_e j\omega + R)\ \overline{U} \qquad D.5$$

and equation (D4) becomes

$$\frac{\partial U}{\partial X} = - \frac{j\omega}{\rho C^2} P \qquad D.6$$

taking divergence of (D4) and substituting (D5) yields

$$- \frac{\partial^2 P}{\partial X^2} = (- K^2 \frac{\rho_e}{\rho_o} + j\ K \frac{R}{\rho_o C})\ P \qquad D.7$$

where

$$K = \omega/C$$

The notation can be condensed by introducing

$$Y_r = - K^2 \frac{\rho_e}{\rho_o} \qquad D.8$$

So (D7) can be written as

$$Y_i = K \frac{R}{\rho_o C} \qquad D.9$$

$$- \frac{\partial^2 P}{\partial X^2} = Y_r \; P_r \; - Y_i \; P_i \qquad D.10$$

$$- \frac{\partial^2 P}{\partial X^2} = Y_r \; P_i \; + Y_i \; P_r \qquad D.11$$

Applying Galerkin's criterion to (D10) gives

$$\int_o^L Ni\left(\frac{\partial^2 P_r}{\partial X^2} + Y_r P_r - Y_i P_i\right) dX = 0 \qquad D.12$$

Integrating by parts gives

$$Ni \frac{\partial P_r}{\partial X} \Big|_o^L - \int_o^L \frac{\partial Ni}{\partial X} \frac{\partial P_r}{\partial X} + Ni \; Y_r P_r - Ni \; Y_i P_i \; dX = 0 \qquad D.13$$

The first term is represents the boundary condition i.e. a) at terminus dp/dx=0 and b) for input Ni(dp/dx) must be evaluated at x=0. The remainder reduces to

$$\int \left\{ \frac{\partial N}{\partial X} \right\} \lfloor \frac{\partial N}{\partial X} \rfloor \; dX = [s] \qquad D.14$$

$$\int \{N\} \lfloor N \rfloor \; dX = [P] \qquad D.15$$

Therefore equation (D13) can be written as

$$[s] \;\; \{P_r\} \; + Y_r[P] \; \{P_r\} - Y_i[P] \; \{P_i\} \;\; = 0 \qquad D.16$$

Treating equation D11 similarly

$$[s]\{P_i\} + Y_i[P]\{P_r\} + Y_r[P]\{P_i\} = 0 \qquad \text{D.17}$$

The boundary condition $Ni \frac{\partial P}{\partial X} \Big|_o^L$ will be evaluated next.

For a rigid terminus dP/dX=0 at X=L. The evaluation of the boundary condition $Ni\frac{\partial P}{\partial X}$ at X=0 (at the open end of the pipe) begins with

$$\frac{\partial P}{\partial X} = (j\ \rho_e\ \omega + R)\ U \qquad \text{D.18}$$

In the real and imaginary components

$$\frac{\partial P_r}{\partial X} = RU_r - \rho_e\ \omega\ U_i \qquad \text{D.19}$$

$$\frac{\partial P_i}{\partial x} = R\ U_i + \rho_e\ \omega\ U_r \qquad \text{D.20}$$

Therefore at the open end

$$Ni\ \frac{\partial P_r}{\partial X} = \{N\} \left\lfloor \frac{\partial N}{\partial X} \right\rfloor \{P_r\}\Big|_{X=0} = R\{N\} \lfloor N \rfloor \{U_r\}\Big|_{X=0} - \rho_e \omega \{N\} \lfloor N \rfloor \{\dot{U}_i\}\Big|_{X=0} \qquad \text{D.21}$$

The input velocity is set to be real only, for convenience.

Defining {Q} as the input array

$$\{Q_r\} = Ni\ \frac{\partial P_r}{\partial X} = R[D]\ \{U_r\} \qquad \text{D.22}$$

$$\{Qi\} = Ni\ \frac{\partial P_i}{\partial X} = \rho_e\ \omega[D]\ \{U_r\} \qquad \text{D.23}$$

where

$$[D] = \{N\} \lfloor N \rfloor \tag{D.24}$$

If a linear interpolation function is used

$$P = \lfloor 1 - X/L, \quad X/L \rfloor \begin{Bmatrix} P1 \\ P2 \end{Bmatrix} \tag{D.25}$$

then

$$[D] = \begin{bmatrix} 1 & 0 \\ 0 & 0 \end{bmatrix} \tag{D.26}$$

The complete equation to be solved is

$$\frac{1}{\rho_o C} \begin{bmatrix} \{Q_r\} \\ \\ \{Q_i\} \end{bmatrix} = \begin{bmatrix} [s] - K^2 \frac{\rho_e}{\rho_o} [P] & -K \frac{R}{\rho_o C} [P] \\ \\ K \frac{R}{\rho_o C} [P] & [s] - K^2 \frac{\rho_e}{\rho_o} [P] \end{bmatrix} \begin{Bmatrix} P_r \\ \\ P_i \end{Bmatrix} \tag{D.27}$$

This gives the pressure distribution along the pipe. To find the impedence of the pipe at the open end the pressure is divided by the velocity at the open end (the velocity is that used to calculate {Q}).

To find the pressure distribution in a pipe of varying area a similar analysis is done by using the wave equation for a horn, which is

$$\frac{\partial^2 P}{\partial t^2} - \frac{C^2}{A} \frac{\partial}{\partial X} \left(A \frac{\partial P}{\partial X}\right) = 0 \tag{D.28}$$

The only difference in the resulting equations is the manner [S] and [P] are calculated and the input term is multiplied by the area at the open end.

The new calculations are

$$[s] = \int_0^L A \left\{\frac{\partial N}{\partial X}\right\} \left\lfloor\frac{\partial N}{\partial X}\right\rfloor dX \qquad D.29$$

$$[P] = \int_0^L A\{N\}\lfloor N\rfloor \, dX \qquad D.30$$

If a linear interpolation function is used

$$[s] = \frac{A_1 + A_2}{2L} \begin{bmatrix} 1 & -1 \\ -1 & 1 \end{bmatrix} \qquad D.31$$

$$[P] = \frac{L}{12} \begin{bmatrix} 3A_1 + A_2 & A_1 + A_2 \\ A_1 + A_2 & A_1 + 3A_2 \end{bmatrix} \qquad D.32$$